THE UNIVERSITY OF CHICAGO

HOST DETERMINANTS OF INFLUENZA VIRUS REPLICATION

A DISSERTATION SUBMITTED TO

THE FACULTY OF THE DIVISION OF THE BIOLOGICAL SCIENCES

AND THE PRITZKER SCHOOL OF MEDICINE

IN CANDIDACY FOR THE DEGREE OF

DOCTOR OF PHILOSOPHY

COMMITTEE ON MICROBIOLOGY

BY

JULIANNA GRACE HAN

CHICAGO, ILLINOIS

DECEMBER 2018

COPYRIGHT © 2018 JULIANNA GRACE HAN

TABLE OF CONTENTS

ACKNOWLEDGEMENTS	iv
LIST OF FIGURES	vi
LIST OF TABLES	viii
CHAPTER I: Introduction	1
CHAPTER II: Materials And Methods	22
CHAPTER III: Genome-wide CRISPR/Cas9 Screen Identifies Host Factors Imperative for Influenza Virus Replication	41
CHAPTER IV: Regulation of Cell Intrinsic Immunity by the Transcriptional Repressor CIC	57
CHAPTER V: Tetracysteine Tagged NP Reveals the Role of Rab11a in Production of Infectious Influenza Virus Particles	74
CHAPTER VI: Discussion	89
BIBLIOGRAPHY	99
APPENDIX A: Figures	125
APPENDIX B: Tables	167
APPENDIX C: Soundtrack	183

ACKNOWLEDGEMENTS

I have been incredibly fortunate to be the first graduate student of my mentor, Dr. Balaji Manicassamy. As one of the most intelligent and scientifically creative people I know, I gratefully took the opportunity to absorb his way of thinking and approaching science. Dr. Jasmine Perez is a brilliant, insightful, and meticulous scientist who has also been a fantastic role model to me in the lab. I cannot thank Balaji and Jasmine enough for their devotion to my intellectual and technical training. Additionally, my thesis committee members, Drs. Glenn Randall, Seungmin Hwang, Michaela Gack, and Raymond Roos, have been instrumental to my Ph.D. success through their insight, advice, and care. Finally, I would not have made it through my second and third years without Cindy Chen in the Manicassamy lab to believe in me and build me up.

Throughout my Ph.D. experience, I relied heavily on my incredible family support system. My parents, Jim and Joycelyn, and siblings, Justin, Jenna, Josh, and Joe, built a solid foundation and motivated me to be my best. They inspire me every day with their passion, talent, courageousness, and kindness. I have also been lucky to extend my family to my husband Brendan's relatives, especially the Prendergasts, Orsers, Bowlings, Woods, and Johnsons. It has been a pleasure to be incorporated into a second closely-knit family of loving and supportive people.

Finally, this tough Ph.D. process has highlighted the immeasurable strength of the bond between my husband, Brendan Prendergast, and me. With his compassionate and

sincere heart and extraordinary intellect, he processed what it means to be a Ph.D. student with me, consoled me and built me up during the trials, and most importantly celebrated my successes and made them even sweeter. I have finished my dissertation due in large part to his belief in me and support.

LIST OF FIGURES

Figure I.1. Intracellular Life Cycle of Influenza Viruses. 125

Figure III.1. GeCKO Screen for Host Factors Essential for IAV Replication. 126

Figure III.2. Analysis of sgRNA Representation in the A549-GeCKO Library and Post H5N1 Selection. 128

Figure III.3. Validation of Selected Hits with Multiple IAV Strains. 130

Figure III.4. Depiction of Individual sgRNA Enrichment for Selected Hits. 132

Figure III.5. Identification of Viral Life-Cycle Defects for Selected Hits. 133

Figure III.6. Complementation of *JAK2* KO cells Increases Viral Replication. 135

Figure III.7. Sialic Acid Transporter SLC35A1 Is Required for IAV Entry. 136

Figure III.8. Enrichment of Host Factors Involved in Sialic Acid Biosynthesis and Related Glycan Modification Pathways. 138

Figure IV.1. Viral Replication is Decreased in CIC KO. 139

Figure IV.2. Viral Replication is Decreased in CIC Knockdown. 141

Figure IV.3. CIC Regulates Antiviral Gene Production. 142

Figure IV.4. CIC Repression of Binding Sites in IFNβ Promoter. 144

Fig IV.5. CIC Repression of Binding Sites in Endogenous Promoters of ISGs. 145

Figure IV.6. Quality Control Checkpoints for RNAseq Analysis of Vector Control and CIC KO2 Cells. 146

Figure IV.7. Global Change in Gene Expression in CIC KO2 Mock vs. Control Mock. 147

Figure IV.8. Enriched Gene Ontology Categories in CIC KO2 Cells. 148

Figure IV.9. CIC KO State: Roadblocks to Multiple Pathogens. 149

Figure IV.10. qPCR Analysis for Confirming Differentially-Expressed Genes Elicited by RNAseq Analysis. 150

Figure IV.11. Importance of Differentially-Expressed Genes During Viral Infection in CIC KO2s Through siRNA Mini-Screen. 151

Figure IV.12. HSV1 Replication is Unaffected in CIC KO2 Cells. 153

Figure IV.13. CIC is Downregulated in Response to Viral Infection. 154

Figure IV.14. Graphical Hypothesis. 155

Figure V.1. Design and characterization of first fluorescently-tagged NP virus. 156

Figure V.2. NP Expression and Dynamics. 158

Figure V.3. NP-Tc allows visualization of vRNP dynamics. 159

Figure V.4. Cytoskeletal components aide in IAV vRNP export. 161

Figure V.5. Rab11a is essential for replication of IAV. 162

Figure V.6. Complementation of Rab11a Restores IAV Replication in Rab11a KO Cells 163

Figure V.7. Loss of Rab11a disrupts trafficking and increases defective particles. 164

Figure V.8. vRNP trafficking is disrupted in Rab11a KO. 166

LIST OF TABLES

Table II.1. Oligonucleotide Sequences for NP-Tc Virus, Rab11a KO, and Gene Segment Sequencing. 167

Table II.2. Oligonucleotide Sequences for Generating and Validating CRISPR KO Cells. 168

Table II.3. FISH Probe Sequences for NP vRNA. 169

Table II.4. FISH Probe Sequences for PB2 vRNA. 171

Table III.1. Enrichment of Selected Top Hits for Validation. 173

Table III.2. Sequence Analysis of sgRNA Target Sites in Clonal KO Cells. 174

Table IV.1. CIC Binding Sites in Antiviral Gene Promoters. 175

Table IV.2. Top 10 Enriched Gene Ontology Terms Between CIC KO Mock vs. Control Mock. 176

Table IV.3. Top 10 Enriched Kyoto Encyclopedia of Genes and Genomes Pathways Between CIC KO Mock vs Control Mock. 177

Table IV.4. Top 10 Enriched Pathways in Ingenuity Pathway Analysis Between CIC KO Mock vs. Control Mock. 178

Table IV.5. Top Enriched MSigDB C3 Transcription Factor Target Motifs Between CIC KO Mock vs. Control Mock. 179

Table IV.6. Top Enriched Genes in CIC KO Mock vs. Control Mock. 180

Table IV.7. DEGs in GO Pathway “Defense Response to Other Organism.” 181

CHAPTER I

Introduction

Some of this chapter includes text and a figure adapted from the published review article 'Influenza Virus: Small Molecule Therapeutics and Mechanisms of Antiviral Resistance,' conceived and written by Julianna Han (Han et al. 2017).

Impact of Influenza Viruses on Global Human Health

Influenza viruses are highly successful pathogens, causing seasonal epidemics of sustained transmission cycles that take a significant toll on public health and remarkably devastating pandemics that spread rapidly across the globe, killing millions of people. Year 2018 marks the 100th anniversary of the 1918 Spanish flu pandemic, which resulted in over 50 million deaths worldwide, yet influenza viruses still evade our best efforts to curb infection and disease. According to World Health Organization reports, seasonal influenza virus epidemics affect 3-5 million people and cause 250,000-500,000 deaths worldwide every year ("World Health Organization" 2016). Influenza viruses cause upper respiratory infections in humans, affecting people of all ages; however, young children and the elderly are the most vulnerable to influenza virus infection. These two groups, in addition to immunocompromised individuals, are considered to be high-risk groups as influenza virus infections are severe in these populations ("Centers for Disease Control and Prevention" 2011). Furthermore, seasonal influenza vaccines do not induce robust and protective immunity in these high-risk groups (Krammer and Palese 2015). Antiviral drugs play a crucial role in impeding influenza virus disease progression and

transmission, especially in these populations ("Centers for Disease Control and Prevention" 2011). However, despite our best efforts, a major hurdle to treating these infections is the propensity of influenza viruses to develop antiviral resistance. Therefore, we must continue to investigate the fundamentals of influenza virus pathogenesis, probing how influenza viruses replicate in conjunction with host factors and pathways. These studies may reveal better targets and methods for combatting influenza virus infection, disease, and pandemic risk.

Ecology of Influenza Virus

Influenza viruses have been circulating among humans for centuries. Indeed, influenza virus is the purported causative agent of a disease recounted by Hippocrates in 412 B.C. (Shaw and Palese 2013). Influenza viruses are members of the *Orthomyxoviridae* family of negative-stranded RNA viruses containing genomes composed of 7-8 segments. The *Orthomyxoviridae* family includes seven genera: influenza viruses A-D, isavirus, thogotovirus, and quaranjavirus ("International Committee on Taxonomy of Viruses: Orthomyxoviridae Current Taxonomy 2015" 2017; Hause et al. 2013). Based on the serology of two viral glycoproteins, hemagglutinin (HA) and neuraminidase (NA), influenza A virus (IAV) can be further classified into subtypes such as H1N1, H2N2, H5N1 etc. Currently, there are at least 18 HA and 11 NA subtypes (Gamblin and Skehel 2010; Wu et al. 2014). IAV and influenza B viruses co-circulate and cause seasonal epidemics in humans.

Of the seven genera, IAV displays broad host species tropism, infecting waterfowl, poultry, horses, pigs, and seals; however, type B and C infections are usually restricted to humans and type D infections are limited to swine and cattle (Shaw and Palese 2013; Ferguson et al. 2016). Aquatic birds are considered to be the natural reservoirs of IAV as they harbor all subtypes of IAV strains (Wahlgren 2011). IAV circulating in wildlife and domestic animals have crossed the species barrier and caused sporadic infection and pandemics in humans.

Zoonotic transmission of IAV has led to the last four influenza pandemics – the 1918 H1N1 Spanish flu, 1957 H2N2 Asian flu, 1968 H3N2 Hong Kong flu, and 2009 H1N1 swine flu (Taubenberger and Morens 2009; Y. Watanabe et al. 2012). Spanish flu was responsible for the most deadly pandemic of any pathogen known in human history, which resulted from a bird IAV strain directly adapting to the human population. 50 million people lost their lives during this pandemic. The Asian and Hong Kong flu pandemics resulted from genetically novel viruses carrying gene segments from both bird and human strains. These pandemics killed several million people. The 2009 swine flu pandemic was caused by melding of the bird IAV strain that generated the Spanish flu with genetic material from pig and human IAV strains. After the pandemic period, the newly introduced strain becomes a seasonal strain and remains in circulation in the human population. The IAV strains currently circulating in humans are H1N1 from the 2009 H1N1 swine flu pandemic and H3N2 from the 1968 H3N2 Hong Kong flu pandemic.

On numerous occasions, IAV strains such as H5N1 and H7N9 that are endemic in domestic poultry have caused wide-spread infections in Southeast Asia with significant loss of human life. While the majority of these avian IAV strains show limited human to human transmission, H5N1 is only a few mutations away from becoming airborne in mammals. Moreover, H5N1 has a very high mortality rate of 60% in humans and is of increasing concern as a pandemic threat (Y. Watanabe et al. 2012; Shi et al. 2014; Taubenberger and Morens 2009). In contrast to IAV, influenza B viruses do not have an animal reservoir outside of humans and thus do not cause pandemics.

Molecular Biology and Life Cycle of Influenza A Virus

The IAV genome is composed of eight negative-sense, single-stranded RNA segments encoding 11 or 12 viral proteins. Additional viral proteins are encoded through mRNA splicing or by utilizing alternate open reading frames for translation (Shaw and Palese 2013). The surface proteins of IAV include hemagglutinin for receptor binding and viral membrane fusion, neuraminidase for cleaving receptors, and matrix 2 ion channel (M2), a proton pump. The capsid is formed by matrix 1 (M1). The RNA genome is formed into viral ribonucleoprotein (RNP) complexes consisting of RNA wrapped around nucleoprotein (NP) with the viral polymerase associated at the ends of the RNA. The viral polymerase is composed of polymerase basic protein 1 (PB1, RNA polymerase), polymerase basic protein 2 (PB2, cap binding protein), and polymerase acidic protein (PA, endonuclease). Nuclear export protein (NEP) escorts RNPs from the nucleus to the plasma membrane. Non-structural protein 1 (NS1) and PB1-F2, expressed from a +1

ORF of PB1 mRNA, counteract host antiviral responses and enable efficient viral replication.

During the intracellular stages of the influenza virus life cycle, viral components need to traffic to and from the plasma membrane, through endosomal and vesicular pathways, and through nuclear import and export pathways, hitchhiking on many trafficking host factors for transportation (Figure I.1) (Hutchinson and Fodor 2013). Most RNA viruses replicate in the cytoplasm because the machinery they need to complete their life cycle is localized there, but in order to maximize its coding capacity, IAV utilizes the host splicing machinery localized in the nucleus to express two of its genes. Moreover, IAV must stealthily accomplish all intracellular stages of its life cycle while subverting the host innate immune system. Studying the dynamics of intracellular IAV replication remains an imperative and ongoing task in order to develop novel therapeutics against IAV.

Influenza A Virus Life Cycle: Entry

The three integral membrane proteins, HA, NA, and M2, are present on the virion surface. HA, a type I membrane protein, facilitates the binding of virus particles to the cell surface receptor (sialic acid) and mediates subsequent entry into host cells. Under low pH conditions, HA undergoes a conformational change in order to fuse the viral envelope with the endosomal membrane. M2, a small integral membrane protein, forms a proton pump on the virion membrane. Under low pH conditions in the late endosome, M2 pumps H^+ into the virion. Virion acidification results in dissociation of M1 from the RNPs, thereby exposing nuclear localization signals critical for the nuclear import of the RNPs.

Influenza A Virus Life Cycle: Transcription and Replication

The heterotrimeric RdRP complex comprised of PB1, PB2, and PA is involved in transcription and replication of the viral genome. Upon entry into the nucleus, the RdRP associated with the viral genomic RNA transcribes viral mRNA. PB2 binds to host 5' 7-methylguanosine caps, PA cleaves 10-13 nucleotides after the cap, and PB1 uses the caps as a primer for initiation of mRNA transcription. Viral mRNA are polyadenylated by PB1 stuttering on a poly-uridine tract. Newly synthesized RdRP proteins replicate the genome: PB1 binds the double-stranded RNA promoter of IAV, formed by the conserved 5' and 3' ends of vRNA, and transcribes a complete complement of vRNA in the positive sense (cRNA) using *de novo* initiation. PB1 retains the newly generated cRNA in a process called antitermination and synthesizes a new vRNA strand using cRNA as a template. NP binds to viral RNA and is critical for both transcription and replication processes. Next, newly replicated RNPs must exit the nucleus and transport through the cytoplasm, undergoing selective packaging of all segments en route to the plasma membrane.

Influenza A Virus Life Cycle: RNP Export and Packaging

As a segmented virus, IAV encodes packaging sequences as a mechanism to ensure complete packaging of all eight gene segments in progeny virions. The packaging signals begin in the noncoding regions at both 3' and 5' ends of vRNA and extend into the coding region of each gene. These signals are sequence-specific to enable specific incorporation of each segment (Lakdawala, Fodor, and Subbarao 2016). After replication, NEP

facilitates the export of newly formed RNP complexes to the plasma membrane for virion assembly and release.

The Importance of Host Factors in RNP Egress

As a virus with a minimal genome, IAV must heavily rely on host proteins and pathways in order to complete its life cycle. A prime example of IAV usurping host pathways occurs during the vRNP egress process. After replication, M1 associates with newly generated vRNPs and binds NEP, which conceals the nuclear localization signal on M1. NEP also has a nuclear export signal that is recognized by the host's nuclear export factor CRM1. This large complexed is shuttled through the nuclear pore complex into the cytoplasm by the CRM1-mediated nuclear export pathway. Then, RNPs take advantage of the Rab11a recycling endosome pathway and the microtubule network to transport to the plasma membrane.

Rab11a belongs to a family of small GTPases that orchestrate membrane trafficking. Rab11a is responsible for retrograde and anterograde delivery of growth factors, peptides, and cytokines between the recycling endosome and the plasma membrane (Guichard, Nizet, and Bier 2014). It interacts with multiple effector proteins and motor proteins in order to traffic along microtubule and actin networks, providing an excellent transportation system for vRNPs. Moreover, due to the massive production of vRNPs, the egress of IAV overwhelms the Rab11a trafficking pathway, jamming cellular recycling and sorting events (Guichard, Nizet, and Bier 2014; Sílvia Vale-Costa and Amorim 2017). Still, the egress process of IAV is not fully understood. Outstanding questions include how

vRNPs gain access to the Rab11a transportation system and how eight RNP segments associate together and specifically package to form infectious virus particles.

Influenza Virus Life Cycle: Virion Budding

Following egress of RNP complexes from the nucleus to the cytoplasm, RNP complexes are packaged into virions at the plasma membrane, with M1 forming the capsid of the virion. The virions bud from the plasma membrane, acquiring a host-derived envelope in the process. NA, a type II membrane protein, removes sialic acid to promote viral spread by preventing the re-attachment of newly formed virions to the surface of already infected cells (Shaw and Palese 2013).

Therapeutics to Control Influenza Viruses

Due in part to its error-prone RdRP and RNA genome, IAV is highly mutagenic, allowing it to quickly diversify its genome to remain pathogenic under selective pressures. Indeed, this antigenic drift enables IAV to escape restriction from seasonal influenza vaccines. Furthermore, as seasonal influenza vaccines contain antigens that induce immunity against seasonal strains but not against novel zoonotic strains, antivirals are the first line of defense against novel IAV strains until sufficient quantities of vaccines are made available.

At present, there are five FDA-approved antivirals for the treatment of influenza virus infection that are categorized into two groups, M2 ion channel inhibitors (adamantanes) and NA inhibitors (NAIs). The adamantane group consists of amantadine and

rimantadine, which target M2 to inhibit IAV disassembly. However, adamantanes are ineffective against the M2 of influenza B viruses because of dissimilarity in the amino acid sequences of the two proteins, resulting in polar residues lining the M2 pore for influenza B viruses rather than hydrophobic residues lining the M2 pore for IAV (C. Ma et al. 2008; Pinto and Lamb 2006). NAIs include zanamivir, oseltamivir, and peramivir and function to prevent the release of nascent virions for both IAV and influenza B viruses. The currently circulating IAV strains are almost fully resistant to adamantanes, thus amantadine and rimantadine are no longer used for the treatment of IAV infection ("Centers for Disease Control and Prevention" 2017a). In contrast, resistance to the available NAIs varies among seasonal strains, and this group of drugs is actively used for the treatment of influenza virus infections in humans (Hurt 2014).

Need for Host-Directed Therapeutics

Elucidating host determinants of influenza virus is crucial not only for our fundamental knowledge of IAV pathogenesis, but also for therapeutic purposes. Antiviral drugs targeting viral proteins can become ineffective due to the ability of the RdRP to mutate the viral genome and generate resistant variants. An alternative strategy is to target the host proteins and pathways critical for the life cycle of influenza virus (T. Watanabe and Kawaoka 2015; T. Watanabe et al. 2014). For example, DAS181 is a sialidase fusion protein that cleaves α2'-6' and α2'-3' sialic acid from epithelial cells, potently blocking influenza virus binding and entry into cells (Malakhov et al. 2006; R. W. Y. Chan et al. 2009; Triana-Baltzer et al. 2009). Currently in clinical trials, DAS181 is administered as an inhalant to cleave sialic acid from the airway epithelium (Zenilman et al. 2015;

Malakhov et al. 2006). Moreover, genome-wide screens have led to the identification of cellular components critical for IAV replication and have elucidated the viral-host interactome. This novel information can be used to develop new host-directed antivirals with reduced predisposition for the development of antiviral resistance (T. Watanabe et al. 2014; T. Watanabe and Kawaoka 2015).

Genome-wide Screens Reveal the Virus:Host Interaction Network

In the last decade, researchers have conducted multiple genome-wide screens for host factors utilized during IAV replication by employing RNA interference (RNAi) technology, a system to knockdown expression of genes through small-interfering RNAs (siRNA) (König et al. 2010; Karlas et al. 2010; Desai et al. 2014; Shapira et al. 2009; Hao et al. 2008). These screens greatly contributed to understanding the intracellular life cycle of IAV by revealing novel host factors such as COPI vesicle transport proteins and RNA splicing machinery that aide IAV replication and IFITM proteins that restrict the entry process of IAV (Mehle and Doudna 2010; Stertz and Shaw 2011).

Several caveats to siRNA genome-wide screens confound the conclusions of these screens. Inherently in the siRNA system, knockdown of genes still enables low amounts of these genes to be expressed. This results in false negatives for genes that may be highly potent for IAV replication, but only needed in low abundance—these genes will not be included as hits in negative selection siRNA screens because knockdown of these genes will still produce minimal protein that could be sufficient to support viral replication. Conversely, siRNAs can target unintended genes, resulting in false positives. The

individual factors uncovered by siRNA genome-wide screens were inconsistent with one another—no single gene was identified by all siRNA screens, and ~92% of the total lists of genes were unique to their respective screens (Mehle and Doudna 2010; Stertz and Shaw 2011). Technical differences between screens, such as cell lines, strains, and end-point assays, contributed to the dissimilarity in gene lists. Regardless, these screens hit on enriched host pathways utilized by IAV, which open avenues for future investigation.

All siRNA genome-wide screens utilized PR8 or WSN33 strains of H1N1, furnishing a thorough assessment of H1N1 host factors, but leaving IAV subtype differences untouched. It would be interesting to compare similarities and differences in host factors between the two seasonal subtypes, H1N1 and H3N2. Investigating and comparing shared and novel host factors between H1N1 and H5N1, a potentially pandemic bird flu strain, is perhaps even more interesting and useful. There is still a great need for more research into host dependency factors of IAV, especially regarding differences between subtypes.

CRISPR/Cas9 Technology

Within the last five years, a new gene editing technique exploded onto the scene of molecular engineering, capturing prizes such as the 2015 *Science* Breakthrough of the Year and the 2015 Kavli Prize in nanoscience, and anticipating a Nobel Prize. The revolutionary gene editing technique involving clustered regularly interspaced short palindromic repeats (CRISPR) and cas (CRISPR associated) enzymes was harnessed by multiple groups led by Drs. Doudna, Charpentier, Siksnys, and Zhang, who

manipulated the endogenous CRISPR/Cas system to tailor genes, including those of the mammalian system on a genome-wide scale.

However, this system is far from new; CRISPRs were described as early as 1987 (Ishino et al. 1987). In fact, CRISPR/Cas is an ancient, conserved defense mechanism in bacteria that utilizes “memory” to provide the organism with an adaptive-like immune system to ward off bacteriophages. In the endogenous system, bacteriophage DNA is inserted as spacers into the CRISPR array in the bacterial genome. These spacers are transcribed and processed to mature CRISPR RNAs (crRNAs) that target foreign DNA through the complementary spacer region and recruit cas enzymes through a repeat region. The bacterial system utilizes protospacer adjacent motifs (PAM), sequences in the invader DNA next to the crRNA target region, to ensure non-self targeting. crRNAs are perpetually on surveillance to recognize their targets and recruit cas enzymes to degrade the foreign DNA, inhibiting reinfection by previous invaders (Doudna and Charpentier 2014).

In the CRISPR/Cas9 gene editing tool, crRNA processing and maturation has been simplified to a single guide RNA (sgRNA) that hybridizes the functions of DNA recognition and cas recruitment. While multiple cas systems exist, Cas9 of *Streptococcus pyogenes* was quickly established as the cas enzyme of choice for gene editing, in part because it did not need protein cofactors to function. Therefore, in this tool, the sgRNA binds to its target sequence in genomic DNA and Cas9 binds and induces a double stranded break (DSB). The cellular repair pathway non-homologous end joining (NHEJ) tries to repair the DSB, but due to the error-prone nature of NHEJ, the repair often contains DNA insertions

and deletions that can disrupt the open reading frame and result in a non-functional gene (Doudna and Charpentier 2014). Therefore, CRISPR gene editing “knocks out” (KO) genes, greatly expanding the potential of molecular engineering.

The invention of CRISPR editing on a genome-wide scale is a result of serendipitous convergence and integration of multiple independent biological fields. Microbiologists discovered the fundamentals of the endogenous CRISPR system as molecular biologists teased apart eukaryotic gene repair pathways and geneticists sequenced the entire human genome. Together, these discoveries spanning multiple disciplines built the pyramid to a truly revolutionary technique.

In CRISPR genome-wide screening, sgRNAs target every gene in the genome of the organism of interest. Researchers commonly use lentiviral systems to deliver Cas9 and the sgRNAs individually or as pooled libraries to cell lines. After researchers apply their selection criteria, next generation sequencing reveals genes of interest. Since the advent of CRISPR genome-wide screening, researchers have capitalized on this technique to elucidate important genes for processes from basal cellular signaling to cancer pathways and viral replication (Sharma and Petsalaki 2018; Gebre, Nomburg, and Gewurz 2018).

Several genome-wide CRISPR screens have been conducted to discover host factors involved in viral life cycles (Han et al. 2018; Zhang et al. 2016; Marceau et al. 2016; B. E. Heaton et al. 2017; H. Ma et al. 2015; Savidis et al. 2016; Orchard et al. 2016; R. J. Park et al. 2017). While both the siRNA and CRISPR systems have off-target caveats, the

CRISPR editing system results in complete KO cells lines, unlike the siRNA system. As such, genes essential for cellular survival are non-viable and are not present in CRISPR KO screens. Therefore, if we identify non-essential genes that are necessary for viral replication, but can be knocked out of cells without affecting cellular survival, then we can try targeting these genes with drugs to combat influenza infection. CRISPR genome-wide screening eliminates a step in the therapeutic pipeline of identifying potential drugs. In order to gain insight into the life cycle of H5N1, we applied a CRISPR genome-wide screen in human lung epithelial cells and elucidated several key host factors imperative for IAV replication as well as a surprising, novel regulator of the human immune system.

Host Antiviral Response

As obligate intracellular pathogens, viruses have been evolving with host organisms for millennia. To fight infection, hosts have evolved extensive immune systems, such as the CRISPR system in bacteria. The immune system in humans is even more complex, containing cell intrinsic and humoral branches to produce a customized response. The pathways in each of these branches are thoroughly selected and adapted, shaping a robust network of host defense.

In order to streamline comprehension of tricky signaling cascades and pathways in intracellular immunity, I have listed the acronyms used in this section here instead of distributing them throughout the text: interferon (IFN); IFN-stimulated genes (ISGs); pathogen-associated molecular patterns (PAMPs); retinoic acid-inducible gene I (RIG-I); melanoma differentiation-associated gene 5 (MDA5); Toll-like receptor (TLR); absent in

melanoma 2 (AIM2); DNA-dependent activator of IFN-regulatory factors (DAI); stimulator of IFN genes (STING); mitochondrial antiviral signaling protein (MAVS); TANK-binding kinase (TBK1); inhibitor of nuclear factor kappa β kinase (IKKε); IFN regulatory factor (IRF); tumor necrosis factor receptor-associated factor (TRAF); IκB kinase (IKK); nuclear factor kappa B (NFκB); NFκB inhibitor (IκB); apoptosis-associated speck-like protein containing a CARD (ASC, also known as PYCARD); interleukin-1 β (IL-1β); IFN-γ inducible protein 16 (IFI16); IFN-α/β receptor (IFNAR); Janus kinase 1 (JAK1); signal transducer and activator of transcription (STAT); IFN-stimulated gene factor 3 (ISGF3); myxovirus resistance A (MxA); IFN induced transmembrane protein (IFITM); IFN induced protein with tetratricopeptide repeats (IFIT); really interesting new gene (RING); tripartite motif containing 25 (TRIM25); protein inhibitor of activated STAT (PIAS); suppressor of cytokine signaling (SOCS); ubiquitin specific peptidase 18 (USP18); small ubiquitin-like modifier (SUMO).

Cell intrinsic immunity, the first line of defense in human immune systems against invaders, is tuned to sense and eliminate RNA and DNA viruses, intracellular bacteria, and parasites. This system involves pathogen detection, IFN and other cytokine signaling and production, stimulation of effector proteins such as ISGs to induce the antiviral state, and regulation of innate immunity (Sun, Liu, and Chen 2010; Schneider, Chevillotte, and Rice 2014).

The innate immune system senses foreign genetic material through PAMPs. Cytosolic PAMPs that recognize foreign RNA include the RIG-I-like receptor family, notably RIG-I

and MDA5. Endosomal PAMPs include members of the TLR family; TLR3 and TLR7 recognize foreign RNA while TLR9 recognizes CpG DNA. AIM2 and DAI are cytosolic PAMPs that recognize foreign DNA (Sun, Liu, and Chen 2010; Y. K. Chan and Gack 2016).

Each PAMP activates a network of signaling cascades to alert the innate immune system to the invasion. Signaling cascades downstream of TLR3, DAI, and the adaptor STING, as well as RIG-I and MDA5 signaling through MAVS, converge on activation of the kinases TBK1 and IKKε to phosphorylate and activate IRF3 and IRF7. These IRFs activate transcription of type I IFNs. Also, endosomal TLRs and MAVS signal through TRAF3 and TRAF6 to activate TBK1 and IKK to phosphorylate and activate IRFs or inactivate the NFκB inhibitor IκB, thus allowing NFκB to activate transcription of a multitude of inflammatory genes and type I IFNs. In addition, the inflammasome also responds to pathogen sensing; DNA sensing through AIM2 stimulates ASC and caspase-1, also cross-activated by RIG-I, to cleave the precursor cytokine pro-IL-1β to mature IL-1β, which mediates the inflammatory response (Poeck et al. 2010). IFI-16 is another cytoplasmic DNA sensor that cross activates several immune pathways: it can activate the inflammasome through complexing with ASC and stimulate production of type I IFN and inflammatory genes through activating STING (Unterholzner et al. 2010; Kerur et al. 2011; Dell'Oste et al. 2015). In this labyrinth of pathogen sensing and signaling including cross talk and cross activation, host sensors respond to invasion, ultimately resulting in production of cytokines such as IFN, inflammatory genes, and a subset of ISGs (Sun, Liu, and Chen 2010; Y. K. Chan and Gack 2016).

Following IFN production, the cell secretes IFN to activate IFN gene response programs in the same cell (autocrine signaling) or in neighboring cells (paracrine signaling). Type I IFNs bind to the cell surface receptor IFNAR, phosphorylating and activating JAK1 and STAT1/STAT2 to complex with IRF9. Together this complex, known as ISGF3, induces transcription of ISGs, which cooperate to attack pathogen replication at multiple stages (Sun, Liu, and Chen 2010).

In the molecular arms race against pathogen invasion, the cell intrinsic immune system evolved a plethora of ISGs and effectors to control pathogens. Immune effectors especially equipped to combat IAV include MxA, IFITMs, and IFITs. The dynamin-like GTPase MxA binds to IAV RNA and prevents nuclear import, halting transcription and replication (47). IFITM3 blocks fusion of viral and endosomal membranes. IFIT1 binds and sequesters the 5' tri-phosphorylated RNA of IAV. ISG15, an ubiquitin-like protein, tags viral proteins for modification. Together, multiple innate immune factors orchestrate a defensive line against the life cycle of IAV (Schneider, Chevillotte, and Rice 2014; Iwasaki and Pillai 2014).

In the struggle to counteract the host, viruses have evolved strategies to evade detection by the innate immune system. One of the most well-characterized examples is the ability of the NS1 protein of IAV to block RIG-I sensing. NS1 inhibits multimerization of TRIM25, a RING-finger E3 ubiquitin ligase crucial for ubiquitinating and activating RIG-I (Gack et al. 2009; Gack et al. 2007). This mechanism enables IAV to subvert host sensing.

Negative regulators are imperative for inhibiting aberrant IFN signaling, and indeed, ISGs include negative regulators to ramp down the IFN response. Some of these IFN desensitizing proteins include PIAS proteins, SOCS proteins, USP18, and phosphatases that inhibit activation of JAKs and STATs. PIAS proteins regulate transcription of IFN responses through SUMOylation, interruption of transcription factor binding partners, and inhibition of STAT dimerization. SOCS proteins inhibit JAK/STAT signaling by binding and hiding phosphorylated residues on JAK and IFNAR. USP18 mediates IFN desensitization through deISGylating proteins as well as by binding IFNAR, barring JAK1 binding. However, negative regulation of IFN responses and cell intrinsic immunity are less studied than their positive effector counterparts. A better understanding of immune regulators can guide efforts to combat viral infections and autoimmunity (Schneider, Chevillotte, and Rice 2014).

Thesis Goals

As highlighted throughout this chapter, host organisms and the viruses that infect them exist in a convoluted interplay with each other. IAV usurps host pathways at every stage of its intracellular life cycle while the host immune system strives to identify and fight off the invasion. In order to limit the extraordinary public health burden of IAV, vaccination and antivirals are our greatest options. While vaccination is the best defensive strategy against seasonal influenza virus outbreaks, antivirals provide a complementary approach to fight influenza virus infection, especially in individuals who are unable to be vaccinated. Moreover, antivirals are the first line of defense for controlling novel influenza virus

outbreaks, as little immunity is present in the human population and vaccine development is time-consuming and laborious. The existing antivirals target the ion-channel activity of M2 or the sialidase activity of NA; however, a major hurdle to their efficacy is the development of resistance to these antivirals. Therefore, identification and characterization of antivirals with an expanded range of viral and host targets are critical to generate novel and effective treatments with less potential for the emergence of resistant variants.

To ultimately uncover novel therapeutic targets, first we must gain a better understanding of the exchange between IAV and the host during intracellular replication. We must pinpoint specific host factors on which IAV depends and also characterize the mechanism and importance of their functions during the life cycle of IAV.

To that end, we employed the powerful new tool of CRISPR genome-wide screening. Using this technique, we added to and strengthened our understanding of the virus:host interaction network. Using a library of KO human lung epithelial cells and a low pathogenic human isolate of H5N1, we selected cells that were resistant to H5N1 infection. This negative selection process elucidated genes that are crucial for the life cycle of IAV; when these factors are knocked out, cells can survive infection. Our top hits clustered into pathways such as proton transport, intracellular signaling, and innate immune regulation. We gleaned host factors involved in individual steps of the life cycle as well as targets that function more broadly in regulation of the immune system. We characterized SLC35A1 as a crucial factor for binding and entry of IAV virions to host cells.

Moreover, we uncovered capicua as a novel negative regulator of cell intrinsic immunity. Multiple viruses from diverse RNA virus families relied on CIC for optimal replication. Without CIC, cells upregulated broad immunity and inflammation pathways, generating a hostile state for pathogen invasion. We identified CIC binding sites in the promoters of immunity and inflammation genes, suggesting a mechanism by which CIC, a DNA repressor, may be regulating these genes. Furthermore, CIC was downregulated during IAV infection, suggesting a host response mechanism exists to control CIC-mediated repression of the antiviral state. As a highly conserved gene, the role of CIC in host defense against pathogens may be evolutionarily significant and applicable to a broad array of species.

One of the greatest challenges in our endeavors to constrain IAV is its propensity to reassort its genome. IAV contains an 8-piece segmented genome that has the ability to recombine genomic segments between IAV strains, spawning antigenically new IAV variants with pandemic potential. Elucidating the mechanism of IAV recombination is crucial to understanding and combatting emerging IAV strains. Again, host factors are at play in this process.

To better understand packaging of IAV segments, we generated tools to assess vRNP dynamics and host factor dependency. Through fluorescent tagging of NP coupled to illumination of vRNA through fluorescence in situ hybridization (FISH), we visualized vRNP transport dynamics. RNP complexes egressed from the nucleus in large

supramolecular complexes in a regulated, polarized fashion as early as 3 hours after infection, localizing with Rab11a and relying on the microtubule network for coordinated transport. Moreover, we revealed novel function for the host protein Rab11a. Loss of Rab11a in cells abrogated supramolecular complex clustering of RNPs in the cytoplasm, potentially hindering selective packaging of vRNPs. Indeed, infectious particle production was significantly attenuated in Rab11a KO cells. Therefore, using Rab11a KOs and the NP-tagged virus to selectively visualize vRNP dynamics, we see that Rab11a is important for clustering RNPs in the cytoplasm to promote efficient packaging of nascent virions, a finding that may nudge the field a step forward in understanding the elaborate process of selective packaging.

Throughout my thesis work, I have been motivated by two major goals. First, I have marveled at the ability of IAV, a genetically-compact virus, to adapt and perpetuate successfully throughout a large array of diverse animal species, all of which have orders of magnitude more sequence space than IAV. During my thesis research, I have investigated the strategies engaged by IAV to be so successful, such as segmented genomes, high mutation rates, and airborne transmission routes. Second, I feel compelled to apply my research and efforts to aide public health. Concordantly, I have also tackled IAV pathogenesis from the host perspective, investigating how the human immune system functions to oppose viral invasion. Moreover, I have uncovered human host factors as potentially druggable targets to add to our arsenal of antivirals. I hope that my findings contribute to our knowledge of biomedical research and can be applied to alleviate human suffering.

CHAPTER II

Materials and Methods

This chapter includes experimental procedures for the published manuscript 'Genome-wide CRISPR/Cas9 Screen Identifies Host Factors Essential for Influenza Virus Replication' (Han et al. 2018). Please access the published manuscript in order to locate the large supplementary tables.

A549-GeCKO Library Generation and H5N1 Screen

The A549-GeCKO library was generated using the lentiGuide-Puro (#52963, Addgene) two-vector system for Cas9 and sgRNA delivery as previously described (Sanjana, Shalem, and Zhang 2014). Briefly, Cas9-A549 cells were generated via lentivirus transduction of the Cas9 transgene (lentiCas9-BLAST, #52962, Addgene) followed by selection with 5μg/ml blasticidin. Clonal Cas9-A549 cells were further transduced with lentivirus particles containing the human sgRNA library (Human GeCKO v2 Library A Cat#1000000049, Addgene) at MOI=0.3 to attain no greater than 1 sgRNA per cell and selected with both 1μg/ml puromycin and 5μg/ml blasticidin for 14 days to achieve >95% gene disruption (Shalem et al. 2014). For the Preliminary Consecutive Screen, $2x10^8$ A549-GeCKO library cells were infected with $VN04_{Low}$ (H5N1) at MOI=5 in infection media for 2 days. Surviving cells were reseeded in DMEM supplemented with 10% FBS and 1% P/S and subjected to four more rounds of infection. The surviving resistant population was expanded to $1x10^7$ cells and subjected to deep sequencing analysis. For the Sequential Screen, $2x10^8$ A549-GeCKO library cells were infected with $VN04_{Low}$ (H5N1) at MOI=5 in infection media for 2 days in biological duplicates, and the surviving cells

were allowed to expand (~2-4x10^7) and 1/5^{th} of the expanded cells were utilized for deep sequencing analysis and 4/5^{th} of the expanded cells were subjected to the next round of infection.

Cell Culture and Viruses

Human embryonic kidney (HEK293) cells, human lung epithelial (A549) cells, African green monkey kidney (Vero) cells, and human bone osteosarcoma epithelial cells (U2OS) were cultured in DMEM supplemented with 10% fetal bovine serum (FBS) and 1% penicillin/streptomycin (P/S). U2OS cells were provided by Dr. Kay Macleod at the University of Chicago. Madin Darby canine kidney (MDCK) cells were cultured in MEM supplemented with 10% FBS and 1% P/S. All IAV strains – A/Puerto Rico/8/1934 (PR8, H1N1), low pathogenic version of A/Vietnam/1203/2004 ($VN04_{Low}$, H5N1), and A/Hong Kong/1/1968 (HK68, H3N2) – were kindly provided by Dr. Adolfo Garcia-Sastre at the Icahn School of Medicine at Mount Sinai, NY. IAV were grown in 10 day old specific pathogen-free eggs (Charles River) and titered by standard plaque assay on MDCK cells, using 2.4% Avicel RC-581 (a kind gift from FMC BioPolymer, Philadelphia PA) as an alternative to oxoid agar (Perez, Garćia-Sastre, and Manicassamy 2013); plaques were quantified 2 days post infection by crystal violet staining. Vesicular stomatitis virus expressing GFP (VSV) was kindly provided by Dr. Glenn Barber at the University of Miami, FL (Stojdl et al. 2003). Encephalomyocarditis virus (EMCV) was obtained from Dr. Seungmin Hwang at the University of Chicago, IL. Zika virus strain MR766 was provided by Dr. Rong Hai at the University of California-Riverside, CA. Herpes Simplex Virus 1 (HSV1) was obtained from Dr. Michaela Gack at the University of Chicago and ΔICP0

HSV1 was obtained from Dr. Bin He at the University of Illinois at Chicago. VSV, EMCV, Zika virus, and HSV1 were grown in Vero cells, ΔICP0 HSV1 was grown in U2OS cells. Briefly, HSV1 was amplified for 3-4 days in Vero or U2OS cells. Supernatant was collected and cell pellets were freeze-thawed three times to release cell-bound virus. Freeze-thawed cell pellets were spun down at 1500 rpm for 5 min, and supernatants were pooled and filtered through a 0.45um filter. Viruses were titered by plaque assay using 1% methylcellulose (Sigma).

Generation of NP-Tc and NP200 Viruses

To generate the tetra-cysteine tag (Tc) in the NP segment, a flexible linker (GTGSGIR) followed by the 6 amino-acid Tc tag (CCPGCC) was inserted before the stop codon of the NP open-reading frame (-GTGSGIRCCPGCC Stop) along with duplication of the 200nt NP packaging sequence (Table II.1) (Tundup et al. 2017). The NP200 control segment contained the duplicated packaging sequence as well. Recombinant NP-Tc and NP200 viruses in the PR8 background were generated using a pDZ vector based reverse genetics system (Perez, Garćia-Sastre, and Manicassamy 2013; Manicassamy et al. 2010). NP-Tc virus stocks were generated by amplification of plaque purified virus in eggs and the presence of the desired modification in NP was confirmed by Sanger sequencing of the NP segment. Briefly, viral RNA from egg grown stock or cell supernatants was isolated using the QIAamp Viral RNA Mini Kit (Qiagen) and cDNA generated using SuperScript II Reverse Transcriptase (Invitrogen). RT-PCR products were separated on a 1% agarose gel, extracted, and sequenced.

Deep Sequencing and Bioinformatics Analysis

Genomic DNA (gDNA) was isolated from $1x10^8$ cells for the A549-GeCKO library and 4-$10x10^6$ cells for the Preliminary Consecutive Screen and the Sequential Screen, using the Blood and Cell Culture Maxi Kit or Mini Kit (Qiagen) per the manufacturer's specifications. The integrated sgRNA cassette was PCR amplified using EconoTaq DNA Polymerase (Lucigen) in two steps as previously described (Shalem et al. 2014). Briefly, the initial PCR for the A549-GeCKO library gDNA consisted of 13 separate reactions using 10µg gDNA each, and the resulting amplicons were combined. Amplification of the sgRNA cassette from the Preliminary Consecutive Screen and the Sequential Screen gDNA was performed as described with 9 separate reactions for the initial PCR. Nested PCR was then performed using 5µl of combined PCR product each in 9 separate reactions to incorporate Illumina linkers and a 1-9nt variable region. The resulting amplicons were gel extracted and combined in equivalent amounts prior to deep sequencing. PCR fragments were assessed using an Agilent 2100 Bioanalyzer and a 4nM library was applied to a standard MiSeq Flow Cell (MiSeq Reagent Kit v3) and run for 150 cycles. The occurrence of sgRNA indexes were summarized with the Bioconductor Biostrings package (PDict class) (Pages et al., Biostrings R package). Enriched genes were identified via MAGeCK, a Model-based Analysis of Genome-wide CRISPR/Cas9 Knockout method for prioritizing single-guide RNAs, genes, and pathways in genome-scale CRISPR/Cas9 knockout screens (Li et al. 2014). For the Preliminary Consecutive Screen, the A549-GeCKO library sample set was used to calculate sgRNA enrichment for Prelim Rd5 and the corresponding genes were identified as candidate hits (p-value <0.1). For the Sequential Screen, the average of the Rd1 sample set was used

to calculate sgRNA enrichment for Rd2 and Rd5, and corresponding genes were identified as candidate hits (p-value <0.05). Pairwise comparison was performed with the top hits from Rd5 of the Sequential Screen, excluding miRNAs, and the validated hits from the 9 published IAV siRNA screens (Hao et al. 2008; Brass et al. 2009; Karlas et al. 2010; König et al. 2010; Shapira et al. 2009; T. Watanabe et al. 2014; Ward et al. 2012; Su et al. 2013; Sui et al. 2009). Gene ontology analysis of hits identified in Rd2 and Rd5 of the Sequential Screen, excluding miRNAs, was performed with an R package for Reactome Pathway Analysis to identify enriched biological processes, and the gene annotations are listed in Table S3 (Yu and He 2016). For analysis, R was used to assist in the exploration and summarization of the results.

Generation of CRISPR KO and Complemented Cells

CRISPR KO A549 cell lines were generated using the lentiCRISPR v2 (#52961, Addgene) single vector system as previously described (Sanjana, Shalem, and Zhang 2014). Briefly, annealed oligonucleotides were cloned into the lentiCRISPR v2 vector via BsmBI sites. Oligonucleotide sequences for the gene specific sgRNAs are listed in Table II.2. Polyclonal CRISPR KO A549 cells were generated via lentivirus transduction of the gene specific sgRNA containing vector followed by selection with 1μg/ml puromycin for 14 days. Vector control cells were generated as above, using the lentiCRISPR v2 vector. For generation of clonal KO A549 cells, lentiCRISPR v2 transduced cells were seeded in limiting dilutions and individual clones were isolated. gDNA was extracted from monoclonal KO cells using the Blood and Cell Culture Mini kit (Qiagen) per the manufacturer's specifications, and the targeted region was PCR amplified using EconoTaq and the gene specific primers listed in Table II.2. Likewise, total RNA was

extracted from clonal KO cells using TRIzol (Invitrogen) per the manufacturer's guidelines, cDNA was generated using Superscript II reverse transcriptase (Invitrogen) and Oligo dT (Invitrogen) per the manufacturer's instructions, and the targeted region was PCR amplified using Econotaq and the gene specific primers listed in Table II.2. PCR products were cloned into pGEM-T (Promega) per the manufacturer's recommendations, and ≥ 8 clones per gene were sequenced by Sanger Sequencing. In/Dels were analyzed for each gene using SeqMan (Lasergene, DNAStar Inc) and are summarized in Table III.2.

Rab11a KO A549 cell lines were generated using two guide RNA (gRNA) targeting the promoter and exon 1 of the Rab11a gene as described above (Table II.1). A549 cells transduced with lentivirus vectors expressing gRNAs were selected in the presence of 2 μg/mL puromycin for 10 days and clonal Rab11a KOs were generated by limiting dilution of the polyclonal population. Rab11a KO were initially screened by PCR of targeted genomic region as well as by western blot analysis for Rab11a.

SLC35A1 cDNA in a lentivirus plasmid (pLX304 vector) was purchased from DNASU Plasmid Repository at Arizona State University (https://dnasu.org/). *SLC35A1* KO cells or WT A549 cells were transduced with lentivirus particles carrying GFP or *SLC35A1* cDNA and selected with 5μg/ml blasticidin for 5 days. *JAK2* cDNA was purchased from Harvard Plasmid Repository and subcloned into the pLX304 vector. *JAK2* cDNA complementation in *JAK2* KO cells was performed as described above. *Rab11a* cDNA was purchased from

Addgene and subcloned into pLX304 with an HA tag. Rab11a cDNA complementation in Rab11a KO cells was performed as described above with 2μg/mL puromycin selection.

Virus Infections

For assessment of viral replication, vector control and CRISPR KO A549 cells were seeded in triplicate at a density of $4x10^5$ cells per well in a 12-well dish, and cell numbers were measured the next day prior to infection. For IAV infections, cells were washed twice with phosphate buffered saline (PBS), placed in ~250μl of infection media (DMEM supplemented with 0.2% bovine serum albumin (BSA), 1μg/ml TPCK-treated trypsin (T1426, Sigma), and 0.01% FBS), and inoculated with ~50μl virus at the MOI indicated in the text. After incubation for 1hr at 37ºC, the inoculum was removed, and cells were washed twice with PBS and placed in 1ml of fresh infection media. For high MOI experiments, infections were performed as above with DMEM supplemented with 0.2% BSA only (without TPCK), and harvested supernatants were treated with 1μg/ml TPCK-treated trypsin prior to tittering. Supernatants were harvested at the times indicated in the text, serially diluted, and titered by plaque assay in MDCK cells. For VSV, EMCV and Zika virus, infections were performed as above with DMEM supplemented with 2% FBS, and supernatant titers were assessed as above by plaque assay in Vero cells using 1% methylcellulose. For HSV1 and ΔHSV1 viruses, infections were performed as above with DMEM supplemented with 10% FBS and 1% penicillin/streptomycin, and virus was incubated on cells for 2-3 hours. HSV1 supernatant titers were assessed as above by plaque assay for 3 days using 1.5mL 1% methylcellulose per well of a 12-well dish. For HSV1 plaque assays, Vero or U2OS cells were seeded at 75% confluency. Infection

experiments were performed with biological triplicates, data are presented as mean percentage titer of the triplicate samples relative to vector control ± SD, and are representative of at least three independent experiments. Routinely, in our infection experiments in vector control or WT A549 cells, we observe a peak viral titer of 10^6-10^7 PFU/ml (IAV), 10^8-10^9 PFU/ml (VSV), and 10^5-10^6 PFU/ml (Zika virus) at 48hpi, and 10^7-10^8 PFU/ml (EMCV) at 24hpi.

For analysis of ISG expression, vector control and clonal KO cells were seeded in triplicate at a density of $1.2x10^6$ cells per well in a 6-well dish, and cell numbers were measured the next day prior to treatment/infection. Cells were mock treated or inoculated with H1N1 (PR8) at MOI=5 in DMEM supplemented with 0.2% BSA and 1% P/S at 37ºC for 16hrs prior to RNA or protein isolation. CIC downregulation experiments were performed in WT A549 cells as described above.

For synchronized infections, cells were seeded as described above. Cells were washed twice with PBS, placed in ~750µl infection media, prechilled on ice for 15min, mock treated or inoculated with H1N1 at MOI=3 for 1hr on ice, washed twice in PBS, and placed in 2ml of fresh infection media for the indicated times at 37ºC prior to RNA isolation or RIPA lysis.

QPCR Analysis of Host Gene Expression

Total RNA was isolated from pooled triplicates using TRIzol (Invitrogen) and residual gDNA was removed with recombinant DNAse I (Roche) per the manufacturer's

recommendations. For analysis of ISG expression, cDNA was generated using Superscript II reverse transcriptase (Invitrogen) and Oligo dT (Invitrogen). qPCR was performed with technical duplicates using gene specific primers and SYBR Green PCR Master Mix (Applied Biosystems) per the manufacturer's guidelines. Delta delta cycle thresholds were calculated using tubulin as the endogenous housekeeping gene and data are represented as fold expression relative to uninfected (mock) vector control cells ± SD or H1N1 infected vector control cells ± SD. For analysis of ETV4 expression, total RNA was isolated from mock vector control or *CIC* KO2 cells, and cDNA was generated in a similar manner. qPCR was performed as detailed above and data are represented as fold expression relative to vector control cells ± SD. For CIC downregulation, cDNA was generated using Superscript III reverse transcriptase (Invitrogen) with equimolar amounts of the reverse CIC and tubulin qPCR primers. qPCR was performed as detailed above and data are represented as fold expression relative to mock treated WT A549 cells ± SD. Data are representative of at least three independent experiments.

RT and qPCR primers are as follows-

hRIG-I: forward CCTACCTACATCCTGAGCTACAT and reverse

TCTAGGGCATCCAAAAAGCCA;

hIFIT-1: forward AGTGTGGGAATACACAACCTACT and reverse

GGTCACCAGACTCCTCACATTT;

hISG15 : forward TCCTGGTGAGGAATAACAAGGG and reverse

GTCAGCCAGAACAGGTCGTC;

hMxA: forward GAAGGGCAACTCCTGACAGT and reverse

GTTTCCGAAGTGGACATCGCA;

hIFNb : forward TCTGGCACAACAGGTAGTAGGC and reverse

GAGAAGCACAACAGGAGAGCAA;

NP mRNA: forward GAGCTCTCGGACGAAAAGG and reverse

TGTCGTACTCCTCTGCATTGTC;

hTub : forward GCCTGGACCACAAGTTTGAC and reverse

TGAAATTCTGGGAGCATGAC;

hCIC-S : forward ATGTATTCGGCCCACAGGC and reverse

CACAGAGCGAGGTTCCACAT;

hCIC-L: forward TTGGTGCCCAGCAGCTATAC and reverse

CACAGAGCGAGGTTCCACAT;

hETV4: forward CATTGAGCCTGAGGAGGTCG and reverse

AAGGCCAAAGAGAAGAGGGC.

RNAseq Experiment and Analysis

Infections in vector control and CIC KO cells were performed as above for analysis of ISG expression. Briefly, cells were infected with PR8 at MOI=5 for 16hours. RNA extraction was performed as above for “QPCR Analysis of Host Gene Expression.” The tenOever lab at the Icahn School of Medicine at Mount Sinai, NY prepared the cDNA library using TruSeq RNA Library Prep Kit v2 (Illumina) and performed deep sequencing using NextSeq 500 sequencer (Illumina). Dr. Lei Huang at the Center for Research Informatics, The University of Chicago, IL analyzed the data and performed gene expression profiling.

Briefly, reads were assessed for quality control (FastQC) and analyzed by both alignment-based and alignment-free methods mostly using R/Bioconductor packages. In the alignment-based pipeline, reads were aligned by reference (STAR), gene expression was quantified (featureCounts), post-alignment reads were quality controlled (Picard, multiQC). In the alignment-free pipeline, reads were estimated for transcript abundance (Kallisto), gene expression was quantified (tximport), and differentially-expressed genes (DEGs) were assessed (Limma-voom). Function (IPA, clusterProfiler) and gene set enrichment (EGSEA) analyses were performed for DEGs.

Primary Transcription and Early Replication Assays

For measurement of viral NP expression during primary transcription, vector control or clonal KO cells were pretreated with ~750µl infection media containing 100µg/ml cycloheximide (MP Biomedicals) for 1hr at 37ºC, synchronized infections were performed as described above, and RNA was isolated at 3hpi. For measurement of viral NP expression during early replication, synchronized infections were performed as described above (without cycloheximide treatment) and RNA was isolated at 6hpi. Total RNA from pooled triplicates was used to generate cDNA with Superscript II reverse transcriptase. For NP mRNA and tubulin levels, reverse transcription was performed with Oligo dT; for NP vRNA and tubulin levels, reverse transcription was performed with equimolar amounts of the reverse NP vRNA and tubulin qPCR primers. qPCR was performed as above and data are represented as percent expression relative to H1N1 infected vector control cells ± SD. Data are representative of at least three independent experiments. Additional qPCR primers are as follows - NP vRNA: forward TTGTCCTCTGATAAGTTGCATCA and reverse ATGACAAAGAAGAAATAAGGCGAATC.

Western Blot Analysis

Whole cell extracts from pooled triplicates were lysed using RIPA buffer containing protease inhibitors and western blot analysis was performed with ~80ug of total protein. Confirmation of gene KO was performed in untreated vector control and clonal KO cells. CIC degradation analysis was carried out in vector control and *CIC* KO2 cells and synchronized infections were performed as described above. Antibodies used for western blot analysis are as follows – JAK2 (#3230T) and MxA (#37849) from Cell Signaling Technologies; β-actin (#A5316) and Ku (#K2882) from Sigma; RIG-I (1C3 clone) (Nistal-Villan et al. 2010); ISG56 or IFIT1 (#PA3-848) from Thermo Scientific, CIC and ATXN1L (Kim et al. 2015).

VLP Entry Assay

The beta-lactamase-M1 (Bla-M1) based VLP assay was performed as previously described (Tscherne, Manicassamy, and García-Sastre 2010). Briefly, VLPs were produced by co-transfecting HEK293s with 3µg Bla-M1 along with 0.5µg pCAGGS-HA and 0.5µg pCAGGS-NA (Flu VLP, VN04 strain, or with 0.5µg pCMV-VSV-G (#8454, Addgene) using 6µl of Lipofectamine 2000 in OptiMEM (Steel et al. 2009). VLPs produced from HEK293 cells transfected with Bla-M1 alone were used as negative controls. At 6hrs post transfection, cells were placed in OptiMEM supplemented with 0.2% BSA, 1µg/ml TPCK-treated trypsin, and 0.01% FBS. At 72hrs post transfection, supernatants were collected and clarified of debris by centrifugation at 3,000rpm for 10min. Vector control and clonal KO cells were seeded in duplicate at a density of $8x10^4$ cells per well in a 24-

well dish the day before infection. For VLP infection, media was removed from cells and replaced with 0.5ml of cleared VLP supernatant, cells were spinoculated by centrifugation at 2,000rpm for 90min at 4ºC, and cells were transferred to 37ºC for an additional 3hrs. VLP entry levels were measured by flow cytometry of duplicate samples loaded with fluorogenic beta-lactamase substrate CCF4-AM (Invitrogen) according to the manufacturer's protocol. Data analysis was performed using FlowJo Software and data are represented as percentage of vector control cells ± SD.

Lectin and HA Binding Assays

Biotinylated Sambucus Nigra (SNA) and Maackia Amurensis Lectin II (MAL) lectins were purchased from Vector Biolabs. Vector control and *SLC35A1* KO cells were fixed with 4% formaldehyde for 10min, washed with PBS twice and incubated with 20µg/ml biotinylated lectin for 1hr on ice, followed by staining with 1µg/ml Streptavidin conjugated to Brilliant Violet 605 (BioLegend). The levels of lectin binding were visualized using a confocal microscope, or analyzed by a BD LSRII flow cytometer. Cell surface binding of HA was performed with purified H5 HA protein (BEI Resources). Briefly, cells were incubated with 5µg of HA on ice for 1hr and the unbound protein was removed by PBS/BSA washes. Cells were fixed with 4% formaldehyde for 10min and washed with PBS/BSA. The amount of bound HA was measured using cell surface staining for HA with an anti-H5 mouse sera followed by a secondary antibody conjugated to Alexa-647, and analyzed by flow cytometry on a BD LSRII instrument. Data analysis was performed using FlowJo Software.

Treatment with 3F-Neu5Ac

3Fax-Peracetyl Neu5Ac (3F-Neu5Ac) was purchased from Millipore. WT A549 cells were treated with DMSO or 200μM 3F-Neu5Ac for a period of 10 days to eliminate residual sialic acid from the cell surface. Lectin binding analysis was performed as described above. Viral infections were performed at an MOI=0.1 and viral titers in the supernatants at 18hpi were assessed by plaque assay as described above.

Mini-Genome Assay

The mini-genome assay was performed by transfecting 0.5 μg each of pDZ WT NP or modified NP with pCAGGS PB1, PB2, and PA of A/WSN/1933 (WSN, H1N1), and a pPolI-Luc (NP gene) reporter into HEK293T cells using polyethylenimine reagent (PEI, MP Biomedicals) at a ratio of 1:5 (DNA:PEI). Forty-eight hours after transfection, cells were lysed with 1x lysis buffer (GoldBio) and supernatant luminescence was analyzed using the Illumination Firefly and Renilla Luciferase Enhanced Assay Kit (GoldBio).

Antiviral Promoter Reporter Assay

Fragments containing ~3kb of the promoters for the antiviral genes *IFIT1* and *MxA* were PCR amplified and cloned into the pXPG vector (Addgene #71248) using hIFIT1: forward GATCCAAGCTCAGATCTCGAGTGGATATTTGAGACCCTTCAGCA and reverse CAGTACCGGAATGCCAAGCTTACATTATGGCAGAGGAGCAAAGA, and hMxA: forward GATCCAAGCTCAGATCTCGAGTTCAGGATCATGAGAACAGCACA and reverse CAGTACCGGAATGCCAAGCTTCTCCTTCCACCTAACGAGAAACA primers. CIC mediated repression of antiviral genes was measured by transfecting

HEK293s with polyethylenimine reagent (PEI, 1:5 DNA:PEI ratio) and a plasmid mixture containing pXPG reporter (100ng, with *MXA* or *IFIT1* promoter) RIG-I-2CARD (50ng), CIC-S (50-150ng), ATXN1 (25-75ng), and SV40 Renilla (50ng). GFP expressing plasmid was included in place of RIG-I-2CARD or CIC/ATXN1 plasmids in the control samples. At 48hrs post-transfection, transfected cells were subjected to lysis in 1x Passive Lysis Buffer (GoldBio). Firefly and Renilla luciferase values were measured using the Illumination Firefly and Renilla Luciferase Enhanced Assay Kit (GoldBio). Data are represented as percent luciferase activity relative to GFP + RIG-I-2CARD transfected control $\pm$ SD. Data are representative of at least three independent experiments. The RIG-I-2CARD plasmid was provided by Dr. Adolfo Garcia-Sastre. The CIC-S expression plasmid was kindly provided by Dr. Carol MacKintosh through the MRC Protein Phosphorylation and Ubiquitylation Unit at the University of Dundee, and was sub-cloned into the pCAGGS vector. The ATXN1 expression plasmid was obtained from Dr. Huda Zoghbi through Addgene (#48189).

RNAi-mediated Knockdown Assays

50nM siRNA targeting host genes (Dharmacon), siControl (irrelevant sequence, Dharmacon and Sigma), and siNP targeting the NP gene of IAV (Sigma) were transfected into A549s using RNAiMAX (Invitrogen). 24 hours post transfection, cells were infected with PR8 at MOI 0.1-0.01 for 48 hours. The siRNA mini-screen was performed in 24-well dishes seeded at $6x10^4$ cells/well. siCIC experiments were performed in 12-well dishes seeded at $1.5x10^5$ cells/well.

Estimation of Defective Particles

PFU to HAU ratio: The amount of virus particles in the supernatants were measured by standard hemagglutinin (HA) assay with serial dilution of cell supernatants in 0.5% chicken red blood cells (RBC). HA units were determined by the highest dilution of virus supernatant positive for RBC agglutination. The levels of infectious particles were determined by plaque assay in MDCK cells as described above. The PFU/ml to HAU/ml ratio was calculated for three replicates and two independent experiments.

Viral RNA copy number to PFU ratio: Viral RNA was isolated from the supernatant using the QIAamp Viral RNA Mini Kit (Qiagen) and viral cDNA was generated using the universal F(A) influenza primer and the Maxima Reverse Transcriptase (Thermo Scientific). RNA Copy Number was quantified by Droplet Digital qPCR (Bio-Rad) of viral cDNA to determine RNA Copy Number/ml for three segments (M, NS, and NA), using sequence specific primers. The RNA Copy Number/ml to PFU/ml ratio was calculated for three replicates and two independent experiments.

FlAsH, Antibody, and FISH Staining and Microscopy Preparation

FlAsH staining: A549 cells were seeded onto coverslips at $1x10^5$ cells/well in 24-well dishes one day prior to infection. Infections were performed as described above, in Opti-Modified Eagle Medium (OMEM). FlAsH staining of cells was started approximately 1hr prior to indicated time points by incubating cells in FlAsH staining solution consisting of 1-1.5 μM FlAsH (Invitrogen) and 10 μM 1,2-ethanedithiol (diluted in DMSO, Sigma) in OMEM at 37°C for 30 min. After incubation, A549 cells were washed once gently with

prewarmed PBS and incubated twice with prewarmed wash buffer (500 μM 1,2-ethanedithiol diluted in DMSO and 1x 2,3-dimercapto-1-propanol (Sigma) in OMEM), each for 7 min at 37°C. Cells were washed once gently with PBS and fixed with 4% Paraformaldehyde (Electron Microscopy Sciences) in PBS for 5 min at room temperature.

Antibody staining: Fixed cells on coverslips were permeabilized with 0.1% Triton X-100 (Sigma) in PBS for 15 min followed by washing in PBS and incubation in a blocking buffer consisting of 1% BSA, 0.5% fish gelatin (Sigma), and 0.01% Tween20 (Sigma) in PBS for 30 min. Permeabilized cells were incubated in primary antibodies diluted in blocking buffer for 1hr (1:1000 PR8 NP polyclonal, gift from Dr. Adolfo Garcia-Sastre; 1:1000 γ-tubulin DQ-19, #T3195 Sigma; 1:1000 α-tubulin, #T6199 Sigma; and 1:250 Rab11a, #715300 Invitrogen) followed by three washes with PBS. Subsequently, cells were incubated with secondary antibodies diluted in blocking buffer for 45 min (1:1000 Alexa-fluor 546 conjugated to mouse or rabbit, Invitrogen) followed by three PBS washes. Coverslips were mounted onto slides using ProLong Gold Antifade Mountant with DAPI (Invitrogen). All incubations involving antibody staining were performed with gentle shaking at room temperature.

FISH staining: Fixed cells on coverslips were permeabilized with 0.05% Triton X-100 in 5mM $MgCl_2$-supplemented PBS (PBSM) for 1 min at room temperature. Cells were incubated in RNA wash buffer (10% formamide [Sigma] in 2xSSC [300mM sodium chloride, 30mM sodium citrate]) for 10min at room temperature. To hybridize FISH probes to cells on coverslips, 40 μL of 10 μM FISH probes in hybridization buffer (10% dextran

sulfate [Sigma], 2mM vanadyl ribonucleoside complexes [#514025, NEB], 0.02% RNAse-free BSA [NEB], 50 μg E.coli tRNA [#10706636, Roche], 10% formamide [Sigma], and 2xSSC) was applied as a droplet onto parafilm. Coverslips were inverted on top of the droplet and this complex was placed in a humidified chamber for 16 hours at 37°C. Coverslips were washed twice, each for 30 min at 37°C without shaking, in RNA wash buffer supplemented with 2mM vanadyl ribonucleoside complexes. Coverslips were mounted onto slides using ProLong Gold Antifade Mountant with DAPI (Invitrogen). Sequences for FISH probes are provided in Table II.3 and II.4 and were generated by LGC Biosearch Technologies.

Imaging was performed at the Integrated Light Microscopy Core Facility at the University of Chicago. The Olympus DSU Spinning Disc confocal microscope was used for general fluorescence imaging. The Leica SP8 3D 3-color Gated Superresolution confocal microscope was used for fluorescence imaging involving FISH probes.

Nocodazole Treatment

A549 cells were seeded and infected as described above. Two hours after initiation of infection, media was replaced with 30 μM Nocodazole (diluted in DMSO, #M1404, Sigma) or the equivalent volume of DMSO in OMEM. FlAsH staining was performed in 30 μM Nocodazole or the equivalent volume of DMSO in OMEM.

Statistical Analysis

Statistical significance was determined by two-tailed unpaired Student's t test, and p-values ≤ 0.05 are considered significant and denoted with an asterisk. Non-significant values are denoted as ns.

CHAPTER III

Genome-wide CRISPR/Cas9 Screen Identifies Host Factors Imperative for Influenza Virus Replication

This chapter is adapted from the published manuscript 'Genome-wide CRISPR/Cas9 Screen Identifies Host Factors Essential for Influenza Virus Replication' (Han et al. 2018). Julianna Han either partially or completely performed all of the experiments in this chapter except for the bioinformatics analysis of the deep sequencing data from the CRISPR screen. Please access the published manuscript from which this chapter is modified in order to locate the large supplementary tables.

INTRODUCTION

Influenza A virus (IAV) is an upper respiratory pathogen in humans with the ability to rapidly evolve, resulting in both seasonal epidemics and occasional pandemics (Shaw and Palese 2013). As the constant emergence of variant and drug resistant strains greatly reduce the efficacy of current vaccines and therapies, there remains a need for host-directed therapeutics against IAV. Multiple genome-wide screening approaches, including siRNA, proteomic, and insertional mutagenesis screens, have been employed to identify host factors involved in IAV infection (Hao et al. 2008; Brass et al. 2009; Karlas et al. 2010; König et al. 2010; Ward et al. 2012; Su et al. 2013; Shapira et al. 2009; Sui et al. 2009; T. Watanabe et al. 2014; Benitez et al. 2015). Although some common hits and pathways were revealed, most notably members of the vacuolar ATPase family,

meta-analyses demonstrated liitle overlap in the identified IAV host factors, likely due to differences in the strains used, time points assayed, and functional readouts chosen (Mehle and Doudna 2010; Stertz and Shaw 2011; T. Watanabe, Watanabe, and Kawaoka 2010). Therefore, alternative screening strategies will provide the flexibility needed to uncover host factors and pathways, as well as validate previously identified hits, to serve as potential targets for the development of anti-influenza therapeutics.

Recent advancements in CRISPR/Cas9 technology (clustered regularly interspaced short palindromic repeat (CRISPR) and CRISPR associated nuclease Cas9) have allowed for gene disruption on a genome-wide scale in mammalian cells (Shalem et al. 2014; T. Wang et al. 2014; Wright, Nunez, and Doudna 2016). Recently, the GeCKO (genome-wide CRISPR knockout) screening strategy has been utilized to investigate virus-host interactions (H. Ma et al. 2015; Marceau et al. 2016; Savidis et al. 2016; R. J. Park et al. 2017; Orchard et al. 2016; Zhang et al. 2016). Here, we generated a GeCKO library in human lung epithelial (A549) cells negatively selected against genes essential for cell viability, and subjected this A549-GeCKO library to five rounds of lethal infection with a human isolate of an avian IAV strain. Deep sequencing analysis of the enriched sgRNA population identified numerous genes involved in the sialic acid biosynthesis and glycosylation pathways, as well as in the regulation of cell intrinsic immunity. Validation studies revealed host factors critical for multiple IAV strains that function at different stages of viral replication, including entry and antiviral responses. Loss of *SLC35A1*, a CMP-sialic acid transporter, rendered cells resistant to IAV infection due to the absence of cell surface sialic acids. Furthermore, GeCKO screening identified capicua (CIC), a

DNA-binding transcriptional repressor, as a negative regulator of cell intrinsic immunity. Loss of *CIC* resulted in upregulation of antiviral responses and restricted replication of viruses from diverse families. Taken together, our studies demonstrate that GeCKO screening is a versatile strategy that can be utilized to identify host factors critical for IAV replication.

RESULTS

Generation of an A549-GeCKO Library

To identify host genes critical for IAV replication, we generated a GeCKO library in A549 cells as previously described and performed a genome-scale loss-of-function genetic screen (Shalem et al. 2014; T. Wang et al. 2014; Zhang et al. 2016). First, we derived a clonal Cas9-expressing A549 cell line (Cas9-A549s) by transducing wild type (WT) A549 cells with lentivirus expressing the Cas9 gene (Figure III.1A, Step 1). Next, Cas9-A549s were transduced with lentivirus containing a pooled human genome-wide sgRNA library (Library A) of 65,383 sgRNAs targeting 19,050 protein-coding genes and 1,864 microRNA (miRNA) precursors, and selected in puromycin for 14 days (Figure III.1A, Steps 2-4) (Sanjana, Shalem, and Zhang 2014; Shalem et al. 2014). To evaluate sgRNA diversity in the A549-GeCKO library, the integrated sgRNA cassettes were PCR amplified from genomic DNA and subjected to Illumina sequencing. Analysis of the 9M reads obtained from $1x10^8$ cells revealed the presence of 62,659 sgRNAs ($\geq$10 reads) in the A549-GeCKO library, representing an average coverage of ~140x per sgRNA (Figure III.2A-B). The loss of ~4.2% of sgRNAs post puromycin selection likely suggests the negative

selection of a non-viable cell population. Thus, we successfully generated a pooled GeCKO library in A549 cells with sufficient coverage to perform genetic screens for IAV host factors.

Preliminary Screen for Positive Selection of H5N1 Resistant Cells in the A549-GeCKO Library

To enrich for a cell population resistant to IAV replication, we subjected the A549-GeCKO library to lethal infection with a human isolate of a low pathogenic avian H5N1 virus (A/Vietnam/1203/04, $VN04_{Low}$; Figure III.1A, Steps 5-7). For our preliminary GeCKO screen, we performed 5 consecutive rounds (Rd) of lethal infection with minimal expansion of cells between rounds (Preliminary Consecutive Screen); the resistant cells were subsequently expanded and sgRNA distribution was assessed by Illumina sequencing (Prelim Rd5; Figure III.1A, Steps 8a-9). For the 8M Illumina reads obtained from Prelim Rd5, we observed robust enrichment of 586 sgRNAs (≥10 reads) representing ~1% of the sgRNAs present in the A549-GeCKO library (Figures III.2A and C). Next, candidate genes were identified and ranked using the Model-based Analysis of Genome-wide CRISPR/Cas9 Knockout (MAGeCK) program (Li et al. 2014). We observed positive selection of 119 genes in Prelim Rd5 ($p<0.1$), with the *SLC35A1* gene (sialic acid transporter) ranked highest and demonstrating representation by all 3 independent sgRNAs (Table S1). Interestingly, the remaining genes showed enrichment for a single sgRNA, likely due to the stringent selection achieved by performing five consecutive rounds of lethal infection with minimal expansion of cells between rounds. Together, our

preliminary screen identified potential host factors whose loss rendered cells highly resistant to H5N1 infection.

Analysis of sgRNA Enrichment during Sequential H5N1 Selection

We next performed a less stringent GeCKO screen by allowing for substantial expansion of surviving cells between each round of H5N1 selection (Sequential Screen; Figure III.1A, Steps 8b-9). This would allow us to determine if progressive enrichment of sgRNAs occurs at each round of selection, such that genes critical for H5N1 replication are represented by multiple sgRNAs in the earlier rounds. We assessed sgRNA representation at each round of infection in duplicate sample sets up to 5 rounds. Comparative analysis of sgRNA representation between the A549-GeCKO library and Rd1 of the Sequential Screen showed no significant differences (Figure III.1B; Figure III.2A). In contrast, we observed robust enrichment of specific sgRNAs at Rd2, with a progressive increase in enrichment occurring between Rd2-5. These data indicate that selection of a cell population less permissive to H5N1 occurs after two rounds of lethal infection.

Next, we performed principle component analysis (PCA) and Pearson correlation analysis to understand the sgRNA distribution pattern between biological replicates in the Sequential Screen. The sgRNA distribution profile of Replicate one (Rep1, red) and Replicate two (Rep2, blue) at Rd1 clustered together and remained close to the A549-GeCKO library; however, in subsequent rounds (Rd2 to Rd5), the samples belonging to each replicate closely clustered within their respective groups, indicating divergence of

replicates after Rd2 (Figure III.2D). Similarly, comparison of individual sample sets showed strong correlation of sgRNA distribution between Rep1 and Rep2 at Rd1, with a correlation coefficient value of 0.92; however, the correlation coefficient value decreased to $\leq$0.25 in subsequent rounds (Figure III.2E). Although replicate divergence occurred at Rd2, we observed enrichment of specific sgRNAs common in both replicates (Table S1). Taken together, these results demonstrate that the robust enrichment seen at Rd2 of the Sequential Screen occurred concurrently with replicate divergence, yet revealed the progressive enrichment of a common sgRNA population between replicates.

Identification of Genes Enriched during Sequential H5N1 Selection

Next, we performed MAGeCK analysis to identify positively selected genes at Rd2 and Rd5 of the Sequential Screen (Table S1). We observed enrichment of 798 genes ($p<0.05$) at Rd2, with 161 genes represented by two or more sgRNAs and 637 genes represented by a single sgRNA (Figure III.1C). However, we observed enrichment of 501 genes ($p<0.05$) at Rd5, with only 16 genes represented by two or more sgRNAs, and 485 genes represented by a single sgRNA. This decrease in the number of genes represented by multiple sgRNAs between Rd2 and Rd5 suggests that stringent H5N1 selection results in the preferential enrichment of individual sgRNAs. To further evaluate the genes identified at Rd5, we compared our hits to factors identified in the nine previously reported genome-wide screens for influenza virus (Hao et al. 2008; Brass et al. 2009; Karlas et al. 2010; König et al. 2010; Ward et al. 2012; Su et al. 2013; Shapira et al. 2009; Sui et al. 2009; T. Watanabe et al. 2014). Comparative analyses of the hits identified at Rd5 ($p<0.05$), excluding miRNAs, indicated that 33 of the 453 hits were also identified in previous

screens (Figure III.1D; Table S2). Vacuolar ATPase family members, which were highly represented in six of the prior screens, were also highly enriched in the Sequential Screen (*ATP6AP1, ATP6AP2, ATP6V0A1, ATP6V0B, ATP6V0C, ATP6V1B2, ATP6V1G1, ATP6V1H*) (Stertz and Shaw 2011; Mehle and Doudna 2010; T. Watanabe, Watanabe, and Kawaoka 2010). In addition, we identified >400 unique genes, demonstrating that GeCKO screening can reveal previously unidentified IAV host factors.

Next, we used the R package for Reactome Pathway Analysis to identify enriched biological processes, and determined that 117 genes from Rd2 and 133 genes from Rd5 ($p<0.05$) mapped to known biological processes (Figure III.1E; Table S3) (Yu and He 2016). We observed enrichment for genes involved in proton transport and vacuolar acidification, which were represented in the prior genome-wide screens for influenza virus (Figure III.1D; Table S2). We also observed enrichment for genes involved in sialic acid biosynthesis, protein glycan modification, and GPI-anchor synthesis, as well as genes involved in intracellular signaling pathways, regulation of cell intrinsic immunity, and autophagy. Therefore, the GeCKO screening confirmed previously described processes such as vacuolar acidification as well as highlighted other processes including sialic acid biosynthesis and glycan modification that are important for IAV replication.

Confirmation of Top Hits via Individual Gene KO

To prioritize the candidate host factors for further validation, we identified the common genes in the Sequential (Rd5) vs. Consecutive (Prelim Rd5) Screens (Figure III.3A; Table S4). Of the 63 genes in common, we selected 11 highly enriched candidates representing

various biological processes for the generation of individual CRISPR KO cell lines (Table III.1). Eight hits (*SLC35A1, GDF11, IRX3, C2CD4C, TRIM23, PIGN, ACADSB,* and *GRAMD2*) were also highly enriched ($p<0.05$) in the early rounds of selection (Rd2), and the remaining three hits (*CIC, JAK2,* and *PIAS3*) demonstrated enrichment only after multiple rounds of selection (Figure III.4). To determine if these candidate genes are important for IAV replication, the 11 generated polyclonal KOs were infected with H5N1 at a low multiplicity of infection (MOI). A >60% reduction in viral titer was observed in eight KOs as compared to vector control cells, demonstrating that GeCKO screening was successful in identifying H5N1 host factors in A549 cells (Figure III.3B).

As we anticipated incomplete disruption of target gene loci in the polyclonal population, we next generated seven clonal KOs for a subset of host factors. Sequence analysis of the sgRNA target sites in the clonal KOs indicated that complete gene disruption was achieved in all but the *CIC* KOs, which contained a WT allele (Table III.2). We evaluated H5N1 replication in the clonal KOs, and observed an ~5 log reduction in viral titer in *SLC35A1* and *CIC* KOs, as well as a >80% reduction in viral titer in the remaining KOs as compared to vector control cells (Figure III.3C). The robust reduction in H5N1 titer observed in the clonal KOs as compared to their respective polyclonal populations suggests that complete gene disruption was required for the validation of candidate host factors. To exclude the possibility of off-target effects in the clonal KOs, we analyzed the sgRNA sequences for potential complementarity in the exons of the human genome (Table S6). A minimum of 3-4 mismatches were required for identification of potential off-target genes, the majority of which were not enriched at Rd2 and Rd5 of the Sequential

Screen ($p<0.05$). As the seven evaluated clonal KOs demonstrated robust reduction in H5N1 viral titer as well as limited potential for off-target effects, we have thus confirmed that these hits are important for H5N1 replication.

Validation of Hits with Multiple IAV Strains

To determine if the validated host factors are required for the replication of multiple IAV strains, we infected the clonal KOs with H1N1 (A/Puerto Rico/8/1934; PR8) and H3N2 (A/Hong Kong/1/1968; HK68) at a low MOI. We observed a >5 log reduction in viral titer in *SLC35A1* KOs and a >3 log reduction in viral titer in *CIC* KOs as compared to vector control cells (Figure III.3C). Interestingly, *PIAS3* KOs demonstrated strain specificity, as a >80% reduction in viral titer was observed for H1N1 and H5N1, yet H3N2 replication was unaffected. The remaining clonal KOs showed a >60% reduction in viral titers for both H1N1 and H3N2, demonstrating that the identified host factors are important for efficient replication of multiple IAV strains.

To distinguish between IAV-specific host factors and those that function in a pan-proviral manner, we assayed the replication of vesicular stomatitis virus (VSV) in the clonal KOs. VSV replication was unaffected in *SLC35A1* and *PIGN* KOs; however, we observed a >2 log reduction in viral titer in *CIC* KOs and a $\geq$50% reduction in viral titer in the remaining KOs (Figure III.3C). Taken together, these data suggest that SLC35A1 and PIGN are IAV specific host factors, whereas C2CD4C, TRIM23, CIC, JAK2, and PIAS3 may function in a pan-proviral manner to support viral replication.

Identification of Viral Life Cycle Defects in Clonal KO Cells

To elucidate the mechanism by which the identified host factors contribute to IAV replication, we evaluated various stages of the viral life cycle in a subset of clonal KOs. First, to identify host factors that are critical for a single IAV infection cycle, we performed synchronized infections at a high MOI with H5N1. We observed an ~1-2 log reduction in viral titer in *SLC35A1 and CIC* KOs as compared to vector control cells, indicating that loss of these host factors resulted in inefficient establishment or completion of the viral life cycle (Figure III.5A). In contrast, the remaining clonal KOs displayed only modest differences in viral titer, suggesting that the defects observed at a low MOI were due to the cumulative effects of multiple replication cycles.

Next, we utilized beta-lactamase carrying influenza virus-like particles (Flu VLPs) to measure the ability of the clonal KOs to support virion entry and/or fusion, in comparison to VSV glycoprotein (VSV-G) VLPs (Tscherne, Manicassamy, and García-Sastre 2010). *SLC35A1* KOs showed robust restriction of IAV entry and/or fusion, as only ~3.6% of cells were positive for Flu VLP infection (Figure III.5B). In addition, only 25% of *PIAS3* KOs were positive for Flu VLP infection, suggesting a role for PIAS3 in IAV entry and/or fusion. In contrast, no defects in Flu VLP infection were observed for the remaining KOs, and VSV-G VLP infection was largely unaffected in all of the tested KOs. These results demonstrate that SLC35A1 and PIAS3 play a critical role in the entry and/or fusion stage of the IAV life cycle.

To determine if the remaining host factors are required at a post-fusion stage of the IAV life cycle, we measured primary viral transcription and viral genome replication of H1N1 in the clonal KOs. At 3hpi, primary nucleoprotein (NP) transcript (NP mRNA) and input viral genomic NP RNA (NP vRNA) levels were measured by qRT-PCR. As *SLC35A1* KOs demonstrated defects in viral entry and/or fusion, we observed low levels of input NP vRNA and consequently low levels of NP transcription as compared to vector control cells (Figure III.5C). Interestingly, NP mRNA levels were reduced >90% in *CIC* KOs as compared to vector control cells, despite displaying similar levels of input NP vRNA. Next, we assessed the clonal KOs for defects in viral genome replication at 6hpi by qRT-PCR. In *CIC* KOs, we observed an ~80% reduction in both NP vRNA and mRNA as compared to vector control cells, indicating that the observed reduction in primary transcription impaired subsequent genome replication. Thus, *CIC* KOs demonstrate a defect in IAV replication at a stage between post-fusion and primary transcription.

As dysregulation of cell intrinsic immunity may inhibit IAV replication, we evaluated the expression of antiviral genes by qRT-PCR under basal (mock) and H1N1 infected conditions. *CIC and JAK2* KOs demonstrated an increase in antiviral gene expression (>2 fold) for both mock and H1N1 infected conditions as compared to vector control cells (Figure III.5D-E; Figure III.6A). Interestingly, in comparison to vector control cells, *PIAS3* KOs displayed higher antiviral gene expression only upon IAV infection. To further validate our findings, we confirmed the loss of JAK2 protein expression in *JAK2* KOs by western blot analysis (Figure III.6B). In addition, we complemented *JAK2* KOs with cDNA expressing *JAK2* and observed increased viral replication (≥1 log) as compared to GFP

expressing *JAK2* KOs, indicating that only loss of the *JAK2* gene resulted in the observed viral replication defects in *JAK2* KOs (Figure III.6C). These data demonstrate that *CIC, JAK2*, and *PIAS3* KOs display dysregulated antiviral gene expression. Taken together, our studies show that *SCL35A1* KOs display defects in viral entry and/or fusion and *CIC* KOs demonstrate restriction of IAV replication between post-fusion and primary transcription as well as dysregulation of antiviral gene expression.

SLC35A1 is Required for IAV Entry

IAV infection of a host cell is initiated by the binding of viral HA to sialic acid moieties, which are terminal sugars on glycans (Figure III.7A). In our GeCKO screen, we observed enrichment of host factors involved in sialic acid biosynthesis (*GNE, CMAS*), transport (*SLC35A1, SCL35A2*), glycan modification/processing (*DPM2, ALG3, ALG4, ALG12, GANAB, A4GALT, B3GAT1, B4GALNT4, CHSY1, CSGALNACT2, HS3ST6*) and GPI-anchor synthesis (*PIGN, DPM2*) (Figure III.7A; Figure III.8A). Of these host factors, *SLC35A1* was the highest enriched gene and was represented by 3 independent sgRNAs (Figure III.4). As SLC35A1 is a CMP-sialic acid (CMP-Neu5Ac) transporter, we hypothesized that *SLC35A1* KOs lack cell surface sialic acids (Hadley et al. 2014). To this end, we used specific lectins to detect 2'-3' (Maackia amurensis lectin - MAL) or 2'-6' (Sambucus nigra lectin - SNA) linked sialic acid on the cell surface. Flow cytometry and confocal microscopy analyses of *SLC35A1* KOs showed a lack of binding for both types of lectins as compared to vector control cells, indicating the loss of cell surface sialic acid in the absence of *SLC35A1* (Figure III.7B-C). Next, we evaluated the efficiency of recombinant HA (H5) binding. *SLC35A1* KOs were unable to support HA binding as

compared to vector control cells, indicating that the reduced susceptibility of *SLC35A1* KOs was due to inefficient binding of IAV particles to the cell surface (Figure III.7D).

As there are currently no inhibitors available against SLC35A1, we sought to determine if inhibition of downstream sialyltransferases with 3Fax-Peracetyl Neu5Ac (3F-Neu5Ac), a CMP-Neu5Ac analog, would inhibit IAV replication (Rillahan et al. 2012). Treatment of WT A549 cells with 3F-Neu5Ac resulted in robust restriction of H1N1 and H3N2 replication as compared to DMSO treated cells (Figure III.7E). Interestingly, H5N1 replication was unaltered in 3F-Neu5Ac treated cells, despite displaying almost complete loss of lectin binding (Figure III.7F). To exclude the possibility of other defects that may result in the restriction of IAV infection in *SLC35A1* KOs, we complemented *SLC35A1* KOs with cDNA expressing *SLC35A1*. We observed increased IAV replication in complemented *SLC35A1* KOs, yet observed no differences in VSV replication (Figure III.7G). In addition, expression of *SLC35A1* in WT A549 cells did not alter IAV replication (Figure III.8B). These studies demonstrate that SLC35A1 facilitates incorporation of sialic acid moieties onto cell surface proteins, and thus is an essential host factor for IAV entry. Taken together, GeCKO screening has identified numerous host factors involved in IAV processes, including SLC35A1, a crucial component of receptor surface expression.

DISCUSSION

Here, we performed a GECKO screen using a human isolate of an avian H5N1 strain and identified host factors critical for IAV entry and regulation of cell intrinsic immunity. Cells

lacking the sialic acid transporter *SLC35A1* were highly enriched post H5N1 selection, as they were deficient in the viral receptor and thus were incapable of supporting HA binding. sgRNAs targeting several genes involved in sialic acid biosynthesis and related glycosylation pathways were also enriched during H5N1 selection. In addition, we identified *CIC*, a DNA-binding transcriptional repressor, as a key regulator of cell intrinsic immunity. *CIC* deficient cells demonstrated upregulated antiviral gene expression and decreased replication of multiple viruses. Taken together, GeCKO screening can be a powerful tool to discover host factors and to highlight biological pathways essential for the replication of intracellular pathogens.

For this study, we employed a pooled GeCKO approach, relying upon gene disruption and stringent selection to enrich for a cell population resistant to IAV infection. As opposed to siRNA based screening, it has been reported that cell survival based GeCKO screens for viral host factors predominantly reveal hits that support early steps of viral replication (Perreira, Meraner, and Brass 2016; Savidis et al. 2016). Similarly, we observed robust enrichment of host factors important for sialic acid (IAV receptor) expression as well as vacuolar acidification and endocytosis (Figure III.1E; Table S3). Of these identified entry factors, several members of the vacuolar ATPase family were previously identified in multiple siRNA screens (Figure III.1D; Table S2). Interestingly, *SLC35A1* was identified in only one of the prior siRNA screens, and knockdown demonstrated an ~50% decrease in H1N1 (PR8) infection (Brass et al. 2009). In this GeCKO screen, *SLC35A1* was the highest enriched hit and gene knockout displayed an ~5 log decrease in viral replication for multiple IAV strains (Figure III.3C). In addition, several host factors critical for sialic

acid biosynthesis and related glycosylation pathways were uniquely enriched in this GeCKO screen (Figure III.7A; Figure III.8A) (de Vries et al. 2012; Chu and Whittaker 2004). In agreement, a survival based haploid screen for Enterovirus D68, which also utilizes sialic acid as an entry receptor, showed enrichment of host factors necessary for cell surface sialic acid expression (Baggen et al. 2016). Thus, survival based GeCKO screening allows for the identification of host factors critical for the early steps of viral replication.

In addition to the identification of viral entry host factors, GeCKO screening revealed factors important for the regulation of cell intrinsic immunity. In our validation studies, we observed higher levels of antiviral gene expression in *CIC, JAK2,* and *PIAS3* KOs (Figure III.5D-E); however, loss of these host factors impacted different steps of the IAV life cycle (Figure III.5A-C). *JAK2* was previously identified in one of the siRNA screens and implicated in IAV entry (König et al. 2010). However, in *JAK2* KOs, we observed no defects in Flu VLP entry, yet genome replication was decreased at 6hpi. It is possible that increased antiviral gene expression may suppress IAV genome replication in *JAK2* KOs. In another study, JAK2 was implicated in the intracellular localization of the viral M1 protein through tyrosine phosphorylation (König et al. 2010; S. Wang et al. 2013). Therefore, further studies are necessary to delineate the role of JAK2 in IAV replication. In *PIAS3* KOs, we observed increased antiviral gene expression only upon IAV infection, as well as defects in Flu VLP entry and primary transcription. Interestingly, PIAS3, an E3 SUMO ligase, has been shown to SUMOylate RAC1 and modulate cytoskeletal rearrangement; thus, it is possible that PIAS3 plays a role in IAV endocytosis (Castillo-

Lluva et al. 2010). In addition, it has previously been shown that PIAS1 and PIAS3 negatively regulate STAT-mediated signaling and IRF1 transcriptional activity, suggesting that PIAS3 may be important for modulating cell intrinsic immunity (Nakagawa and Yokosawa 2002). These findings suggest that JAK2 and PIAS3 are important for the regulation of cell intrinsic immunity, yet may function at different steps of the IAV life cycle.

In conclusion, GeCKO screening is a powerful alternative strategy for the identification of host factors and biological pathways critical for the replication of multiple influenza viruses. Host pathways required for expression of the viral receptor sialic acid were uniquely enriched in this GeCKO screen, with the highest enrichment observed for SLC35A1, a sialic acid transporter. In addition to highlighting biological pathways, our GeCKO screen identified CIC as a host factor important for the regulation of cell intrinsic immunity. Our studies show that CIC suppresses antiviral gene expression and suggest that CIC levels are regulated during viral infection to facilitate robust induction of antiviral responses. Therefore, we demonstrate that GeCKO screening is an invaluable tool for the discovery of host factors essential for the replication of intracellular pathogens and for the identification of targets for the development of host-directed therapeutics.

CHAPTER IV

Regulation of Cell Intrinsic Immunity by the Transcriptional Repressor CIC

Some material in this chapter is adapted from the published manuscript 'Genome-wide CRISPR/Cas9 Screen Identifies Host Factors Essential for Influenza Virus Replication' (Han et al. 2018). Julianna Han performed all of the experiments and analysis in this chapter except for the bioinformatics analysis of RNAseq data.

INTRODUCTION

Humans constantly face assaults from numerous pathogens and are successfully able to prevent establishment of infection. As such, the host is perpetually on the alert, using innate immune pathways to sense and respond rapidly to viral infection. However, checks and balances of innate immunity, in the form of negative regulation, are critical to prevent erroneous antiviral responses and to ramp down these responses after the threat has been cleared. Through a genome-wide CRISPR/Cas9 screening strategy, we identified capicua (CIC), a DNA binding repressor, as a novel host factor critical for optimal replication of IAV and VSV (Figure III.3).

CIC is a highly-conserved gene encoding the protein capicua, aptly meaning head and tail in Catalan because it plays a crucial role in terminal patterning during *Drosophila* embryogenesis (Jiménez, Shvartsman, and Paroush 2012; C. J. Lee et al. 2002). CIC is a DNA binding transcriptional repressor that functions in conjunction with the co-repressor

Ataxin1 (ATXN1) or its paralog ATXN1-Like (ATXN1L) to regulate genes controlled by receptor tyrosine kinase signaling (Jiménez, Shvartsman, and Paroush 2012; Ajuria et al. 2011). There are two major isoforms of CIC: short (CIC-S) and long (CIC-L), expressed from independent start codons (Figure IV.1.A). Importantly, in human systems, defects in CIC or its co-repressor ATXN1 have been thoroughly characterized to cause spinocerebellar ataxia (SCA1) neuropathogenesis and neurodegeneration, and mice recover from SCA1 disease when genetically rescued with CIC (Pavlovic et al. 1990; Bowman et al. 2007; Crespo-Barreto et al. 2010; Lam et al. 2006; Lu et al. 2017; Zoghbi and Orr 2009; John D Fryer et al. 2011). Moreover, mutations and gene fusions of CIC have been linked to cancer progression (Bettegowda et al. 2011; Chittaranjan et al. 2014; Kawamura-Saito et al. 2006). Recently, CIC has been revealed as a critical regulator of autoimmunity, preventing hyperactivation of T cell receptors to maintain T cell homeostasis (S. Park et al. 2017). CIC is an extraordinary transcriptional regulator that controls severe pathologies including neurodegeneration, cancer, and autoimmunity.

Now, we illuminate another novel and broadly influential role for the transcriptional repressor CIC in disease prevention: regulation of antiviral immunity. Our CRISPR/Cas9 screen identified CIC as a pan-proviral factor critical for both IAV and VSV replication (Figure III.3). CIC is crucial for viral RNA production and is thus important for individual cycles of IAV replication (Figure III.5). Moreover, antiviral genes are overexpressed in cells lacking CIC (Figure III.5). Next we wished identify the mechanism by which CIC aides viral replication.

This chapter is dedicated to characterizing a novel function of CIC in modulating cell intrinsic immunity through the regulation of antiviral gene expression. Our studies demonstrate that loss of CIC results in upregulation of interferon and interferon stimulated genes, thus creating a heightened antiviral status in the cells that prevents replication of viruses from diverse families. In contrast, ectopic expression of CIC suppresses promoters of antiviral genes containing CIC binding sites. Importantly, CIC protein levels and mRNA levels are downregulated during influenza virus infection. We hypothesize that under steady-state conditions CIC represses the transcription of antiviral genes, and upon viral infection, CIC is downregulated to facilitate robust expression of antiviral genes. Our studies illuminate a novel mechanism for the regulation of the intracellular antiviral state by CIC and could have large implications in our understanding of innate immune regulation.

RESULTS

Viral Replication is Decreased in CIC KO and CIC KD

To further understand the role of CIC in virus replication, we first confirmed our findings in new *CIC* KOs generated with an independent sgRNA (*CIC* KO2s). Loss of CIC expression in *CIC* KO2s was confirmed by western blot analysis and sequencing of the sgRNA target site (Figure IV.1A-B; Table III.2). In agreement with previous findings, we observed decreased levels of ATXN1L protein as well as increased expression of a CIC-regulated gene, *ETV4*, in *CIC* KO2s (Figure IV.1C) (Y. Lee et al. 2011; Dissanayake et

al. 2011). These results demonstrate that loss of the CIC/ATXN1 co-repressor complex allowed for expression of target genes in *CIC* KO2 cells (Lam et al. 2006; Kawamura-Saito et al. 2006; Dissanayake et al. 2011). As previously observed, *CIC* KO2s also demonstrated an ~2-3 log reduction in the replication of various IAV strains, as well as a ≥1 log reduction in VSV, encephalomyocarditis virus (EMCV), and Zika virus replication (Figure IV.1D).

Typical analysis for confirming genetic loss-of-function phenotypes involves reconstituting gene expression through ectopic expression of the gene of interest. However, our studies on ectopic expression of CIC have encountered technical challenges: as CIC KOs exist in an antiviral state, the cells are already resistant to expression of exogenous plasmids. Therefore, to further validate the phenotype observed in CIC KO cells, we utilized RNAi-mediated knockdown of CIC. Diminished expression of CIC resulted in a 10-fold reduction in H1N1 replication (Figure IV.2A and B). As a positive control, knockdown of NP also decreased H1N1 replication (Figure IV.2A).

Taken together, two independent CIC KO cell lines and RNAi-mediated knockdown of CIC have confirmed the role of CIC in supporting virus replication. As CIC is a DNA binding transcriptional repressor, we hypothesize that loss of CIC results in altered expression of antiviral genes and thus affects the replication of multiple viruses. This hypothesis could also encompass our observations that CIC impacts viral RNA production, as some antiviral genes, such as MxA, antagonize IAV nuclear import and

RNA expression (Haller et al. 2015; Ferris et al. 2013; Pavlovic et al. 1990; Schuster et al. 1996; Schwemmle et al. 1995; Xiao et al. 2013; Zürcher, Pavlovic, and Staeheli 1992).

CIC Regulates Antiviral Gene Production

Several of the top hits identified through CRISPR screening were crucial for replication of both IAV and VSV (Figure III.3). Profiling antiviral gene expression in the KOs revealed upregulated antiviral responses in cells lacking these pan-viral factors, most prominently CIC (Figure III.5). Our next step was to confirm this phenotype in CIC KO2s. Upon infection, NP expression was decreased in CIC KO2s at 8 and 24 hpi, but increased at 16 hpi (Figure IV.3A). In CIC KO2 mock conditions, IFNβ and antiviral genes were upregulated 5- to 20-fold compared to vector mock conditions (Figure IV.3B-D). Upon infection, vector cells induced antiviral genes over time, to levels comparable to CIC KO2 mock conditions (Figure IV.3B-D). Upon infection of CIC KO2s, antiviral genes were dramatically over-induced (Figure IV.3B-D). Together, as anticipated, these data confirm previous findings and suggest that loss of *CIC* results in a heightened antiviral state, rendering cells less permissive to viral replication.

CIC binds specific oligomeric sequences in target gene promoters to repress gene expression. Our bioinformatics analyses indicate the presence of canonical and putative CIC binding elements in antiviral gene promoters, including those of IFNβ, IFN transcription factors, and ISGs such as MxA, and RIG-I (Table IV.1). We hypothesize that CIC binds to its consensus binding site(s) in antiviral genes and represses transcription.

As the first step to assess if CIC could repress gene transcription in the context of RIG-I induction, we generated a minimal IFNβ-luciferase reporter construct with six CIC binding sites (IFNβ 6x CBS; Figure IV.4A). We activated the RIG-I pathway using a constitutively active RIG-I 2-CARD construct and measured luciferase activity. Expression of RIG-I 2-CARD resulted in increased luciferase levels, demonstrating activation of the IFNβ promoter. However, expression of the CIC and ATXN1 co-repressor complex repressed IFNβ 6x CBS reporter induction (Figure IV.4B). As a control, we mutated the CIC binding sites in the IFNβ 6x CBS reporter construct and observed that CIC/ATXN1 could no longer control expression of the reporter (Figure IV.4C).

As loss of *CIC* resulted in higher antiviral gene expression, we hypothesized that ectopic expression of *CIC* would suppress the activity of antiviral gene promoters. Thus, we generated luciferase reporters under the control of the human *IFIT1* and *MxA* promoters. Co-expression of *CIC* and *ATXN1* resulted in a dose dependent decrease in IFIT1 reporter activity (up to ~50%) upon RIG-I stimulation as compared to GFP control, to a greater extent than expression of *CIC* or *ATXN1* alone (Figure IV.5A). Similarly, an ~40% reduction in MxA reporter activity was observed upon co-expression of *CIC* and *ATXN1* (Figure IV.5B). Therefore, CIC and ATXN1 suppress antiviral gene expression potentially through CIC binding sites in antiviral gene promoters.

CIC Regulates Pathways that Control Multiple Pathogens

The mechanism by which CIC controls antiviral gene expression could be by directly repressing multiple antiviral genes or by suppressing the production of type I IFN, thereby

suppressing type I IFN-induced antiviral genes by proxy. It is conceivable that both of these possibilities may occur: CIC may repress both type I IFN and antiviral genes directly. To gain insight into pathways regulated by CIC, we performed RNA sequencing (RNAseq) analysis of CIC KO2 cells and vector control cells in the presence and absence of H1N1 infection (16 hpi; MOI = 3).

To assess the quality of our RNAseq data, we analyzed coverage and variance. Coverage uniformity of the gene body was evaluated by normalizing transcripts to 100nt and calculating read coverage per nucleotide. Our RNAseq data proportionately covered the gene body with no bias toward either 5' or 3' end of transcripts (Figure IV.6A). After normalization, we performed multidimensional scaling (MDS) analysis and observed that each sample differed from each other while replicates were very similar, as expected (Figure IV.6B).

We performed confident effect (confect) analysis to determine differentially-expressed genes (DEG) in our conditions. This statistically rigorous method identifies and ranks DEGs based on p-value, false discovery rate, and effect size, which is the difference in mean values compared to the standard deviation. Through this analysis we identified 413 DEGs in CIC KO2 mock conditions versus control mock conditions (Figure IV.7A and B). DEGs clustered into categories that demonstrated broad upregulation in pathogen defense systems. Enriched gene ontology (GO) pathways in CIC KO2s included interferon, cytokine, and inflammatory pathways that result in enhanced defense responses to pathogens (Figure IV.8 and Table IV.2). Likewise, enriched Kyoto ensemble

of genes and genomes (KEGG) pathways included cytokine interactions, NFκB signaling, and responses to viruses, bacteria, and parasites (Table IV.3). Ingenuity pathway analysis (IPA), an experimentally-validated categorization program, also highlighted interferon signaling and pathogen recognition pathways (Table IV.4). Using the Molecular Signatures Database, we saw that transcription factors hypothesized to regulate these DEGs included IRFs and ISREs (Table IV.5), further emphasizing that genes enriched in CIC are regulated by interferon signaling (Liberzon et al. 2011; Subramanian et al. 2005).

Our top DEGs included genes involved in cell growth and cancer, (e.g., KRT19, PCDH10, and CAVIN3) confirming enrichment in previously known functions of CIC (Table IV.6) (Simón-Carrasco et al. 2018). Moreover, top DEGs in CIC KO2s included genes which recognize foreign genetic material, transcription factors of interferons, various cytokines, interferon-stimulated genes, and components of the caspase-1 inflammasome (Table IV.6 and 7, Figure IV.9). Multiple immunity-related DEGs contained many iterations of CIC binding sites, hinting at potential regulation by CIC (Table IV.7). We confirmed these DEGs through qPCR analysis and saw that these immunity-related DEGs were indeed enriched in CIC KO2s (Figure IV.10). Therefore, our RNAseq analysis identified CIC as a regulator of remarkably broad defense systems.

In order to evaluate the importance of individual DEGs in controlling IAV infection, we performed a miniature siRNA screen in CIC KO2 cells. We targeted top immunity- and inflammation-related genes, silenced these genes in CIC KO2 cells, and infected with H1N1 (MOI 0.1, 48hpi). As expected, IAV replicated similarly in irrelevant siRNA control

conditions (non-targeting siRNA and siRNA to GAPD, which is not differentially-expressed in CIC KO2s) but was restricted in siNP conditions compared to control conditions (Figure IV.11A). We anticipated that if a single DEG was crucial for restricting IAV replication in CIC KO2s, silencing this gene would restore IAV replication. Knockdown of IFITM3, IFIT1, and STAT2 modestly restored IAV replication, however, we did not identify any single gene that was crucial for IAV restriction (Figure IV.11B). Therefore, CIC negatively regulates multiple genes in tandem to inhibit the antiviral state.

In conclusion, our RNAseq examination characterized CIC as a pivotal element in cell intrinsic immunity and inflammation. We did not identify a single gene modulated by CIC that was responsible for regulation of these pathways. However, the increased IFNβ production in CIC KO2 cells will result in increased ISG production, which complicates the interpretation of our results. We will dissect the confounding effect of IFN-induced ISG expression by generating CIC/STAT1 double knockout cell lines and/or carrying out experiments in the presence of IFN neutralizing antibodies. Through RNAseq comparisons in these systems, we will be able to decipher the regulation of CIC independently of IFN signaling.

HSV1 Replication is Unaltered in CIC KOs

Interferonγ-inducible protein 16 (IFI16) was the top ranked immunity and inflammation DEG, contained many CIC binding sites regulating its isoforms, and is dramatically overexpressed in CIC KO2s (Figure IV.10 and IV.12A, Table IV.7). IFI16 is an intracellular DNA sensor that signals through STING to activate type I IFN and pro-inflammatory

cytokines through IRF3 and NFκB (Y. K. Chan and Gack 2016). As an AIM2-like receptor, IFI16 also activates the inflammasome in response to viral infection (Unterholzner et al. 2010; Kerur et al. 2011). While IFI16 recognizes cytosolic DNA, Herpesviruses are DNA viruses that have evolved intricate mechanisms to subvert innate immune recognition and control, including the ICP0 gene of Herpes Simplex Virus 1 (HSV1) that targets IFI16 for degradation (Orzalli, DeLuca, and Knipe 2012). Therefore, we hypothesized that HSV1 replication may be unrestricted in CIC KOs, but that an ICP0-deficient HSV1 (ΔICP0) may be controlled in CIC KOs. Upon HSV1 infection of Vector control and CIC KO2 cells, we observed no difference in replication kinetics, demonstrating that HSV1 is not restricted in CIC KO2s (Figure IV.12B). Interestingly, we also did not observe any difference in ΔICP0 replication in CIC KO2s either (Figure IV.12C). It is likely that even without ICP0, the multiple defense mechanisms of HSV1 are able to compensate to subvert immune detection. These findings unveil questions of how HSV1 is able to replicate in such a hostile state, and what happens to CIC during HSV1 infection.

CIC is Downregulated in Response to Viral Infection

As our results indicate that CIC can repress antiviral gene expression, we investigated if downregulation of CIC occurs upon infection to facilitate the induction of antiviral genes. Western blot analysis of H1N1 infected vector control cells demonstrated a rapid decline in CIC-L and ATXN1L protein levels at 40 min post-infection (Figure IV.13A). qRT-PCR analysis of H1N1 infected vector control cells showed an ~70-90% decrease in CIC-S, CIC-L, and ATXN1 mRNA levels, demonstrating that the co-repressor complex mRNA and protein levels are downregulated in response to IAV infection (Figure IV.13B). These

results suggest that there is a host-encoded strategy for regulating CIC mediated repression of host defenses.

DISCUSSION

The innate immune system is the host's first line of defense, paramount in detecting viral invasion and mounting a strong and swift protective response. Nevertheless, the innate immune system must be tightly controlled, because aberrant activation can result in autoimmune diseases. Therefore, negative regulators of the innate immune system are crucial. CIC in conjunction with the co-repressor Ataxin1 (ATXN1) or its paralog ATXN1-Like (ATXN1L) has been implicated in cancer development and progression, as well as neuropathology and autoimmunity (Okimoto et al. 2017; Bettegowda et al. 2011; Lam et al. 2006; S. Park et al. 2017). However, CIC has not been shown to play a role in the regulation of cell intrinsic immunity.

Our CRISPR/Cas9 screen identified CIC as a proviral host factor for IAV replication and RNA production (Chapter III). In confirmation studies knocking out CIC using new gRNAs or knocking down CIC using RNAi, we observed significantly reduced viral replication in CIC KO or KD cells by viruses from four different families, including IAV, VSV, Zika and encephalomyocarditis virus (EMCV) (Figure IV.1 and 2). Similar to our prior findings, cells lacking CIC expressed higher levels of antiviral genes under basal conditions, demonstrating a heightened antiviral state, and overexpressed antiviral genes upon IAV infection (Figure IV.3). Furthermore, CIC repressed antiviral genes containing CIC binding

sites in their promoters (Figure IV.4 and 5). We observed broad upregulation of immunity and inflammation pathways in CIC KO2 cells, suggesting that a variety of intracellular pathogens may be restricted in cells lacking CIC (Figure IV.8 and IV.9). However, HSV1 replication was unrestricted, potentially due to the finely tuned ability of HSV1 to subvert the antiviral state in order to replicate undetected (Figure IV.12). Finally, in order to induce the antiviral state, CIC is regulated in response to viral infection at both the protein and mRNA level (Figure IV.13). We hypothesize that CIC and ATXN1 form a co-repressor complex and repress the promoters of inflammation and immunity genes under basal conditions, keeping the antiviral state in check in the absence of infection (Figure IV.14). Upon infection, CIC-mediated repression is relieved, allowing the induction of the antiviral state (Figure IV.14). Taken together, these findings strongly demonstrate that CIC is a critical host factor involved in regulating cell intrinsic immunity.

We observed robust restriction of RNA viruses from diverse families in CIC KO2 cells, yet restriction of Zika virus and EMCV was not as strong as the attenuation observed for IAV and VSV (Figure IV.1). While IAV restricts host sensing of foreign genetic material at the RIG-I level through inhibition of TRIM25, Zika virus and EMCV contain mechanisms to subvert immune responses downstream of host sensing: the non-structural protein NS5 of Zika virus degrades STAT2 to prevent IFN signaling and the protease 3C of EMCV degrades TANK, a scaffolding protein that aides in IRF3 phosphorylation and activation (Gack et al. 2009; Grant et al. 2016; Huang et al. 2017). This may suggest that, while it is still possible that CIC blocks antiviral gene expression downstream of IFN production

and signaling, some of the target antiviral genes of CIC must be effectors involved in pathogen sensing and IFN production.

In addition, we observed repression of IFIT1 and MxA reporter activity upon ectopic expression of *CIC* with the co-repressor *ATXN1* (Figure IV.5). As CIC has been previously demonstrated to function as a DNA binding transcriptional repressor, it is possible that CIC suppresses antiviral gene expression via its transcriptional repressor activity (Jiménez, Shvartsman, and Paroush 2012). Mutational analysis obscuring the endogenous CIC binding sites in the promoters of IFIT1 and MxA reporters will be crucial to assess direct regulation of these promoters by CIC. Moreover, Electrophoretic Mobility Shift Assay (EMSA) will provide mechanistic insight into binding ability and strength of CIC on target antiviral gene promoters, especially in combination with mutants of CIC in key interaction domains, such as the MAPK regulation sites, DNA binding region (HMG box), the ATXN1/ATXN1L binding domain, and finally the C1 domain that binds a motif on target DNA recently identified to improve target specificity (Jiménez, Shvartsman, and Paroush 2012; Simón-Carrasco et al. 2018; Fores et al. 2017). Additionally, while our reporter assays demonstrate that the co-repressor complex CIC and ATXN1 together are needed for optimal repression (Figure IV.4 and IV.5), and the co-repressor is also regulated in response to viral infection (Figure IV.13), we need to confirm the role of the co-repressor by CRISPR/Cas9 KO or RNAi KD analysis. Using these approaches, we will elucidate the mechanism by which CIC basally represses antiviral gene expression.

CIC widely regulates pathways involved in inflammation and immunity, as elicited by RNAseq analysis (Figure IV.8 and IV.9; Tables IV.2-5 and IV.7). We observed enrichment in gene categories involving host defense responses to pathogens, cytokine signaling, type I interferon signaling, and inflammatory responses. In agreement, a previous study demonstrated increased levels of proinflammatory cytokines in CIC-L deficient mice (Kim et al. 2015). Taken together, defense pathways, especially type I interferon signaling, are broadly upregulated in CIC KO cells. The type I interferon pathway occurs through a two-step process: in the first step, receptors sense foreign genetic material and signal through MAVS and interferon transcription factors to produce type I interferons. In the second step, newly produced type I interferons signal in an autocrine and paracrine manner through the IFNα receptor and the JAK/STAT cascade to induce expression of effector proteins such as interferon-induced genes (Schneider, Chevillotte, and Rice 2014). CIC may regulate type I interferon signaling during the first step, where suppression of type I interferons, such as IFNβ, or suppression of a factor controlling type I interferon production blocks the induction of the antiviral state. Alternatively, CIC may regulate individual effector proteins downstream of interferon signaling. To compound matters further, these two possibilities are not mutually exclusive—CIC may repress the antiviral state at multiple nodes. Likewise, CIC may be repressing other defense response pathways, such as inflammatory responses and caspase activation, in a similar fashion.

CIC binds to octameric sequences in the promoters of target genes and represses transcription, and we find CIC binding sites in many promoters of antiviral DEGs from our RNAseq analysis (Table IV.7) (Kawamura-Saito et al. 2006; J. D. Fryer et al. 2011; Ajuria

et al. 2011). In order to assess whether CIC is regulating antiviral gene repression directly through repression of individual promoters, or indirectly, through repression of an upstream gene such as IFNβ, we must employ ChIPseq. In addition, to determine if CIC is regulating genes upstream or downstream of IFN signaling, we can compare DEG profiles through RNAseq comparison of cell knocked out for both CIC and STAT1 versus cells knocked out for CIC alone. In tandem, IFN neutralizing antibodies will complement these assessments. These studies will elucidate the exact targets of CIC repression.

Furthermore, our studies demonstrate downregulation of CIC protein and RNA levels upon IAV infection (Figure IV.13). This regulation may be a two-wave process by which CIC protein is downregulated in a rapid but unsustained manner upon viral infection, but CIC mRNA is downregulated multiple hours after infection from 8 hpi to at least 24 hpi (Figure IV.13 and data not shown). As viral infections activate MAPK pathways, and the activation of MAPK pathways result in the downregulation of CIC, it is possible that CIC downregulation during IAV infection occurs via MAPK signaling (Ajuria et al. 2011; Dissanayake et al. 2011; Pleschka 2008). RTK signaling activates extracellular signal-regulated kinase, which phosphorylates CIC to relieve repression, shunting CIC to the cytoplasm for degradation (John D Fryer et al. 2011; Futran et al. 2015; Lam et al. 2006; Ajuria et al. 2011; Kawamura-Saito et al. 2006; Grimm et al. 2012). For known CIC target genes, well-characterized strategies exist to shut down CIC mediated repression in order to allow for gene expression. Using inhibitors of the proteasome and kinases in the MAPK pathway as well as phospho-mutant and phospho-mimetic constructs of CIC, we can evaluate how CIC is regulated upon infection. Then, we can illuminate what viral

component triggers the degradation of CIC by treating cells with various stimuli (WT IAV, UV-inactivated IAV, viral RNA, virus like particles (VLP) without viral genome, etc.) and performing a time course for CIC protein degradation. These studies will allow us to decipher host pathways important for derepression of CIC target genes during IAV infection.

If these known mechanisms are not responsible for regulation of CIC, or are only responsible for one node of a two-wave regulation process, then CIC may be regulated independently of RTK signaling. Indeed, a new study identified an RTK-independent mechanism of regulating CIC in the Drosophila system, through co-binding DNA with Dorsal protein, an NFκB ortholog (Papagianni et al. 2018). This may be counter-intuitive when applied to the mammalian system, however—if CIC as a repressor works in tandem with NFκB, an activator, then are the target genes repressed or activated? This mode of regulation may be specific to the *Drosophila* setting, or maybe a fine balance exists in CIC-mediated gene regulation.

Previous studies show that CIC degradation can be inhibited by the COP9 signalosome (Suisse et al. 2017). Interestingly, multiple members of the COP9 complex have been identified as IAV host factors; thus, it is tempting to speculate that viruses may usurp the COP9 signalosome to prevent CIC degradation and thereby repress host antiviral gene expression (Tripathi et al. 2015). Intriguingly, HSV1 replication is unhindered in CIC KOs. Could herpesviruses, which stealthily replicate without alarming the immune system, be

co-opting CIC as a mechanism to replicate undetected? It would be interesting to see if CIC is downregulated during HSV1 infection as well.

Once we have discovered the mechanism by which CIC targets and represses antiviral genes and the strategy the host employs to regulate CIC mediated suppression, we wish to assess the broad impact of CIC in controlling viral invasion and identify cellular signals that block CIC repression. Is CIC used in the same manner during infection by DNA viruses? Does the activation of other innate immune RNA/DNA sensors result in inactivation of CIC? Moreover, numerous cancer studies have revealed mutations in CIC that contribute to cancer progression (Bettegowda et al. 2011; Chittaranjan et al. 2014; Simón-Carrasco et al. 2018). Could these individuals be at a lower risk for viral infection due to upregulation of innate immune responses by mutated CIC? It would be intriguing to obtain tissue samples and cell lines from these patients or recapitulate these mutations in A549 cells to analyze viral replication in a background where CIC is naturally mutated and inactivated. In addition, we can utilize CIC-L KO mice (Kim et al. 2015) to determine the role of CIC in IAV and VSV replication, as well as other virus families, *in vivo*. Illuminating CIC as a potent negative regulator of innate immunity, conserved from *Drosophila* to humans, may have universal and immense consequences in our understanding of viral infection, viral control, and the host-pathogen arms race.

CHAPTER V

Tetracysteine Tagged NP Reveals the Role of Rab11a in Production of Infectious Influenza Virus Particles

This chapter is adapted from the manuscript 'Tetracysteine Tagged NP Reveals the Role of Rab11a in Production of Infectious Influenza Virus Particles.' Julianna Han performed all of the experiments in this chapter, except for the defective particle analysis which was performed by the Lowen lab at Emory University.

ABSTRACT

Fluorescent reporter viruses aide investigation of influenza A virus biology. Viral ribonucleoprotein complex egress is not fully understood and studies to understand this process have been hampered by the lack of appropriate tools, including NP-tagged reporter viruses. To probe the dynamics of ribonucleoprotein (vRNP) export and evaluate the significance of cellular factors in genomic packaging, we generated an influenza reporter virus carrying a tetra-cysteine tag in the C-terminus of the NP gene (NP-Tc reporter virus) and utilized the biarsenical labeling reagent FlAsH to visualize NP protein by fluorescence microscopy. Using this new tool, we followed the dynamics of NP localization during the replication of influenza A virus. At early time points, bright NP puncta clustered around the microtubule organizing center (MTOC) that were positive for viral RNA detected via fluorescence *in situ* hybridization, indicating vRNP complexes are preferentially exported to the MTOC. In addition, these vRNP complexes co-localized with the egress factor Rab11a and were transported to the plasma membrane in a regulated and polarized fashion on microtubule networks. We propose that mixing of vRNP segments occurs near MTOCs on Rab11a positive vesicles prior to trafficking through the microtubule network. As vesicles

containing Rab11a may be important for facilitating association of RNP segments, we generated Rab11a knock-out cell lines using CRISPR/Cas9 gene editing and probed the dynamics of Rab11a-mediated organization and egress of vRNP complexes with our NP-Tc reporter virus. In Rab11a KO cells, we observed decreased accumulation of RNP complexes in the cytoplasm and significantly lower production of infectious virus. Importantly, loss of Rab11a resulted in an increased production of defective particles. In summary, the novel reporter virus NP-Tc is a powerful tool for dissecting the molecular dynamics of vRNP export and selective packaging of influenza virus segments.

One of the greatest challenges in our endeavors to constrain IAV is its propensity to reassort its genome. IAV contains a segmented genome of eight pieces that has the ability to recombine genomic segments between IAV strains, spawning antigenically new IAV variants with pandemic potential. Research defining the assembly and packaging of this complicated genome is still inconclusive and the field needs tools to probe these pathways. Elucidating the mechanism of IAV recombination is crucial to understanding and combatting emerging IAV strains.

INTRODUCTION

Influenza viruses are RNA viruses of the *Orthomyxovirus* family that feature several distinctive replication strategies, including possessing a segmented genome and replicating in the nucleus (Shaw and Palese 2013). As such, influenza viruses face several challenges atypical of non-segmented, cytoplasm-replicating RNA viruses. These

unique demands posed by IAV make studying these properties not only intriguing, but also imperative to our understanding of IAV biology in order to fight disease.

The genome of influenza A viruses (IAV) is composed of 8 segments of RNA encoding 11 proteins. Each segment of IAV is wrapped into viral ribo-nucleoprotein (vRNP) complexes containing the genomic RNA encircling oligomerized nucleoprotein (NP) and associated with the proteins of the RNA-dependent RNA polymerase: polymerase basic 1 (PB1), polymerase basic 2 (PB2), and polymerase acidic (PA). Unlike cytoplasm-replicating RNA viruses, IAV replicates in the nucleus in order to access the host's mRNA splicing machinery by which IAV expresses all of its genes. The newly replicated genomic segments are then exported to the cytoplasm; nuclear export protein (NEP) and matrix protein (M1) bind the genomic segments and associated with CRM1 for active transport through nuclear pore complexes. Once in the cytoplasm, vRNP complexes traffic to the plasma membrane in conjunction with Rab11a-associated vesicles on the microtubule network, egressing in an apically-polarized fashion (Guichard, Nizet, and Bier 2014; Lakdawala, Fodor, and Subbarao 2016; S Vale-Costa et al. 2016).

As a virus with a segmented genome, one of the hurdles IAV must address is how to transport and package each segment of its genome into nascent virions. The selective packaging process is still not completely understood; while this process is completed during transport within the cytoplasm, studies also suggest that this process can begin as early as within the nucleus (Chou et al. 2013; Lakdawala et al. 2014). Several host components are crucial for the assembly and packaging of vRNPs, but several key

questions remain. The role of the Rab11 pathway and transport along the microtubule and actin cytoskeletal networks in vRNP complex dynamics during egress is unclear. For example, it is still uncertain how Rab11a associates with vRNPs after nuclear export and subsequently hands off vRNPs at the plasma membrane. Similarly, it is unknown when and where supramolecular complexes of vRNPs are assembled, and whether this is a progressive process during vRNP egress (Gerber et al. 2014; Sílvia Vale-Costa and Amorim 2017).

Fluorescent reporter viruses are useful to illuminate IAV biology, including vRNP dynamics. Several reporter viruses tagging the non-structural protein 1 (NS1) and polymerase basic protein 2 (PB2) with fluorescent proteins have revealed key components of IAV pathogenesis (Manicassamy et al. 2010; Perez, Garćia-Sastre, and Manicassamy 2013; Lakdawala et al. 2014). However, fusing fluorescent proteins to NP have been unsuccessful, most likely because large fusion constructs may disrupt the delicate balance of NP oligomerization and contacts with RNA. Moreover, NP has roles in viral transcription and replication, and NP fused to fluorescent proteins may conflict with these processes. Therefore, we engineered a small peptide tag into NP and analyzed vRNP complex dynamics by employing FlAsH-EDT_2 (fluorescence arsenical hairpin binder—ethane di-thiol) technology. FlAsH is a small dye that fluoresces when bound to a compact tetra-cysteine peptide tag (Tc), therefore allowing simplified tagging of a protein of interest with minimal risk of disrupting protein folding (Hoffmann et al. 2005; Hoffmann et al. 2010). FlAsH binds di-thiols present in the Tc tag or ethane di-thiol molecules, a compound used to wash away unbound FlAsH, eliminating non-specific

signal. Utilizing FlAsH-EDT_2 and the Tc tag inserted into the NP protein (NP-Tc), we generated a reporter virus with a better likelihood of maintaining the delicate balance of NP contacts.

In this study using the NP-Tc tagged virus, we aimed to understand the biology of how cellular factors and cytoskeletal networks facilitate viral vRNP complex transport and promote selective packaging of IAV's genomic segments. Though mildly attenuated, NP-Tc virus replicates efficiently in Madin-Darby canine kidney (MDCK) cells and supports replication activity of the viral polymerase. FlAsH marking of NP selectively detects vRNP complexes, which export from the nucleus to cluster around the microtubule-organizing center (MTOC) before egressing with Rab11a-associated vesicles on the microtubule network in a polarized manner. Using newly-generated Rab11a knock out cells, we see that vRNPs do not accumulate in the cytoplasm and virion populations have more defective particles without Rab11a, suggesting that Rab11a is crucial for cytoplasmic clustering of vRNP complexes for optimal specific infectivity–novel information that will boost our understanding of the Rab11 recycling endosome pathway's role on packaging IAV. Therefore, the NP-Tc virus is a pivotal tool that will augment our knowledge of the IAV egress pathway, selective packaging, and specific infectivity of nascent virions.

RESULTS

Design and Characterization of Tetracysteine-tagged NP Reporter Virus

Influenza virus NP is important for transcription and replication of viral RNA segments. To determine if NP can be tagged with foreign sequences without significantly affecting its function, we C-terminally tagged NP with a small 6-amino acid tetracysteine tag CCPGCC (NP-Tc) or with RFP (NP-RFP) and evaluated its ability to support a vRNA-mimicking reporter construct in a mini-genome assay. The NP-Tc construct supported nearly 70% reporter activity in the mini-genome assay as compared to wild-type NP (Fig V.1A). However, NP-RFP showed very little reporter activity in the mini-genome assay (Fig V.1A), suggesting that the addition of larger C-terminal tags affect NP functions. We also observed that NP-Tc protein expression was similar to WT NP (Fig V.2). Next to generate a recombinant A/Puerto Rico/8/1934 virus carrying Tc-tagged NP, we engineered a NP-Tc segment, in which the small Tc tag was introduced right before the Stop codon (Fig V.1B). As the insertion of the Tc-tag likely disrupts the 5' NP vRNA packaging sequence, we duplicated the 200nt sequence at the 5' end (negative sense genomic RNA) of the NP segment to maintain signals necessary for vRNA packing into the progeny virions (Tundup et al. 2017). As a control, we generated an NP segment with the duplicated packaging sequence (NP200, Fig V.1B). Next, using the influenza virus reverse genetics system, we rescued recombinant NP-Tc virus and confirmed the presence of Tc tag in the purified virus by sequencing of viral genomic RNA.

Next, we compared the growth kinetics of the NP-Tc virus (NP-Tc) and WT virus in MDCK cells. In this replication assay, the WT PR8 virus reached peak titers of ~10^8 PFU/mL while the NP-Tc virus reached peak titers of ~10^6 PFU/mL (Fig V.1C). The NP-Tc virus replicated robustly, though not as high as the replication of PR8, demonstrating an

attenuated phenotype (Fig V.1C). To assess the potential of the NP-Tc virus as a new tool to visualize NP dynamics during replication, we infected A549 cells with NP-Tc virus, stained with FlAsH reagent and analyzed by fluorescent microscopy. We observed NP-Tc in distinct green fluorescent puncta in the cytoplasm infected cells, which also co-stained with an NP antibody (Fig V.1D). A549 cells infected with NP200 virus showed similar NP puncta in the cytoplasm, suggesting that the NP-Tc puncta are genuine NP structures (Fig V.1D). Together, these results indicate that NP-Tc virus, despite decreased peak titer, is capable of undergoing multiple rounds of replication. FlAsH only fluoresces upon binding Tc motifs, enabling selective marking of NP particles.

As other influenza reporter viruses have a tendency to lose foreign reporter genes, we performed a passaging experiment in MDCK cells to determine the stability of the Tc tag. After 10 passages (p10) in MDCK cells, we compared the parental NP-Tc (p1) and passaged NP-Tc virus p10 by fluorescence microscopy (Fig V.1E). Both NP-Tc p1 and NP-Tc p10 showed similar patterns of FlAsH and NP antibody staining, demonstrating that the Tc tag is stable in the NP-Tc virus (Fig V.1E). In addition, sequencing of the NP-Tc segment indicated no changes in NP-Tc coding sequence after the tenth passage. These results demonstrate that the Tc tag accurately marks NP and remains stably integrated and functional throughout passaging.

NP-Tc Allows Visualization of vRNP Dynamics

To determine if the cytoplasmic puncta visualized upon FlAsH and anti-NP staining of NP-Tc virus infected cells are vRNP complexes, we performed fluorescence *in situ*

hybridization (FISH) using probes against the NP vRNA segment (genome) along with FlAsH-staining. A549 cells were infected with NP-Tc virus (MOI=1) and stained with FlAsH reagent at 7hpi followed by FISH analysis. The cytoplasmic NP-Tc puncta observed by FlAsH staining showed the presence of viral genomic RNA via FISH staining, suggesting that the FlAsH-positive NP-Tc puncta are indeed vRNP complexes (Fig V.3A). Through a time course of infection, we observed small NP-Tc puncta outside the nucleus as early as 3hpi, suggesting initiation of vRNP export from the nucleus. Over time, we observed an increase in the size of the NP-Tc puncta in the cytoplasm, suggesting the likely formation of supramolecular complexes of multiple vRNPs. In addition, these large NP-Tc puncta trafficked away from the nucleus towards the plasma membrane in an organized and polarized fashion (Fig V.3B). Taken together, the NP-Tc virus can serve as a novel tool to assess vRNP trafficking during infection.

Cytoskeletal Components Aide in the Regulated Transport of vRNP

Previous research indicates that vRNPs export from the nucleus to Rab11a+ vesicles around the microtubule organizing center (MTOC) and transport along microtubules to the plasma membrane, forming vRNP sub-bundles and supramolecular structures to increase selective packaging during transit (Giese, Bolte, and Schwemmle 2016; Lakdawala, Fodor, and Subbarao 2016; Eisfeld, Neumann, and Kawaoka 2014). To further validate the NP-Tc system, we examined the role of the microtubule network in vRNP trafficking by co-staining for different component of the cytoskeletal network. Using γ-tubulin as a marker for the microtubule organizing center (MTOC), we determined that NP-Tc puncta accumulates near the MTOC, encircling γ-tubulin positive puncta as 3-5 hpi

(Fig V.4A). This indicates that vRNP complexes are exported from the nucleus to the MTOC. At later times during infection, the sizes of NP-Tc puncta increased and co-localized with the cellular factor Rab11a prior to regimented and polarized trafficking on the microtubule network (Fig V.4A). Next, we assessed the importance of the microtubule network for vRNP trafficking by treating NP-Tc virus infected A549 cells with the microtubule depolymerizing agent nocodazole starting treatment at 3hpi. Confirming previous findings in the literature, nocodazole treatment resulted in the loss of organized NP-Tc puncta structures, with the majority of large NP-Tc puncta observed at the plasma membrane (Fig V.4B) (Amorim et al. 2011; Momose et al. 2007; Liu et al. 2015; Nturibi et al. 2017). To determine if nocodazole treatment diminished association of different vRNP complexes, we performed FISH analysis for NP and PB2 vRNA segments and observed no significant difference in co-localization of NP/PB2 segments through Manders co-efficient analysis (Fig V.4C and D). These data demonstrate that the microtubule network is not required for association of vRNP segments and that vRNP egress of NP-Tc virus is identical to egress of WT IAV strains as reported by other groups (Amorim et al. 2011; Momose et al. 2007; Liu et al. 2015; Nturibi et al. 2017).

Rab11a Knock-out A549 Cells Show Decreased Viral Replication

Prior studies indicate that the Rab11a recycling pathway is important for transport of vRNP complexes to the plasma membrane. Most of the studies investigating Rab11a utilized either siRNA mediated knockdown or overexpression of Rab11a mutants (Eisfeld et al. 2011; Bruce, Digard, and Stuart 2010; Amorim et al. 2011; Momose et al. 2011). To further investigate the importance of Rab11a in the NP-Tc system, we generated Rab11a

KO A549 cells using the CRISPR/Cas technique and evaluated viral replication (Fig V.5A). In three independent Rab11a KO clones, we observed over ~3 logs lower replication of a H5N1 strain (A/Vietnam/1203/04, low pathogenic) in Rab11a KO cells as compared to control cells (Fig V.5B). In addition, analysis of replication kinetics of a H7N7 strain (A/Netherlands/219/03, low pathogenic) showed no significant change in viral titers over time and remained around ~10^2 PFU/mL (Fig V.5C). In contrast, H7N7 replication increased steadily and reached peak titers of 10^5-10^6 PFU/mL in control cells (Fig V.5C). Moreover, replication of several different strains of influenza virus were lowered by 1000-fold in Rab11a KO cells as compared to control cells (Fig V.5D). In contrast, the replication of vesicular stomatitis virus in Rab11a KO and control cells was similar. Together this data demonstrates that while Rab11a KOs adequately support replication of viruses such as VSV, IAV replication is greatly attenuated in these cells (Fig V.5B-D). These data highlight Rab11a as a crucial host factor for replication of a broad variety of human IAV strains.

In order to validate the role of Rab11a in IAV replication, we ectopically expressed Rab11a constructs in Rab11a KOs (Fig V.6). Reconstitution of Rab11a KOs with Rab11a restored H5N1, H1N1, and H7N7 replication by >100-fold compared to Rab11a KOs alone or Rab11a KOs expressing empty vector (Fig V.6). These findings clarify that the defects in IAV replication in Rab11a KOs are due specifically to the absence of Rab11a in these cells.

Loss of Rab11a Disrupts Trafficking and Increases Defective Particles

To assess the functional consequences of loss of Rab11a on vRNP trafficking, we infected Rab11a KO cells with NP-Tc virus (MOI=1) and analyzed vRNP localization by FlAsH and FISH staining at 18hpi. Interestingly, in Rab11a KO cells we did not observe any large, bright FlAsH puncta or FISH puncta outside the nucleus; indeed, vRNP complexes were mostly retained in the nucleus, indicating that loss of Rab11a likely prevents the formation of large supramolecular vRNP complexes in the cytoplasm (Fig V.7A and Fig V.8). In contrast, control cells showed significant accumulation of supramolecular vRNP structures in the cytoplasm in a polarized pattern (Fig V.7A and Fig V.8). In addition, faint, cytoplasmic staining of NP and PB2 FISH probes do not appear to co-localize, demonstrating the importance of Rab11a for association of different vRNP segments. This is in contrast to prior studies which showed cytoplasmic accumulation of vRNP complexes that are enriched in the nucleus and perinuclear space upon knockdown of Rab11a (Eisfeld et al. 2011). Moreover, luciferase activity of PR8 PB2-GLUC, a reporter virus marking viral replication processes, was unaffected between control and Rab11a KO cells, suggesting that the defect in Rab11a KO cells occurs after replication of the viral genome (Figure V.7B) (N. S. Heaton et al. 2013). Our results demonstrate that Rab11a is essential for the formation of supramolecular vRNP complexes and is potentially involved in receiving vRNP complexes as they are exported from the nucleus.

As we did not observe significant cytoplasmic localization of NP and PB2 vRNP segments in the Rab11a KO cells, we next investigated if the lack of Rab11a resulted in the formation of defective particles. We assessed the levels of defective particles in the viral supernatant from Rab11a KO and control cells by measuring the ratios of PFU to HA

(Infectious particles to total particles) as well as the ratios of vRNA copy number to PFU (Fig V.7C and D). The supernatants from infected Rab11a KOs displayed a lower ratio of PFU to HA units (Fig V.7C) and a higher ratio of viral RNA copy per PFU (Fig V.7D) as compared to supernatants from infected control cells, suggesting that there are higher numbers of defective particles in supernatants from Rab11a KOs. Taken together, these results suggest that the loss of Rab11a results in attenuated IAV titers, disrupted vRNP egress and defective packaging of vRNP segments into nascent virions. Therefore, using NP-Tc as a tool to selectively visualize NP in vRNP complexes, our studies elicit vRNP dynamics and suggest a novel element of Rab11a in the life cycle of influenza virus.

DISCUSSION

Unraveling the IAV egress pathway is crucial for understanding and combatting IAV pathogenesis. However, dissecting the mechanism of IAV assembly and packaging has remained elusive. We designed and characterized the NP-Tc virus as a novel tool for investigating vRNP dynamics. Using biarsenical probes and a simple tetra-cysteine motif inserted into the NP gene, we created an NP-Tc virus capable of tracking vRNP complexes in conjunction with cellular factors and cytoskeletal networks.

The NP-Tc virus grows robustly, though attenuated compared to the parental virus, and supports polymerase activity, while fusion of NP to RFP is inoperable (Fig V.1). WT IAV strains replicate quickly and vigorously, packed with puncta during the egress process. These features present a challenge to dissecting and tracking vRNP complexes.

Therefore, the slower growth kinetics of the NP-Tc virus may have a silver lining—the slackened dynamics may enable clearer visualization of the interactions between vRNP complexes and cellular factors. Using this virus, we see that vRNP complexes export to the MTOC and cluster in supramolecular assemblies in the cytoplasm (Fig V.3 and V.4). Rab11a is critical for formation of large vRNP congregations in the cytoplasm, ultimately leading to optimal infectivity of virions (Fig V.7 and V.8).

Notably, previous literature describing the temporal and spatial process of genomic packaging is inconclusive. Studies suggest that IAV's vRNPs assemble into individual supramolecular complexes in a hierarchical manner through RNA contacts (Gerber et al. 2014). However, it is unclear where and when these complexes come together. Our findings corroborate studies demonstrating that the microtubule network plays a crucial role in regulating vRNP export (Amorim et al. 2011; Liu et al. 2015; Nturibi et al. 2017; Momose et al. 2007). Indeed, upon disruption of the microtubule network, vRNPs quickly disperse to the plasma membrane and are contained in smaller supramolecular complexes (Fig V.4B and C). Cells with intact microtubules exhibit organized egress which likely supports presence of a cytoplasmic hub for efficient mixing of vRNPs.

Multiple studies also show that the Rab11a trafficking pathway is imperative for transport of vRNP complexes to the plasma membrane (Eisfeld et al. 2011; Silvia Vale-Costa and Amorim 2016; Amorim et al. 2011; Horgan et al. 2010; Momose et al. 2011; Avilov et al. 2012). Using complementary techniques including fluorescence microscopy, FRET, and IP, Rab11a has been shown to interact with vRNPs (Lakdawala, Fodor, and Subbarao

2016). Furthermore, a study showed that RNPs traffic with Rab11a on ER-derived membranes rather than on recycling endosomes (De Castro Martin et al. 2017). However, it is unknown whether Rab11a plays a more direct role in packaging or assembly. Is Rab11a involved in progressively assembling vRNPs during trafficking to the plasma membrane? How do vRNP complexes transfer from Rab11a-associated endosomes to the plasma membrane? A less-studied open issue is whether Rab11a plays a separate role from transportation during IAV egress. Insight into this issue has so far been limited due to small amounts of Rab11a still present in RNAi studies.

Using CRISPR/Cas9 gene editing to create cell lines completely devoid of Rab11a, we confirmed the importance of Rab11a in the replication cycle of IAV (Fig V.5 and V.6). Crucially, we see an almost complete lack of vRNP assemblies in the cytoplasm of Rab11a KO cells. Virions egressing from Rab11a KO cells exhibited packaging defects, as they were lacking segments and had decreased infectivity compared to their WT counterparts. Therefore, association of vRNP complexes with Rab11a is critical for amassing supramolecular assemblies for production of infectious particles. Previous literature knocking-down Rab11a still showed cytoplasmic conglomerations of vRNPs enriched in the perinuclear region (Eisfeld et al. 2011; Bruce, Digard, and Stuart 2010; Momose et al. 2011). Minimal amounts of Rab11a may be sufficient to collect vRNPs in higher-order cytoplasmic assemblies. Therefore, our findings in Rab11a KO cells clarify the role of Rab11a in vRNP assembly.

Upon trafficking out of the nucleus, cellular export machinery may hand-off vRNPs to Rab11a, building supramolecular complexes in the cytoplasm. This platform, in conjunction with the cytoskeleton, enriches vRNP interactions within the hub of the Rab11a recycling endosome network for organized, polarized egress to promote correct packaging of nascent virions. Following segment mixing within the supramolecular complex stage, correctly arranged genomic particles may then section off of the stage and conclude trafficking to the plasma membrane in smaller complexes. In our model, Rab11a acts as a staging area after nuclear export, not only to promote selective packaging, but primarily to associate vRNPs together. This model highlights questions in the assembly process of IAV: when and how do multiplexes of vRNPs and Rab11a form at the beginning of cytoplasmic transport, how are vRNPs handed off from nuclear export machinery to Rab11a-mediated vesicles, and finally how do sorted vRNP complexes leave the supramolecular complex stage and traffic to the plasma membrane?

CHAPTER VI

Discussion

One hundred years ago, the worst pandemic known to humans emerged across the globe. This pandemic was caused by the “Spanish flu,” an H1N1 IAV strain, and was responsible for the deadliest pandemic in human history. As illustrated by previous pandemics as well as seasonal epidemics, influenza A viruses are particularly resilient and adept at evading selection pressures, blocking our containment and elimination efforts (Belser and Terrence 2018). Because of its wide host range, there is a diverse pool of IAV strains potentially capable of causing disease in humans. When IAV strains from other species cross the species barrier into humans, devastating pandemics can result, as the human population is naïve to the incoming IAV strains. Indeed, many scientists believe another flu pandemic is inevitable, underscoring our need to be prepared. What insight have we gleaned from the past IAV pandemics, how are we applying these experiences, and how are we preparing for the next threat?

Since the bird flu (H5N1) and swine flu (H1N1) pandemic threats, many governmental and independent agencies, notably the United States Homeland Security Council, the CDC, and the WHO, have generated national and global pandemic response strategies (“Homeland Security Council” 2005; “Centers for Disease Control and Prevention” 2017b; “World Health Organization” 2017). These efforts helped spur laudable multi-sector collaborations for combatting these global threats, including unifying pandemic strategies, sharing programs and materials, and coordinating surveillance and reporting systems.

Pillars central to these strategies include preparedness, surveillance, containment, and global cooperation.

The United States government maintains stockpiles of vaccines and antivirals, but it is impossible to predict whether these countermeasures will be cross-protective for the next novel pandemic strain. Moreover, well-documented evidence and surveillance demonstrates that IAV strains easily develop resistance to currently-licensed antivirals, and sporadic resistance has already been observed in H5N1 (Han et al. 2017). It is crucial to identify novel targets for therapeutic intervention and implement countermeasures against the emergence of resistance.

IAV proteins have extraordinary plasticity and can morph away from restriction imposed on them. Hence, as IAV relies on many host pathways during its replication cycle, some therapeutic efforts have turned to targeting host factors instead of viral factors. Targeting a host pathway that may be conserved among IAV strains could generate a more substantial replication block; the virus will be forced to find an alternate route in its life cycle, and this block might be effective against novel IAV strains.

Therefore, pandemic response strategies recognize and highlight the need for science advancement and therapeutic development. Basic research underscores pandemic preparedness, as it both broadens and tailors our understanding of the threat. Consequently, it is crucial to evaluate molecular determinants of likely culprits, such as H5N1. IAV adaptation is largely due to its ability to access and commandeer host proteins

and pathways. Gaining access to these mechanisms in different species is a major determinant in IAV interspecies transmission. The knowledge gained from studying the role of these host factors in IAV replication will provide valuable insight into how IAV exploits host factors and crosses the species barrier, revealing potentially druggable targets.

Next Generation Techniques for Detecting Druggable Targets

To identify and define the roles of cellular factors that aid in the viral life cycle, we took advantage of CRISPR/Cas gene editing and next generation sequencing. The combination of these new tools enabled precise evaluation of host factors through successive elimination of individual genes—a loss-of-function screen. We generated a human lung epithelial cell line library in which ~30,000 genes were targeted by the CRISPR/Cas9 gene editing system and performed stringent selection using a human isolate of H5N1 avian IAV followed by deep sequencing (Han et al. 2018). In general, this rigorous selection process enriched for the most effective gRNA per gene, rather than allowing multiple gRNA per gene to exist in the population.

We observed enrichment in pathways already detected by siRNA screens using H1N1 strains, such as endosomal acidification and sialic acid transport pathways. Our strongest hit, the sialic acid transporter SLC35A1, was also identified by an siRNA screen (Brass et al. 2009). These shared factors spanning multiple screens and techniques provide further evidence of the importance of these pathways in pan-influenza life cycles.

We identified numerous novel factors, some of which were strain-specific, such as PIAS3. Loss of PIAS3 in cells reduced H5N1 and H1N1 replication by 10-fold but did not affect H3N2 replication. PIAS3 is an E3 SUMO ligase, involved in post-translationally conjugating SUMO residues onto target proteins for functions such as cell motility (Castillo-Lluva et al. 2010). IAV usurps post-translational modifications, including the highly dynamic and wide-ranging SUMOylation system, for optimal intracellular transport and viral growth (Pal et al. 2011; Wimmer, Schreiner, and Dobner 2012). Indeed, multiple IAV proteins are SUMOylated and IAV infection induces a global increase in SUMOylation that results in increased viral replication, although the functional necessities of the modifications are still not understood (Pal et al. 2011). In regard to the strain-specificity of PIAS3, perhaps several strains of IAV rely on PIAS3 for SUMOylation, but H3N2 has adopted another method by which to SUMOylate viral proteins. As there are multiple SUMO ligases, redundancy in the SUMOylation pathway may also explain why loss of PIAS3 only decreased IAV replication by 10-fold (Pichler et al. 2017). Because of this redundancy in SUMOylating ligases, as well as the dispensability of PIAS3 in H3N2 replication, one of the circulating IAV strains, PIAS3 is not an ideal antiviral target.

The CRISPR KO system contains an intrinsic benefit of eliminating host factors crucial for cellular survival; knockout of any factor that a cell needs to survive will result in a non-viable cell. Therefore, it is less likely that we will encounter cytotoxicity if we target any of our hits for therapeutic intervention, increasing our likelihood of generating druggable targets. Next, we cross-checked our factors against databases of drugs, to see if any of our factors were already targeted by FDA-approved remedies for other processes.

We detected one of our top hits, acyl-CoA dehydrogenase short/branched chain (ACADSB) as a potential target of valproic acid, a well-known medicine. Valproic acid is a branched short-chain fatty acid known since 1962 as an anti-convulsant drug and commonly used to treat epilepsy, bipolar disorder, and migraines (Loscher 1999). ACADSB is an enzyme in the mitochondrial β-oxidation pathway, involved in degrading leucine, valine, and isoleucine (Ito et al. 1990; Luís et al. 2011). While the mechanism(s) of action of valproic acid are still not understood, valproic acid structurally resembles the natural substrate of ACADSB, the metabolite 2-methylbutyryl-CoA, and has been shown to competitively inhibit ACADSB (Luís et al. 2011; Činčárová, Zdráhal, and Fajkus 2013). Therefore, valproic acid may be a candidate anti-influenza drug against ACADSB. As valproic acid affects multiple pathways and enzymes, it has substantial side effects. However, for the purposes of an acute, relatively short-lived IAV infection, the benefit valproic acid may have to fighting infection is probably greater than the potential side effects. Therefore, as an already tested and approved therapy with dosage and regimes established in humans, valproic acid could have great potential as an antiviral, either by itself or in combination with other antivirals.

CIC Negatively Regulates Cell Intrinsic Immunity

Perhaps the most note-worthy result of the CRISPR screen was the hit CIC, which modulates immune control of multiple viral families. CIC is a transcriptional repressor that regulates gene expression in response to receptor tyrosine kinase signaling. We observed that CIC was pivotal for replication of *Orthomyxoviruses, Rhabdoviruses,*

Flaviviruses, and *Picornaviruses,* and loss of CIC highly upregulated expression of immunity and inflammation genes, rendering CIC KO cells robustly resistant to viral infection. We hypothesize that CIC negatively regulates the innate immune response. CIC repressed binding sites endogenous in MxA and IFIT1 promoters, lending evidence that CIC may be directly repressing promoters of certain antiviral genes in order to control type I IFN signaling. Finally, CIC mRNA and protein were downregulated upon IAV infection, further supporting the hypothesis of CIC as a negative regulator of the antiviral state by revealing the regulation of CIC to activate defense systems in response to infection (Han et al. 2018). As discussed in detail in Chapter IV, further research into the role of CIC in regulating antiviral and inflammation pathways, using techniques such as EMSA, ChIPseq, RNAseq of CIC/STAT1 double KO cells, and RTK/EGFR inhibitors, will reveal the targets and mechanism by which CIC represses these states as well as identify the signal and pathway necessary for alleviating CIC mediated repression in the context of viral infection, augmenting our fundamental knowledge of the immune response to pathogens.

How can CIC be controlling broad defense responses to pathogens, including sensing of RNA and DNA viruses, intracellular bacteria, and parasites, type I IFN signaling, and inflammasome activation? Is CIC a true global regulator of immunity and inflammation, or is it a potent regulator of a central node, such as type I IFN signaling, that affects and potentiates other pathways through cross-talk? For instance, during RNA virus sensing, RIG-I can signal through ASC to induce caspase1 and the inflammasome, thus connecting type I IFN signaling and inflammasome activation (Poeck et al. 2010). Though,

RIG-I itself is induced by type I IFN signaling—is inflammasome activation part of the type I IFN-mediated antiviral state (Kopitar-Jerala 2017)? Moreover, the DNA virus sensor IFI-16 is one of the most robustly upregulated genes in CIC KO cells. IFI16 also activates multiple pathways, including the inflammasome, the NFκB gene program, and type I IFN signaling, and is itself induced by IFNγ (Dell'Oste et al. 2015; Kerur et al. 2011; Unterholzner et al. 2010; Orzalli, DeLuca, and Knipe 2012). These circuitous pathways regulated by CIC are true chicken-and-egg scenarios and must be solved by ChIPseq to undeniably detect CIC repression of endogenous promoters.

CIC studies *in vivo* will be crucial for cementing the importance of CIC during viral infection. CIC-L KO mice and hematopoietic lineage-specific CIC full KO mice show upregulated IFNγ and pro-inflammatory cytokines, supporting our observations of upregulated immunity and inflammation pathways in CIC KO cells, and suggesting that CIC may regulate immune activation and autoimmune diseases *in vivo* (Kim et al. 2015; S. Park et al. 2017; Tan et al. 2018). Through future IAV infections in CIC-L KO mice, we will determine whether CIC-L is important for *in vivo* infection. We expect that IAV infection will be stunted in CIC-L KO mice, as aberrantly upregulated inflammation pathways and potentially upregulated antiviral pathways should defend against IAV infection. However, if we do not observe IAV replication differences in CIC-L KO mice, then perhaps CIC-S may be the isoform important for modulating antiviral pathways. Also, CIC-L KO mice die within 4-5 weeks of birth, most likely due to lung defects and bile acid disequilibrium (S. Park et al. 2017). In addition, these lung defects in CIC-L KO mice may pose a caveat to interpreting flu infection results. Potential differences in viral replication in CIC-L KO mice

could be due to viral restriction by the immune system or mere physical restrictions in IAV transmission throughout the lungs.

Our work demonstrates a new but complementary function of CIC, in regulating responses to intracellular pathogens. Our observations that CIC suppresses aberrant expression of antiviral and inflammatory genes can also be applied to explain and unify the mechanisms of CIC's role in autoimmunity and cancer. Indeed, several sarcomas and gliomas have been linked to mutations found in CIC (Kawamura-Saito et al. 2006; Bettegowda et al. 2011; Chittaranjan et al. 2014; Simón-Carrasco et al. 2018). Aberrant deregulation of CIC or loss of CIC function observed in some autoimmunity and cancer states can increase pro-inflammatory and immunity genes, advancing these diseases.

As CIC controls progression to multiple severe disease pathways, targeting regulators of CIC with antivirals may be risky, though this remains possible for acute treatment. Perhaps if our future studies can pinpoint the mechanism to selectively release CIC's control of immune genes while maintaining cell growth checkpoints, then we can attempt to target those kinases to specifically release CIC's hold on the subset of immunity genes, amplifying the host's defense responses to viral infection.

Genetic Reassortment and the Role of Rab11a

One of IAV's most potent strategies is genetic reassortment, by which IAV spawns a vast repertoire of genetic variants that confound containment efforts. How and when does IAV reassort its genome, and how are these dynamics orchestrated? To investigate this

question, we generated the first NP-tagged virus in order to monitor the RNP packaging process. Our studies illuminated the importance of the microtubule cytoskeleton and the recycling endosome trafficking factor Rab11a in polarized, coordinated, and clustered egress of RNP complexes from nucleus to plasma membrane.

Crucially, our work revealed a novel function for the Rab11a GTPase in RNP egress; Rab11a is imperative for clustering RNPs in the cytoplasm in order to produce infectious particles. Rab11a may even serve as a target for delivery of RNPs from the nucleus to the cytoplasm, as the nuclei of Rab11a KO cells were enriched for RNPs. Without Rab11a, virions no longer contained the correct number or proportion of RNP segments, resulting in defective particles. Therefore, Rab11a may play an important scaffolding role in selectively packaging RNP segments, aiding reassortment of IAV. Using live cell microscopy and collaborating with the Lowen lab at Emory University to assess reassortment dynamics, our future studies will investigate the involvement of Rab11a on selective packaging and its potential ability to drive reassortment.

Is Rab11a a druggable target? A small molecule drug still in the experimental phase, the GTP analog 5'-Guanosine-diphosphate-monothiophosphate, is purported to inhibit Rab11a (DrugBank database version 5.1.1, www.drugbank.ca). However, there are many small GTPases, and they have myriad functions throughout the cell. For example, there are 60 members in the largest family of GTPases, the Rab GTPases, and they are involved in most intracellular membrane trafficking events (Stenmark 2009). Hence, as a GTP analog, 5'-Guanosine-diphosphate-monothiophosphate may have too many off-

target effects. More research will decipher whether this small molecule is specific enough to Rab11a to be effective, and if the potential antiviral effects outweigh the side effects.

Concluding Remarks

Influenza viruses are constantly evolving targets. IAV usurps host pathways during its intracellular life cycle, and pandemic strains must be able to gain access to these pathways in new organisms during cross-species transmission. Therefore, uncovering the molecular basis of pandemic IAV strains is central to our preparedness against pandemics. Throughout my thesis work, I have thoroughly explored the virus:host interaction network of the potentially pandemic strain H5N1, identifying and characterizing host factors, including a novel regulator of cell intrinsic immunity, and defining new roles for already known host factors. These findings elicit druggable host factors for IAV, augmenting our potential antiviral stockpile. Moreover, this work enhances our understanding of central pillars of the immune response, broadening the scope of this research to the control of multiple viruses and potentially other disease states.

BIBLIOGRAPHY

Ajuria, Leiore, Claudia Nieva, Clint Winkler, Dennis Kuo, Núria Samper, María José Andreu, Aharon Helman, et al. 2011. “Capicua DNA-Binding Sites Are General Response Elements for RTK Signaling in Drosophila.” *Development (Cambridge, England)* 138 (5): 915–24. doi:10.1242/dev.057729.

Amorim, Maria Joao, Emily a Bruce, Eliot K C Read, Agnes Foeglein, Robert Mahen, Amanda D Stuart, and Paul Digard. 2011. “A Rab11- and Microtubule-Dependent Mechanism for Cytoplasmic Transport of Influenza A Virus Viral RNA.” *Journal of Virology* 85 (9): 4143–56. doi:10.1128/JVI.02606-10.

Avilov, Sergiy V, Dorothée Moisy, Nadia Naffakh, and Stephen Cusack. 2012. “Influenza A Virus Progeny VRNP Trafficking in Live Infected Cells Studied with the Virus-Encoded Fluorescently Tagged PB2 Protein.” *Vaccine* 30 (51). Elsevier Ltd: 7411–17. doi:10.1016/j.vaccine.2012.09.077.

Baggen, Jim, Hendrik Jan Thibaut, Jacqueline Staring, Lucas T Jae, Yue Liu, Hongbo Guo, Jasper J Slager, et al. 2016. “Enterovirus D68 Receptor Requirements Unveiled by Haploid Genetics.” *Proceedings of the National Academy of Sciences of the United States of America* 113 (5). United States: 1399–1404. doi:10.1073/pnas.1524498113.

Belser, Jessica A., and M. Terrence. 2018. “The 1918 Flu, 100 Years Later.” *Science* 359 (6373): 255. doi:10.1126/science.aas9565.

Benitez, Asiel A, Maryline Panis, Jia Xue, Andrew Varble, Jaehee V Shim, Amy L Frick, Carolina B Lopez, David Sachs, and Benjamin R tenOever. 2015. “In Vivo RNAi

Screening Identifies MDA5 as a Significant Contributor to the Cellular Defense against Influenza A Virus." *Cell Reports* 11 (11). United States: 1714–26. doi:10.1016/j.celrep.2015.05.032.

Bettegowda, Chetan, Nishant Agrawal, Yuchen Jiao, Mark Sausen, Laura D. Wood, Ralph H. Hruban, Fausto J. Rodriguez, et al. 2011. "Mutations in CIC and FUBP1 Contribute to Human Oligodendroglioma." *Science* 21 (September): 1453–56.

Bowman, Aaron B, Yung C Lam, Paymaan Jafar-Nejad, Hung-Kai Chen, Ronald Richman, Rodney C Samaco, John D Fryer, Juliette J Kahle, Harry T Orr, and Huda Y Zoghbi. 2007. "Duplication of Atxn1l Suppresses SCA1 Neuropathology by Decreasing Incorporation of Polyglutamine-Expanded Ataxin-1 into Native Complexes." *Nature Genetics* 39 (3): 373–79. doi:10.1038/ng1977.

Brass, a L, I C Huang, Y Benita, S P John, M N Krishnan, E M Feeley, B J Ryan, et al. 2009. "The IFITM Proteins Mediate Cellular Resistance to Influenza A H1N1 Virus, West Nile Virus, and Dengue Virus." *Cell* 139: 1243–54. doi:10.1016/j.cell.2009.12.017.

Bruce, Emily a, Paul Digard, and Amanda D Stuart. 2010. "The Rab11 Pathway Is Required for Influenza A Virus Budding and Filament Formation." *Journal of Virology* 84 (12): 5848–59. doi:10.1128/JVI.00307-10.

Castillo-Lluva, Sonia, Michael H Tatham, Richard C Jones, Ellis G Jaffray, Ricky D Edmondson, Ronald T Hay, and Angeliki Malliri. 2010. "SUMOylation of the GTPase Rac1 Is Required for Optimal Cell Migration." *Nature Cell Biology* 12 (October). Nature Publishing Group, a division of Macmillan Publishers Limited. All Rights Reserved.: 1078. http://dx.doi.org/10.1038/ncb2112.

"Centers for Disease Control and Prevention." 2011. "Antiviral Agents for the Treatment and Chemoprophylaxis of Influenza --- Recommendations of the Advisory Committee on Immunization Practices (ACIP)." *MMWR. Recommendations and Reports : Morbidity and Mortality Weekly Report. Recommendations and Reports / Centers for Disease Control* 60 (1): 1–24. doi:10.1086/598513.

———. 2017a. "CDC: Influenza Antiviral Medications: Summary for Clinicians." *Centers for Disease Control*. http://www.cdc.gov.ez.urosario.edu.co/flu/professionals/antivirals/summary-clinicians.htm.

———. 2017b. "Pandemic Influenza Plan - Update IV (December 2017)." *Office of the Assistant Secretary for Preparedness, HHS*. https://www.cdc.gov/flu/pandemic-resources/pdf/pan-flu-report-2017v2.pdf.

Chan, Renee W Y, Michael C W Chan, Adam C N Wong, Rositsa Karamanska, Anne Dell, Stuart M. Haslam, Alan D L Sihoe, et al. 2009. "DAS181 Inhibits H5N1 Influenza Virus Infection of Human Lung Tissues." *Antimicrobial Agents and Chemotherapy* 53 (9): 3935–41. doi:10.1128/AAC.00389-09.

Chan, Ying Kai, and Michaela U. Gack. 2016. "Viral Evasion of Intracellular DNA and RNA Sensing." *Nature Reviews Microbiology* 14 (6). Nature Publishing Group: 360–73. doi:10.1038/nrmicro.2016.45.

Chittaranjan, Suganthi, Susanna Chan, Cindy Yang, Kevin C Yang, Vincent Chen, Annie Moradian, Marlo Firme, et al. 2014. "Mutations in CIC and IDH1 Cooperatively Regulate 2-Hydroxyglutarate Levels and Cell Clonogenicity." *Oncotarget* 5 (17): 7960–79.

Chou, Yi Ying, Nicholas S. Heaton, Qinshan Gao, Peter Palese, Robert Singer, and Timothée Lionnet. 2013. “Colocalization of Different Influenza Viral RNA Segments in the Cytoplasm before Viral Budding as Shown by Single-Molecule Sensitivity FISH Analysis.” *PLoS Pathogens* 9 (5). doi:10.1371/journal.ppat.1003358.

Chu, Victor C, and Gary R Whittaker. 2004. “Influenza Virus Entry and Infection Require Host Cell N-Linked Glycoprotein.” *Proceedings of the National Academy of Sciences of the United States of America* 101 (52). United States: 18153–58. doi:10.1073/pnas.0405172102.

Činčárová, Lenka, Zbyněk Zdráhal, and Jiří Fajkus. 2013. “New Perspectives of Valproic Acid in Clinical Practice.” *Expert Opinion on Investigational Drugs* 22 (12). Taylor & Francis: 1535–47. doi:10.1517/13543784.2013.853037.

Crespo-Barreto, Juan, John D. Fryer, Chad A. Shaw, Harry T. Orr, and Huda Y. Zoghbi. 2010. “Partial Loss of Ataxin-1 Function Contributes to Transcriptional Dysregulation in Spinocerebellar Ataxia Type 1 Pathogenesis.” *PLoS Genetics* 6 (7): 1–17. doi:10.1371/journal.pgen.1001021.

De Castro Martin, Isabel Fernández, Guillaume Fournier, Martin Sachse, Javier Pizarro-Cerda, Cristina Risco, and Nadia Naffakh. 2017. “Influenza Virus Genome Reaches the Plasma Membrane via a Modified Endoplasmic Reticulum and Rab11-Dependent Vesicles.” *Nature Communications* 8 (1). Springer US. doi:10.1038/s41467-017-01557-6.

de Vries, E., R. P. de Vries, M. J. Wienholts, C. E. Floris, M.-S. Jacobs, A. van den Heuvel, P. J. M. Rottier, and C. A. M. de Haan. 2012. “Influenza A Virus Entry into Cells Lacking Sialylated N-Glycans.” *Proceedings of the National Academy of*

Sciences 109 (19): 7457–62. doi:10.1073/pnas.1200987109.

Dell'Oste, Valentina, Deborah Gatti, Alessandro G. Giorgio, Marisa Gariglio, Santo Landolfo, and Marco De Andrea. 2015. "The Interferon-Inducible DNA-Sensor Protein IFI16: A Key Player in the Antiviral Response." *New Microbiologica* 38 (1): 5–20.

Desai, Tanay M., Mariana Marin, Christopher R. Chin, George Savidis, Abraham L. Brass, and Gregory B. Melikyan. 2014. "IFITM3 Restricts Influenza A Virus Entry by Blocking the Formation of Fusion Pores Following Virus-Endosome Hemifusion." *PLoS Pathogens* 10 (4): e1004048. doi:10.1371/journal.ppat.1004048.

Dissanayake, Kumara, Rachel Toth, Jamie Blakey, Olof Olsson, David G. Campbell, Alan R. Prescott, and Carol MacKintosh. 2011. "ERK/P90 ^{RSK} /14-3-3 Signalling Has an Impact on Expression of PEA3 Ets Transcription Factors via the Transcriptional Repressor Capicúa." *Biochemical Journal* 433 (3): 515–25. doi:10.1042/BJ20101562.

Doudna, Jennifer, and Emmanuelle Charpentier. 2014. "The New Frontier of Genome Engineering with CRISPR-Cas9." *Science* 346 (6213). doi:10.1126/science.1258096.

Eisfeld, Amie J, Eiryo Kawakami, Tokiko Watanabe, Gabriele Neumann, and Yoshihiro Kawaoka. 2011. "RAB11A Is Essential for Transport of the Influenza Virus Genome to the Plasma Membrane." *Journal of Virology* 85 (13): 6117–26. doi:10.1128/JVI.00378-11.

Eisfeld, Amie J, Gabriele Neumann, and Yoshihiro Kawaoka. 2014. "At the Centre: Influenza A Virus Ribonucleoproteins." *Nature Reviews Microbiology*, no.

November (November). Nature Publishing Group. doi:10.1038/nrmicro3367.

Ferguson, Lucas, Alicia K. Olivier, Suzanne Genova, William B. Epperson, David R. Smith, Liesel Schneider, Kathleen Barton, Katlin McCuan, Richard J. Webby, and Xiu-Feng Wan. 2016. “Pathogenesis of Influenza D Virus in Cattle.” *Journal of Virology* 90 (March): JVI.03122-15. doi:10.1128/JVI.03122-15.

Ferris, Martin T., David L. Aylor, Daniel Bottomly, Alan C. Whitmore, Lauri D. Aicher, Timothy A. Bell, Birgit Bradel-Tretheway, et al. 2013. “Modeling Host Genetic Regulation of Influenza Pathogenesis in the Collaborative Cross.” *PLoS Pathogens* 9 (2). doi:10.1371/journal.ppat.1003196.

Fores, Marta, Lucia Simon-Carrasco, Leiore Ajuria, Nuria Samper, Sergio Gonzalez-Crespo, Matthias Drosten, Mariano Barbacid, and Gerardo Jimenez. 2017. “A New Mode of DNA Binding Distinguishes Capicua from Other HMG-Box Factors and Explains Its Mutation Patterns in Cancer.” *PLoS Genetics* 13 (3): 1–22. doi:10.1371/journal.pgen.1006622.

Fryer, J. D., P. Yu, H. Kang, C. Mandel-Brehm, A. N. Carter, J. Crespo-Barreto, Y. Gao, et al. 2011. “Exercise and Genetic Rescue of SCA1 via the Transcriptional Repressor Capicua.” *Science* 334 (6056): 690–93. doi:10.1126/science.1212673.

Fryer, John D, Peng Yu, Hyojin Kang, Caleigh Mandel-brehm, Angela N Carter, Juan Crespo-barreto, Yan Gao, Adriano Flora, and Chad Shaw. 2011. “Exercise and Genetic Rescue of SCA1 via the Transcriptional Repressor Capicua.” *Science* 334 (November): 690–93.

Futran, Alan S., Saw Kyin, Stanislav Y. Shvartsman, and a. James Link. 2015. “Mapping the Binding Interface of ERK and Transcriptional Repressor Capicua

Using Photocrosslinking." *Proceedings of the National Academy of Sciences* 112 (28): 201501373. doi:10.1073/pnas.1501373112.

Gack, Michaela U., Randy Allen Albrecht, Tomohiko Urano, Kyung-Soo Inn, I-Chueh Huang, Elena Carnero, Michael Farzan, Satoshi Inoue, Jae Ung Jung, and Adolfo García-Sastre. 2009. "Influenza A Virus NS1 Targets the Ubiquitin Ligase TRIM25 to Evade Recognition by the Host Viral RNA Sensor RIG-I." *Cell Host & Microbe* 5 (5): 439–49. doi:10.1016/j.chom.2009.04.006.

Gack, Michaela U., Young C. Shin, Chul Hyun Joo, Tomohiko Urano, Chengyu Liang, Lijun Sun, Osamu Takeuchi, et al. 2007. "TRIM25 RING-Finger E3 Ubiquitin Ligase Is Essential for RIG-I-Mediated Antiviral Activity." *Nature* 446 (7138): 916–20. doi:10.1038/nature05732.

Gamblin, S. J., and J. J. Skehel. 2010. "Influenza Hemagglutinin and Neuraminidase Membrane Glycoproteins." *Journal of Biological Chemistry* 285 (37): 28403–9. doi:10.1074/jbc.R110.129809.

Gebre, Makda, Jason L. Nomburg, and Benjamin E. Gewurz. 2018. "Crispr–Cas9 Genetic Analysis of Virus–Host Interactions." *Viruses* 10 (2): 1–22. doi:10.3390/v10020055.

Gerber, Marie, Catherine Isel, Vincent Moules, and Roland Marquet. 2014. "Selective Packaging of the Influenza A Genome and Consequences for Genetic Reassortment." *Trends in Microbiology* 22 (8). Elsevier Ltd: 446–55. doi:10.1016/j.tim.2014.04.001.

Giese, Sebastian, Hardin Bolte, and Martin Schwemmle. 2016. "The Feat of Packaging Eight Unique Genome Segments." *Viruses* 8 (6): 165. doi:10.3390/v8060165.

Grant, Alesha, Sanket S. Ponia, Shashank Tripathi, Vinod Balasubramaniam, Lisa Miorin, Marion Sourisseau, Megan C. Schwarz, et al. 2016. “Zika Virus Targets Human STAT2 to Inhibit Type i Interferon Signaling.” *Cell Host and Microbe* 19 (6): 882–90. doi:10.1016/j.chom.2016.05.009.

Grimm, O., V. S. Zini, Y. Kim, J. Casanova, S. Y. Shvartsman, and E. Wieschaus. 2012. “Torso RTK Controls Capicua Degradation by Changing Its Subcellular Localization.” *Development* 139 (21): 3962–68. doi:10.1242/dev.084327.

Guichard, Annabel, Victor Nizet, and Ethan Bier. 2014. “RAB11-Mediated Trafficking in Host-Pathogen Interactions.” *Nature Reviews. Microbiology* 12 (9): 624–34. doi:10.1038/nrmicro3325.

Hadley, Barbara, Andrea Maggioni, Angel Ashikov, Christopher J. Day, Thomas Haselhorst, and Joe Tiralongo. 2014. “Structure and Function of Nucleotide Sugar Transporters: Current Progress.” *Computational and Structural Biotechnology Journal* 10 (16). Elsevier B.V.: 23–32. doi:10.1016/j.csbj.2014.05.003.

Haller, Otto, Peter Staeheli, Martin Schwemmle, and Georg Kochs. 2015. “Mx GTPases: Dynamin-like Antiviral Machines of Innate Immunity.” *Trends in Microbiology*, January. Elsevier Ltd, 1–10. doi:10.1016/j.tim.2014.12.003.

Han, Julianna, Jasmine Perez, Adam Schafer, Han Cheng, Norton Peet, and Lijun Rong. 2017. “Influenza Virus: Small Molecule Therapeutics and Mechanisms of Antiviral Resistance.” *Current Medicinal Chemistry* in revision.

Han, Julianna, Jasmine T Perez, Cindy Chen, Yan Li, Asiel Benitez, Matheswaran Kandasamy, Yoontae Lee, Jorge Andrade, Benjamin R. TenOever, and Balaji Manicassamy. 2018. “Genome-Wide CRISPR / Cas9 Screen Identifies Host

Factors Essential for Influenza Virus Replication." *Cell Reports* 23 (2). ElsevierCompany.: 596–607. doi:10.1016/j.celrep.2018.03.045.

Hao, Linhui, Akira Sakurai, Tokiko Watanabe, Ericka Sorensen, Chairul a Nidom, Michael a Newton, Paul Ahlquist, and Yoshihiro Kawaoka. 2008. "Drosophila RNAi Screen Identifies Host Genes Important for Influenza Virus Replication." *Nature* 454. doi:10.1038/nature.

Hause, Ben M., Mariette Ducatez, Emily A. Collin, Zhiguang Ran, Runxia Liu, Zizhang Sheng, Anibal Armien, et al. 2013. "Isolation of a Novel Swine Influenza Virus from Oklahoma in 2011 Which Is Distantly Related to Human Influenza C Viruses." *PLoS Pathogens* 9 (2). doi:10.1371/journal.ppat.1003176.

Heaton, Brook E, Edward M Kennedy, Rebekah E Dumm, Alfred T Harding, Matthew T Sacco, David Sachs, and Nicholas S Heaton. 2017. "A CRISPR Activation Screen Identifies a Pan-Avian Influenza Virus Inhibitory Host Factor." *Cell Reports* 20 (7). ElsevierCompany.: 1503–12. doi:10.1016/j.celrep.2017.07.060.

Heaton, N. S., V. H. Leyva-Grado, G. S. Tan, D. Eggink, R. Hai, and P. Palese. 2013. "In Vivo Bioluminescent Imaging of Influenza A Virus Infection and Characterization of Novel Cross-Protective Monoclonal Antibodies." *Journal of Virology* 87 (15): 8272–81. doi:10.1128/JVI.00969-13.

Hoffmann, Carsten, Guido Gaietta, Moritz Bünemann, Stephen R. Adams, Silke Oberdorff-Maass, Björn Behr, Jean Pierre Vilardaga, Roger Y. Tsien, Mark H. Ellisman, and Martin J. Lohse. 2005. "A FlAsH-Based FRET Approach to Determine G Protein-Coupled Receptor Activation in Living Cells." *Nature Methods* 2 (3): 171–76. doi:10.1038/nmeth742.

Hoffmann, Carsten, Guido Gaietta, Alexander Zürn, Stephen R. Adams, Sonia Terrillon, Mark H. Ellisman, Roger Y. Tsien, and Martin J. Lohse. 2010. “Fluorescent Labeling of Tetracysteine-Tagged Proteins in Intact Cells.” *Nature Protocols* 5 (10). Nature Publishing Group: 1666–77. doi:10.1038/nprot.2010.129.

“Homeland Security Council.” 2005. “National Strategy for Pandemic Influenza.”

Horgan, Conor P, Sara R Hanscom, Rushee S Jolly, Clare E Futter, and Mary W McCaffrey. 2010. “Rab11-FIP3 Links the Rab11 GTPase and Cytoplasmic Dynein to Mediate Transport to the Endosomal-Recycling Compartment.” *Journal of Cell Science* 123 (Pt 2): 181–91. doi:10.1242/jcs.052670.

Huang, Li, Tao Xiong, Huibin Yu, Quan Zhang, Kunli Zhang, Changyao Li, Liang Hu, et al. 2017. “Encephalomyocarditis Virus 3C Protease Attenuates Type I Interferon Production through Disrupting the TANK–TBK1–IKKε–IRF3 Complex.” *Biochemical Journal* 474 (12): 2051–65. doi:10.1042/BCJ20161037.

Hurt, Aeron C. 2014. “The Epidemiology and Spread of Drug Resistant Human Influenza Viruses.” *Current Opinion in Virology* 8. Elsevier B.V.: 22–29. doi:10.1016/j.coviro.2014.04.009.

Hutchinson, Edward C, and Ervin Fodor. 2013. “Transport of the Influenza Virus Genome from Nucleus to Nucleus.” *Viruses* 5 (10): 2424–46. doi:10.3390/v5102424.

“International Committee on Taxonomy of Viruses: Orthomyxoviridae Current Taxonomy 2015.” 2017. Accessed May 3. https://talk.ictvonline.org/ictv-reports/ictv_online_report/positive-sense-rna-viruses/w/flaviviridae/360/genus-flavivirus.

Ishino, Y, H Shinagawa, K Makino, M Amemura, and A Nakata. 1987. “Nucleotide Sequence of the Iap Gene, Responsible for Alkaline Phosphatase Isozyme Conversion in Escherichia Coli, and Identification of the Gene Product.” *Journal of Bacteriology* 169 (12): 5429–33. doi:10.1128/jb.169.12.5429-5433.1987.

Ito, Michinori, Yasuyuki Ikeda, John G. Arnez, Gaetano Finocchiaro, and Kay Tanaka. 1990. “The Enzymatic Basis for the Metabolism and Inhibitory Effects of Valproic Acid: Dehydrogenation of Valproyl-CoA by 2-Methyl-Branched-Chain Acyl-CoA Dehydrogenase.” *BBA - General Subjects* 1034 (2): 213–18. doi:10.1016/0304-4165(90)90079-C.

Iwasaki, Akiko, and Padmini S. Pillai. 2014. “Innate Immunity to Influenza Virus Infection.” *Nature Reviews Immunology* 14 (5). Nature Publishing Group: 315–28. doi:10.1038/nri3665.

Jiménez, Gerardo, Stanislav Y. Shvartsman, and Ze’ev Paroush. 2012. “The Capicua Repressor--a General Sensor of RTK Signaling in Development and Disease.” *Journal of Cell Science* 125 (Pt 6): 1383–91. doi:10.1242/jcs.092965.

Karlas, Alexander, Nikolaus Machuy, Yujin Shin, Klaus-Peter Pleissner, Anita Artarini, Dagmar Heuer, Daniel Becker, et al. 2010. “Genome-Wide RNAi Screen Identifies Human Host Factors Crucial for Influenza Virus Replication.” *Nature* 463 (February): 818–22. doi:10.1038/nature08760.

Kawamura-Saito, Miho, Yukari Yamazaki, Keiko Kaneko, Noriyoshi Kawaguchi, Hiroaki Kanda, Hiroyuki Mukai, Takahiro Gotoh, et al. 2006. “Fusion between CIC and DUX4 Up-Regulates PEA3 Family Genes in Ewing-like Sarcomas with t(4;19)(Q35;Q13) Translocation.” *Human Molecular Genetics* 15 (13): 2125–37.

doi:10.1093/hmg/ddl136.

Kerur, Nagaraj, Mohanan Valiya Veettil, Neelam Sharma-Walia, Virginie Bottero, Sathish Sadagopan, Pushpalatha Otageri, and Bala Chandran. 2011. “IFI16 Acts as a Nuclear Pathogen Sensor to Induce the Inflammasome in Response to Kaposi Sarcoma-Associated Herpesvirus Infection.” *Cell Host and Microbe* 9 (5). Elsevier Inc.: 363–75. doi:10.1016/j.chom.2011.04.008.

Kim, Eunjeong, Sungjun Park, Nahyun Choi, Jieon Lee, Jeehyun Yoe, Soeun Kim, Hoe-Yune Jung, et al. 2015. “Deficiency of Capicua Disrupts Bile Acid Homeostasis.” *Scientific Reports* 5: 8272. doi:10.1038/srep08272.

König, Renate, Silke Stertz, Yingyao Zhou, Atsushi Inoue, H-Heinrich Hoffmann, Suchita Bhattacharyya, Judith G Alamares, et al. 2010. “Human Host Factors Required for Influenza Virus Replication.” *Nature* 463 (February): 813–17. doi:10.1038/nature08699.

Kopitar-Jerala, Nataša. 2017. “The Role of Interferons in Inflammation and Inflammasome Activation.” *Frontiers in Immunology* 8 (JUL). doi:10.3389/fimmu.2017.00873.

Krammer, Florian, and Peter Palese. 2015. “Advances in the Development of Influenza Virus Vaccines.” *Nature Reviews Drug Discovery* 14 (March): 167–82. doi:10.1038/nrd4529.

Lakdawala, Seema S., Ervin Fodor, and Kanta Subbarao. 2016. “Moving On Out: Transport and Packaging of Influenza Viral RNA into Virions.” *Annual Review of Virology* 3 (1): 411–27. doi:10.1146/annurev-virology-110615-042345.

Lakdawala, Seema S, Yicong Wu, Peter Wawrzusin, Juraj Kabat, Andrew J Broadbent,

Elaine W Lamirande, Ervin Fodor, Nihal Altan-Bonnet, Hari Shroff, and Kanta Subbarao. 2014. “Influenza a Virus Assembly Intermediates Fuse in the Cytoplasm.” *PLoS Pathogens* 10 (3): e1003971. doi:10.1371/journal.ppat.1003971.

Lam, Yung C., Aaron B. Bowman, Paymaan Jafar-Nejad, Janghoo Lim, Ronald Richman, John D. Fryer, Eric D. Hyun, et al. 2006. “ATAXIN-1 Interacts with the Repressor Capicua in Its Native Complex to Cause SCA1 Neuropathology.” *Cell* 127 (7): 1335–47. doi:10.1016/j.cell.2006.11.038.

Lee, Ching Jung, Wai In Chan, Martin Cheung, Yi Chuan Cheng, Vanessa J. Appleby, Alex T. Orme, and Paul J. Scotting. 2002. “CIC, a Member of a Novel Subfamily of the HMG-Box Superfamily, Is Transiently Expressed in Developing Granule Neurons.” *Molecular Brain Research* 106 (1–2): 151–56. doi:10.1016/S0169-328X(02)00439-4.

Lee, Yoontae, John D. Fryer, Hyojin Kang, Juan Crespo-Barreto, Aaron B. Bowman, Yan Gao, Juliette J. Kahle, et al. 2011. “ATXN1 Protein Family and CIC Regulate Extracellular Matrix Remodeling and Lung Alveolarization.” *Developmental Cell* 21 (4). Elsevier Inc.: 746–57. doi:10.1016/j.devcel.2011.08.017.

Li, Wei, Han Xu, Tengfei Xiao, Le Cong, Michael I Love, Feng Zhang, Rafael A Irizarry, Jun S Liu, Myles Brown, and X Shirley Liu. 2014. “MAGeCK Enables Robust Identification of Essential Genes from Genome-Scale CRISPR/Cas9 Knockout Screens.” *Genome Biology* 15 (12): 554. doi:10.1186/s13059-014-0554-4.

Liberzon, Arthur, Aravind Subramanian, Reid Pinchback, Helga Thorvaldsdóttir, Pablo Tamayo, and Jill P. Mesirov. 2011. “Molecular Signatures Database (MSigDB) 3.0.” *Bioinformatics* 27 (12): 1739–40. doi:10.1093/bioinformatics/btr260.

Liu, Shu-lin, Li-juan Zhang, Zhi-gang Wang, Zhi-ling Zhang, Qiu-mei Wu, En-ze Sun, Yun-bo Shi, and Dai-wen Pang. 2015. “Globally Visualizing the Microtubule-Dependent Transport Behaviors of In Fl Uenza Virus in Live Cells.”

Loscher, Wolfgang. 1999. “The Discovery of Valproate.” In *Milestones in Drug Therapy*, edited by Wolfgang Loscher. Basel: Birkhäuser, Basel. doi:10.1007/978-3-0348-8759-5_1.

Lu, Hsiang-Chih, Qiumin Tan, Maxime W C Rousseaux, Wei Wang, Ji-Yoen Kim, Ronald Richman, Ying-Wooi Wan, et al. 2017. “Disruption of the ATXN1–CIC Complex Causes a Spectrum of Neurobehavioral Phenotypes in Mice and Humans.” *Nature Genetics* 49 (4). Nature Publishing Group: 527–36. doi:10.1038/ng.3808.

Luís, Paula B.M., Jos P.N. Ruiter, Lodewijk IJlst, Isabel Tavares De Almeida, Marinus Duran, Al Walid Mohsen, Jerry Vockley, Ronald J.A. Wanders, and Margarida F.B. Silva. 2011. “Role of Isovaleryl-CoA Dehydrogenase and Short Branched-Chain Acyl-CoA Dehydrogenase in the Metabolism of Valproic Acid: Implications for the Branched-Chain Amino Acid Oxidation Pathway.” *Drug Metabolism and Disposition* 39 (7): 1155–60. doi:10.1124/dmd.110.037606.

Ma, Chunlong, Cinque S. Soto, Yuki Ohigashi, Albert Taylor, Vasilios Bournas, Brett Glawe, Maria K. Udo, William F. DeGrado, Robert A. Lamb, and Lawrence H. Pinto. 2008. “Identification of the Pore-Lining Residues of the BM2 Ion Channel Protein of Influenza B Virus.” *Journal of Biological Chemistry* 283 (23): 15921–31. doi:10.1074/jbc.M710302200.

Ma, Hongming, Ying Dang, Yonggan Wu, Gengxiang Jia, Edgar Anaya, Junli Zhang,

Sojan Abraham, et al. 2015. “A CRISPR-Based Screen Identifies Genes Essential for West-Nile-Virus-Induced Cell Death.” *Cell Reports* 12 (4). The Authors: 673–83. doi:10.1016/j.celrep.2015.06.049.

Malakhov, Michael P, Laura M Aschenbrenner, F Donald, Miles K Wandersee, Robert W Sidwell, V Larisa, Vasiliy P Mishin, et al. 2006. “Sialidase Fusion Protein as a Novel Broad-Spectrum Inhibitor of Influenza Virus Infection Sialidase Fusion Protein as a Novel Broad-Spectrum Inhibitor of Influenza Virus Infection.” *Antimicrobial Agents and Chemotherapy* 50 (4): 1470–79. doi:10.1128/AAC.50.4.1470.

Manicassamy, B., S. Manicassamy, A. Belicha-Villanueva, G. Pisanelli, B. Pulendran, and A. Garcia-Sastre. 2010. “Analysis of in Vivo Dynamics of Influenza Virus Infection in Mice Using a GFP Reporter Virus.” *Proceedings of the National Academy of Sciences* 107 (25): 11531–36. doi:10.1073/pnas.0914994107.

Marceau, Caleb D., Andreas S. Puschnik, Karim Majzoub, Yaw Shin Ooi, Susan M. Brewer, Gabriele Fuchs, Kavya Swaminathan, et al. 2016. “Genetic Dissection of Flaviviridae Host Factors through Genome-Scale CRISPR Screens.” *Nature* 535 (7610). Nature Publishing Group: 159–63. doi:10.1038/nature18631.

Mehle, Andrew, and Jennifer A. Doudna. 2010. “A Host of Factors Regulating Influenza Virus Replication.” *Viruses* 2 (2): 566–73. doi:10.3390/v2020566.

Momose, Fumitaka, Yuji Kikuchi, Katsuhiro Komase, and Yuko Morikawa. 2007. “Visualization of Microtubule-Mediated Transport of Influenza Viral Progeny Ribonucleoprotein.” *Microbes and Infection / Institut Pasteur* 9 (12–13): 1422–33. doi:10.1016/j.micinf.2007.07.007.

Momose, Fumitaka, Tetsuya Sekimoto, Takashi Ohkura, Shuichi Jo, Atsushi Kawaguchi, Kyosuke Nagata, and Yuko Morikawa. 2011. “Apical Transport of Influenza A Virus Ribonucleoprotein Requires Rab11-Positive Recycling Endosome.” *PloS One* 6 (6): e21123. doi:10.1371/journal.pone.0021123.

Nakagawa, Koji, and Hideyoshi Yokosawa. 2002. “PIAS3 Induces SUMO-1 Modification and Transcriptional Repression of IRF-1.” *FEBS Letters* 530 (1–3). England: 204–8.

Nistal-Villan, Estanislao, Michaela U Gack, Gustavo Martinez-Delgado, Natalya P Maharaj, Kyung-Soo Inn, Heyi Yang, Rong Wang, Aneel K Aggarwal, Jae U Jung, and Adolfo Garcia-Sastre. 2010. “Negative Role of RIG-I Serine 8 Phosphorylation in the Regulation of Interferon-Beta Production.” *The Journal of Biological Chemistry* 285 (26). United States: 20252–61. doi:10.1074/jbc.M109.089912.

Nturibi, Eric, Amar R. Bhagwat, Stefanie Coburn, Mike M. Myerburg, and Seema S. Lakdawala. 2017. “Intracellular Colocalization of Influenza Viral RNA and Rab11A Is Dependent upon Microtubule Filaments.” *Journal of Virology*, no. July: JVI.01179-17. doi:10.1128/JVI.01179-17.

Okimoto, Ross A, Frank Breitenbuecher, Victor R Olivas, Wei Wu, Beatrice Gini, Matan Hofree, Saurabh Asthana, et al. 2017. “Inactivation of Capicua Drives Cancer Metastasis” 49 (1). doi:10.1038/ng.3728.

Orchard, Robert C., Craig B. Wilen, John G. Doench, Megan T. Baldridge, Broc T. McCune, Ying Chiang J. Lee, Sanghyun Lee, et al. 2016. “Discovery of a Proteinaceous Cellular Receptor for a Norovirus.” *Science* 353 (6302): 933–36. doi:10.1126/science.aaf1220.

Orzalli, M. H., N. A. DeLuca, and D. M. Knipe. 2012. “Nuclear IFI16 Induction of IRF-3

Signaling during Herpesviral Infection and Degradation of IFI16 by the Viral ICP0 Protein." *Proceedings of the National Academy of Sciences* 109 (44): E3008–17. doi:10.1073/pnas.1211302109.

Pages, H, P Aboyoun, R Gentleman, and S DebRoy. n.d. "Biostrings: String Objects Representing Biological Sequences, and Matching Algorithms." R package version 2.42.1.

Pal, Sangita, Andres Santos, Juan M. Rosas, Joshua Ortiz-Guzman, and Germán Rosas-Acosta. 2011. "Influenza A Virus Interacts Extensively with the Cellular SUMOylation System during Infection." *Virus Research* 158 (1–2). Elsevier B.V.: 12–27. doi:10.1016/j.virusres.2011.02.017.

Papagianni, Aikaterini, Marta Forés, Wanqing Shao, Shuonan He, Nina Koenecke, and María José. 2018. "Capicua Controls Toll / IL-1 Signaling Targets Independently of RTK Regulation" 115 (8). doi:10.1073/pnas.1713930115.

Park, Ryan J., Tim Wang, Dylan Koundakjian, Judd F. Hultquist, Pedro Lamothe-Molina, Blandine Monel, Kathrin Schumann, et al. 2017. "A Genome-Wide CRISPR Screen Identifies a Restricted Set of HIV Host Dependency Factors." *Nature Genetics* 49 (2). Nature Publishing Group: 193–203. doi:10.1038/ng.3741.

Park, Sungjun, Seungwon Lee, Choong-Gu Lee, Guk Yeol Park, Hyebeen Hong, Jeon-Soo Lee, Young Min Kim, et al. 2017. "Capicua Deficiency Induces Autoimmunity and Promotes Follicular Helper T Cell Differentiation via Derepression of ETV5." *Nature Communications* 8 (May). Nature Publishing Group: 16037. doi:10.1038/ncomms16037.

Pavlovic, Jovan, Thomas Zurcher, Otto Haller, and Peter Staeheli. 1990. "Resistance to

Influenza Virus and Vesicular Stomatitis Virus Conferred by Expression of Human MxA Protein . Resistance to Influenza Virus and Vesicular Stomatitis Virus Conferred by Expression of Human MxA Protein" 64 (7): 3370–75.

Perez, Jasmine T., Adolfo Garćia-Sastre, and Balaji Manicassamy. 2013. "Insertion of a GFP Reporter Gene in Influenza Virus." *Current Protocols in Microbiology*, no. SUPPL.29: 1–16. doi:10.1002/9780471729259.mc15g04s29.

Perreira, Jill M, Paul Meraner, and Abraham L Brass. 2016. "Functional Genomic Strategies for Elucidating Human-Virus Interactions: Will CRISPR Knockout RNAi and Haploid Cells?" *Advances in Virus Research* 94. United States: 1–51. doi:10.1016/bs.aivir.2015.11.001.

Pichler, Andrea, Chronis Fatouros, Heekyoung Lee, and Nathalie Eisenhardt. 2017. "SUMO Conjugation - A Mechanistic View." *Biomolecular Concepts* 8 (1): 13–36. doi:10.1515/bmc-2016-0030.

Pinto, Lawrence H., and Robert A. Lamb. 2006. "The M2 Proton Channels of Influenza A and B Viruses." *Journal of Biological Chemistry* 281 (14): 8997–9000. doi:10.1074/jbc.R500020200.

Pleschka, Stephan. 2008. "RNA Viruses and the Mitogenic Raf/MEK/ERK Signal Transduction Cascade." *Biological Chemistry* 389 (10): 1273–82. doi:10.1515/BC.2008.145.

Poeck, Hendrik, Michael Bscheider, Olaf Gross, Katrin Finger, Susanne Roth, Manuele Rebsamen, Nicole Hannesschläger, et al. 2010. "Recognition of RNA Virus by RIG-I Results in Activation of CARD9 and Inflammasome Signaling for Interleukin 1B Production." *Nature Immunology* 11 (1): 63–69. doi:10.1038/ni.1824.

Rillahan, Cory D., Aristotelis Antonopoulos, Craig T. Lefort, Roberto Sonon, Parastoo Azadi, Klaus Ley, Anne Dell, Stuart M. Haslam, and James C. Paulson. 2012. “Global Metabolic Inhibitors of Sialyl- and Fucosyltransferases Remodel the Glycome.” *Nature Chemical Biology* 8 (7). Nature Publishing Group: 661–68. doi:10.1038/nchembio.999.

Sanjana, Neville E, Ophir Shalem, and Feng Zhang. 2014. “Improved Vectors and Genome-Wide Libraries for CRISPR Screening.” *Nature Methods* 11 (July). Nature Publishing Group, a division of Macmillan Publishers Limited. All Rights Reserved.: 783. http://dx.doi.org/10.1038/nmeth.3047.

Savidis, George, William M Mcdougall, Paul Meraner, Sharone Green, Timothy F Kowalik, Abraham L Brass, George Savidis, et al. 2016. “Identification of Zika Virus and Dengue Virus Dependency Factors Using Functional Genomics Resource Identification of Zika Virus and Dengue Virus Dependency Factors Using Functional Genomics.” *CellReports* 16 (1). ElsevierCompany.: 1–15. doi:10.1016/j.celrep.2016.06.028.

Schneider, William M, Meike Dittmann Chevillotte, and Charles M Rice. 2014. “Interferon-Stimulated Genes: A Complex Web of Host Defenses.” *Annual Review of Immunology* 32: 513–45. doi:10.1146/annurev-immunol-032713-120231.

Schuster, A, I C Johnston, T Das, A K Banerjee, J Pavlovic, V ter Meulen, and S Schneider-Schaulies. 1996. “Expression of the Human MxA Protein Is Associated with Hyperphosphorylation of VSV P Protein in Human Neural Cells.” *Virology* 220 (1): 241–45. doi:10.1006/viro.1996.0308.

Schwemmle, Martin, Kirsten C. Weining, Marc F. Richter, Beats Schumacher, and Peter

Staeheli. 1995. “Vesicular Stomatitis Virus Transcription Inhibited by Purified MxA Protein.” *Virology* 206 (1): 545–54. doi:10.1016/S0042-6822(95)80071-9.

Shalem, Ophir, Neville E Sanjana, Ella Hartenian, Xi Shi, David a Scott, Tarjei S Mikkelsen, Dirk Heckl, et al. 2014. “Genome-Scale CRISPR-Cas9 Knockout Screening in Human Cells.” *Science (New York, N.Y.)* 343 (6166): 84–87. doi:10.1126/science.1247005.

Shapira, Sagi D., Irit Gat-Viks, Bennett O V Shum, Amelie Dricot, Marciela M. de Grace, Liguo Wu, Piyush B. Gupta, et al. 2009. “A Physical and Regulatory Map of Host-Influenza Interactions Reveals Pathways in H1N1 Infection.” *Cell* 139 (7). Elsevier Ltd: 1255–67. doi:10.1016/j.cell.2009.12.018.

Sharma, Sumana, and Evangelia Petsalaki. 2018. “Application of CRISPR-Cas9 Based Genome-Wide Screening Approaches to Study Cellular Signalling Mechanisms.” *International Journal of Molecular Sciences* 19 (4). doi:10.3390/ijms19040933.

Shaw, Megan L;, and Peter Palese. 2013. “Orthomyxoviridae: The Viruses and Their Replication.” In *Fields Virology*, edited by D.M. Knipe and P.M. Howley, 6th ed., 1647–89. Philadelphia: Lippincott Williams & Wilkins.

Shi, Yi, Ying Wu, Wei Zhang, Jianxun Qi, and George F Gao. 2014. “Enabling the ‘Host Jump’: Structural Determinants of Receptor-Binding Specificity in Influenza A Viruses.” *Nature Reviews. Microbiology* 12 (12). Nature Publishing Group: 822–31. doi:10.1038/nrmicro3362.

Simón-Carrasco, Lucía, Gerardo Jiménez, Mariano Barbacid, and Matthias Drosten. 2018. “The Capicua Tumor Suppressor: A Gatekeeper of Ras Signaling in Development and Cancer.” *Cell Cycle (Georgetown, Tex.)* 4101: 1–33.

doi:10.1080/15384101.2018.1450029.

Steel, John, Anice C Lowen, Lindomar Pena, Matthew Angel, Alicia Solorzano, Randy Albrecht, Daniel R Perez, Adolfo Garcia-Sastre, and Peter Palese. 2009. “Live Attenuated Influenza Viruses Containing NS1 Truncations as Vaccine Candidates against H5N1 Highly Pathogenic Avian Influenza.” *Journal of Virology* 83 (4). United States: 1742–53. doi:10.1128/JVI.01920-08.

Stenmark, Harald. 2009. “Rab GTPases as Coordinators of Vesicle Traffic.” *Nature Reviews Molecular Cell Biology* 10 (8). Nature Publishing Group: 513–25. doi:10.1038/nrm2728.

Stertz, Silke, and Megan L. Shaw. 2011. “Uncovering the Global Host Cell Requirements for Influenza Virus Replication via RNAi Screening.” *Microbes and Infection* 13 (5). Elsevier Masson SAS: 516–25. doi:10.1016/j.micinf.2011.01.012.

Stojdl, David F., Brian D. Lichty, Benjamin R. TenOever, Jennifer M. Paterson, Anthony T. Power, Shane Knowles, Ricardo Marius, et al. 2003. “VSV Strains with Defects in Their Ability to Shutdown Innate Immunity Are Potent Systemic Anti-Cancer Agents.” *Cancer Cell* 4 (4): 263–75. doi:10.1016/S1535-6108(03)00241-1.

Su, Wen-Chi, Yung-Chia Chen, Chung-Hsin Tseng, Paul Wei-Che Hsu, Kuo-Feng Tung, King-Song Jeng, and Michael M C Lai. 2013. “Pooled RNAi Screen Identifies Ubiquitin Ligase Itch as Crucial for Influenza A Virus Release from the Endosome during Virus Entry.” *Proceedings of the National Academy of Sciences of the United States of America* 110 (43). United States: 17516–21. doi:10.1073/pnas.1312374110.

Subramanian, A., P. Tamayo, V. K. Mootha, S. Mukherjee, B. L. Ebert, M. A. Gillette, A.

Paulovich, et al. 2005. “Gene Set Enrichment Analysis: A Knowledge-Based Approach for Interpreting Genome-Wide Expression Profiles.” *Proceedings of the National Academy of Sciences* 102 (43): 15545–50. doi:10.1073/pnas.0506580102.

Sui, Baoquan, Douty Bamba, Ke Weng, Huong Ung, Shaojing Chang, Jessica Van Dyke, Michael Goldblatt, Roxanne Duan, Michael S Kinch, and Wu-Bo Li. 2009. “The Use of Random Homozygous Gene Perturbation to Identify Novel Host-Oriented Targets for Influenza.” *Virology* 387 (2). United States: 473–81. doi:10.1016/j.virol.2009.02.046.

Suisse, Annabelle, Danqing He, Kevin Legent, and Jessica E Treisman. 2017. “COP9 Signalosome Subunits Protect Capicua from MAPK-Dependent and -Independent Mechanisms of Degradation,” 2673–82. doi:10.1242/dev.148767.

Sun, Lijun, Siqi Liu, and Zhijian J. Chen. 2010. “SnapShot: Pathways of Antiviral Innate Immunity.” *Cell* 140 (3): 436–436.e2. doi:10.1016/j.cell.2010.01.041.

Tan, Qiumin, Lorenzo Brunetti, Maxime W C Rousseaux, Hsiang-chih Lu, and Ying-wooi Wan. 2018. “Loss of Capicua Alters Early T Cell Development and Predisposes Mice to T Cell Lymphoblastic Leukemia / Lymphoma,” 1511–19. doi:10.1073/pnas.1716452115.

Taubenberger, J K, and D M Morens. 2009. “Pandemic Influenza--Including a Risk Assessment of H5N1.” *Rev Sci Tech* 28 (1): 187–202. doi:10.1016/j.bbi.2008.05.010.

Triana-Baltzer, Gallen B., Larisa V. Gubareva, John M. Nicholls, Melissa B. Pearce, Vasiliy P. Mishin, Jessica A. Belser, Li Mei Chen, et al. 2009. “Novel Pandemic Influenza A(H1N1) Viruses Are Potently Inhibited by DAS181, a Sialidase Fusion

Protein.” *PLoS ONE* 4 (11): 12–14. doi:10.1371/journal.pone.0007788.

Tripathi, Shashank, Marie O. Pohl, Yingyao Zhou, Ariel Rodriguez-Frandsen, Guojun Wang, David A. Stein, Hong M. Moulton, et al. 2015. “Meta- and Orthogonal Integration of Influenza ‘OMICs’ Data Defines a Role for UBR4 in Virus Budding.” *Cell Host and Microbe* 18 (6): 723–35. doi:10.1016/j.chom.2015.11.002.

Tscherne, Donna M., Balaji Manicassamy, and Adolfo García-Sastre. 2010. “An Enzymatic Virus-like Particle Assay for Sensitive Detection of Virus Entry.” *Journal of Virological Methods* 163 (2): 336–43. doi:10.1016/j.jviromet.2009.10.020.

Tundup, Smanla, Matheswaran Kandasamy, Jasmine T. Perez, Nacho Mena, John Steel, Tamas Nagy, Randy A. Albrecht, and Balaji Manicassamy. 2017. “Endothelial Cell Tropism Is a Determinant of H5N1 Pathogenesis in Mammalian Species.” *PLoS Pathogens* 13 (3): 1–21. doi:10.1371/journal.ppat.1006270.

Unterholzner, Leonie, Sinead E Keating, Marcin Baran, Kristy A Horan, B Søren, Shruti Sharma, Cherilyn M Sirois, et al. 2010. “IFI16 Is an Innate Immune Sensor for Intracellular DNA.” *Nature Immunology* 11 (11): 997–1004. doi:10.1038/ni.1932.IFI16.

Vale-Costa, S, M Alenquer, A L Sousa, B Kellen, J Ramalho, E M Tranfield, and M J Amorim. 2016. “Influenza A Virus Ribonucleoproteins Modulate Host Recycling by Competing with Rab11 Effectors.” *J Cell Sci*, 1697–1710. doi:10.1242/jcs.188409.

Vale-Costa, Silvia, and Maria Joao Amorim. 2016. “Clustering of Rab11 Vesicles in Influenza A Virus Infected Cells Creates Hotspots Containing the 8 Viral Ribonucleoproteins.” *Small GTPases* 8 (2): 1–7. doi:10.1080/21541248.2016.1199190.

Vale-Costa, Sílvia, and Maria João Amorim. 2017. “Clustering of Rab11 Vesicles in Influenza A Virus Infected Cells Creates Hotspots Containing the 8 Viral Ribonucleoproteins.” *Small GTPases* 8 (2). Taylor & Francis: 71–77. doi:10.1080/21541248.2016.1199190.

Wahlgren, John. 2011. “Influenza A Viruses: An Ecology Review.” *Infection Ecology & Epidemiology* 1: 1–7. doi:10.3402/iee.v1i0.6004.

Wang, Shanshan, Zhendong Zhao, Yuhai Bi, Lei Sun, Xiaoling Liu, and Wenjun Liu. 2013. “Tyrosine 132 Phosphorylation of Influenza A Virus M1 Protein Is Crucial for Virus Replication by Controlling the Nuclear Import of M1.” *Journal of Virology* 87 (11). United States: 6182–91. doi:10.1128/JVI.03024-12.

Wang, Tim, Jenny J Wei, David M Sabatini, and Eric S Lander. 2014. “Genetic Screens in Human Cells Using the CRISPR-Cas9 System.” *Science (New York, N.Y.)* 343 (6166). United States: 80–84. doi:10.1126/science.1246981.

Ward, Samuel E., Hyun Seok Kim, Kakajan Komurov, Saurabh Mendiratta, Pei Ling Tsai, Mirco Schmolke, Neal Satterly, et al. 2012. “Host Modulators of H1N1 Cytopathogenicity.” *PLoS ONE* 7 (8): 1–12. doi:10.1371/journal.pone.0039284.

Watanabe, Tokiko, Eiryo Kawakami, Jason E Shoemaker, Tiago J S Lopes, Yukiko Matsuoka, Yuriko Tomita, Hiroko Kozuka-Hata, et al. 2014. “Influenza Virus-Host Interactome Screen as a Platform for Antiviral Drug Development.” *Cell Host & Microbe* 16 (6). Elsevier Inc.: 795–805. doi:10.1016/j.chom.2014.11.002.

Watanabe, Tokiko, and Yoshihiro Kawaoka. 2015. “Influenza Virus-Host Interactomes as a Basis for Antiviral Drug Development.” *Current Opinion in Virology* 14. Elsevier B.V.: 71–78. doi:10.1016/j.coviro.2015.08.008.

Watanabe, Tokiko, Shinji Watanabe, and Yoshihiro Kawaoka. 2010. “Cellular Networks Involved in the Influenza Virus Life Cycle.” *Cell Host & Microbe* 7 (6). United States: 427–39. doi:10.1016/j.chom.2010.05.008.

Watanabe, Yohei, Madiha S. Ibrahim, Yasuo Suzuki, and Kazuyoshi Ikuta. 2012. “The Changing Nature of Avian Influenza A Virus (H5N1).” *Trends in Microbiology* 20 (1). Elsevier Ltd: 11–20. doi:10.1016/j.tim.2011.10.003.

Wimmer, P., S. Schreiner, and T. Dobner. 2012. “Human Pathogens and the Host Cell SUMOylation System.” *Journal of Virology* 86 (2): 642–54. doi:10.1128/JVI.06227-11.

“World Health Organization.” 2016. “WHO: Influenza (Seasonal) Fact Sheet.” *World Health Organization*. http://www.who.int/mediacentre/factsheets/fs211/en/.

———. 2017. “Pandemic Influenza Risk Management Guidance.”

Wright, Addison V, James K Nunez, and Jennifer A Doudna. 2016. “Biology and Applications of CRISPR Systems: Harnessing Nature’s Toolbox for Genome Engineering.” *Cell* 164 (1–2). United States: 29–44. doi:10.1016/j.cell.2015.12.035.

Wu, Ying, Yan Wu, Boris Tefsen, Yi Shi, and George F. Gao. 2014. “Bat-Derived Influenza-like Viruses H17N10 and H18N11.” *Trends in Microbiology* 22 (4). Elsevier Ltd: 183–91. doi:10.1016/j.tim.2014.01.010.

Xiao, Han, Marian J. Killip, Peter Staeheli, Richard E. Randall, and David Jackson. 2013. “The Human Interferon-Induced MxA Protein Inhibits Early Stages of Influenza A Virus Infection by Retaining the Incoming Viral Genome in the Cytoplasm.” *Journal of Virology* 87 (23): 13053–58. doi:10.1128/JVI.02220-13.

Yu, Guangchuang, and Qing-Yu He. 2016. “ReactomePA: An R/Bioconductor Package

for Reactome Pathway Analysis and Visualization." *Molecular BioSystems* 12 (2). England: 477–79. doi:10.1039/c5mb00663e.

Zenilman, Jonathan M., Edward J. Fuchs, Craig W. Hendrix, Christine Radebaugh, Robert Jurao, Seema U. Nayak, Robert G. Hamilton, and J. McLeod Griffiss. 2015. "Phase 1 Clinical Trials of DAS181, an Inhaled Sialidase, in Healthy Adults." *Antiviral Research* 123. Elsevier B.V.: 114–19. doi:10.1016/j.antiviral.2015.09.008.

Zhang, Rong, Jonathan J. Miner, Matthew J. Gorman, Keiko Rausch, Holly Ramage, James P. White, Adam Zuiani, et al. 2016. "A CRISPR Screen Defines a Signal Peptide Processing Pathway Required by Flaviviruses." *Nature* 535 (7610). Nature Publishing Group: 164–68. doi:10.1038/nature18625.

Zoghbi, Huda Y., and Harry T. Orr. 2009. "Pathogenic Mechanisms of a Polyglutamine-Mediated Neurodegenerative Disease, Spinocerebellar Ataxia Type 1." *Journal of Biological Chemistry* 284 (12): 7425–29. doi:10.1074/jbc.R800041200.

Zürcher, T, J Pavlovic, and P Staeheli. 1992. "Mechanism of Human MxA Protein Action: Variants with Changed Antiviral Properties." *The EMBO Journal* 11 (4): 1657–61. http://www.pubmedcentral.nih.gov/articlerender.fcgi?artid=556616&tool=pmcentrez&rendertype=abstract.

APPENDIX A

Figures

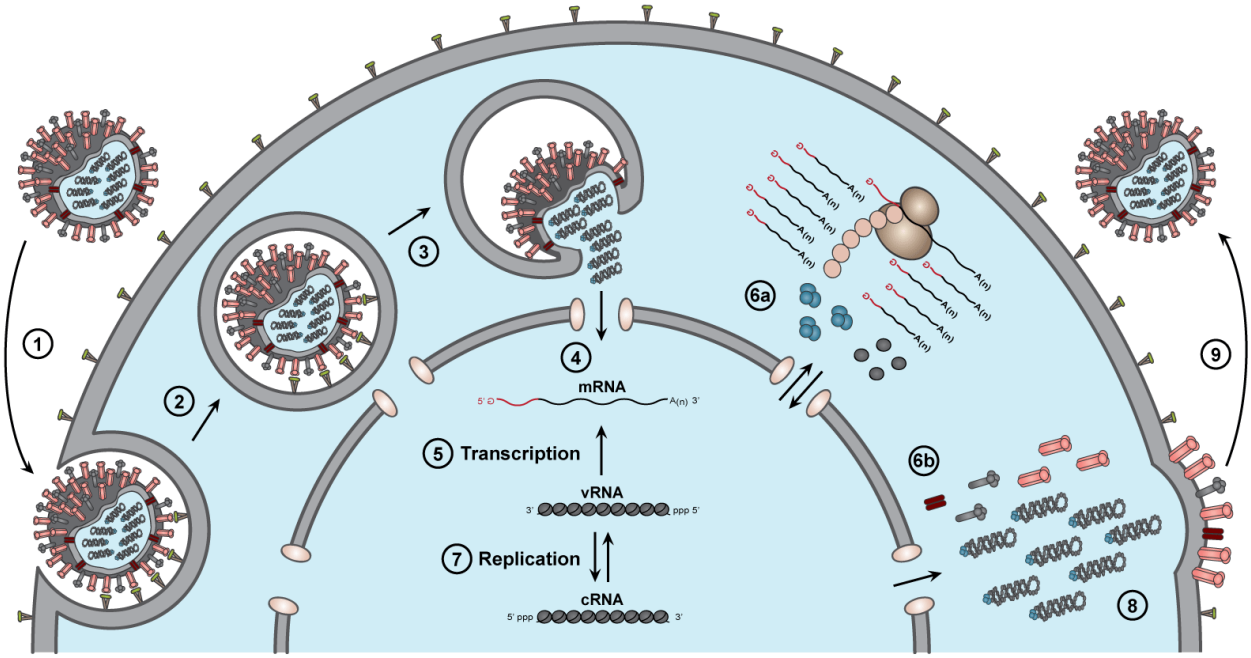
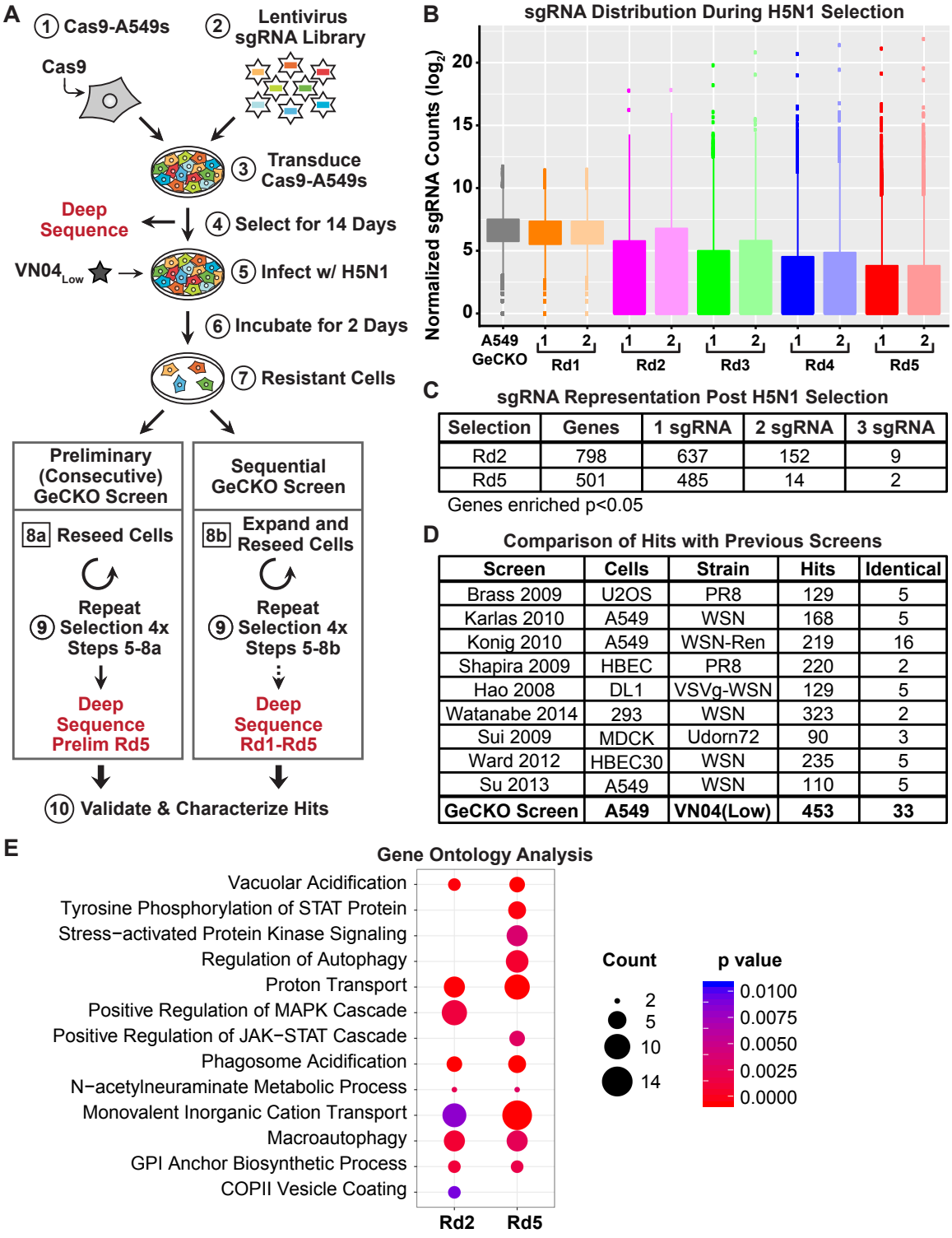


Figure I.1. Intracellular Life Cycle of Influenza Viruses.
Step 1: Binding of influenza virus particle to sialic acid and uptake of virion via endocytosis. Step 2: Acidification of the virion in the endosome for virion disassembly. Step 3: HA-mediated fusion of the viral membrane and endosomal membrane. Step 4: Import of RNP complexes into the nucleus where viral transcription and replication occur. Step 5: Primary viral transcription by genome-associated RdRP complex. Step 6a: Export of viral mRNA and synthesis of viral proteins. Step 6b: Import of newly synthesized viral proteins and trafficking of HA, NA, and M2 to the plasma membrane. Step 7: Replication of viral genome by newly synthesized RdRP proteins. Step 8: Export of RNP complexes from the nucleus to plasma membrane for virion assembly and release. Step 9: Release of virion from plasma membrane.



Selection	Genes	1 sgRNA	2 sgRNA	3 sgRNA
Rd2	798	637	152	9
Rd5	501	485	14	2

Screen	Cells	Strain	Hits	Identical
Brass 2009	U2OS	PR8	129	5
Karlas 2010	A549	WSN	168	5
Konig 2010	A549	WSN-Ren	219	16
Shapira 2009	HBEC	PR8	220	2
Hao 2008	DL1	VSVg-WSN	129	5
Watanabe 2014	293	WSN	323	2
Sui 2009	MDCK	Udorn72	90	3
Ward 2012	HBEC30	WSN	235	5
Su 2013	A549	WSN	110	5
GeCKO Screen	**A549**	**VN04(Low)**	**453**	**33**

Figure III.1. GeCKO Screen for Host Factors Essential for IAV Replication.
(A) Overview of GeCKO screen in human lung epithelial (A549) cells. Steps 1–4: Cas9-expressing A549 (Cas9-A549) cells were transduced with lentivirus containing sgRNA library A and selected for 14 days in puromycin to generate the A549-GeCKO library.

Fig. III.1, continued. Steps 5–7: the A549-GeCKO library was infected with a low-pathogenic H5N1 (VN04Low) to obtain resistant cells. Steps 8a–9: preliminary consecutive screen: surviving cells were subjected to a total of five rounds of H5N1 infection with minimal expansion of resistant cells. Steps 8b–9: sequential screen: surviving cells were subjected to a total of five rounds of H5N1 infection with substantial expansion of resistant cells between each round. Step 10: validation and characterization of selected hits. (B) Boxplot of sgRNA distribution in the A549-GeCKO library and after each round (Rd) of the sequential screen. Biological replicates are shown as Rep1 and Rep2; values are represented in $\log_2$ scale; and sgRNAs are median-normalized to account for differences in total Illumina read counts. Each point represents individual sgRNAs. sgRNAs are distributed by quartile, where the boxes represent the middle quartiles (25%–75% distribution), and the lines and dots represent sgRNAs in the upper and the lower 25% of the distribution. (C) Summary of genes enriched at Rd2 and Rd5 of the sequential screen. sgRNAs enriched during H5N1 selection were identified using the MAGeCK program ($p < 0.05$) and mapped to corresponding genes. (D) Comparison of hits identified at Rd5 of the sequential screen, excluding miRNAs, with nine genome-wide screens performed for IAV. See also Table S2 in Han et al., *Cell Reports,* 2018 (Han et al. 2018). (E) Gene ontology analysis of Rd2 and Rd5 hits from the sequential screen, excluding miRNAs.

A

A549 GeCKO Library	
Reads	sgRNA Counts
9,072,253	62,659

Consecutive Screen (Prelim Rd5)	
Reads	sgRNA Counts
8,138,970	586

Sequential Screen: Rd1-Rd5										
	Rd1		Rd2		Rd3		Rd4		Rd5	
	Reads	sgRNA Counts	Reads	sgRNA Counts	Reads	sgRNA Counts	Reads	sgRNA Counts	Reads	sgRNA Counts
Rep1	11,388,638	61,677	12,612,908	21,336	10,622,535	19,538	12,340,246	18,544	11,975,021	16,875
Rep2	11,344,521	61,864	12,155,402	27,942	11,013,842	24,859	11,102,179	21,452	11,973,987	17,495

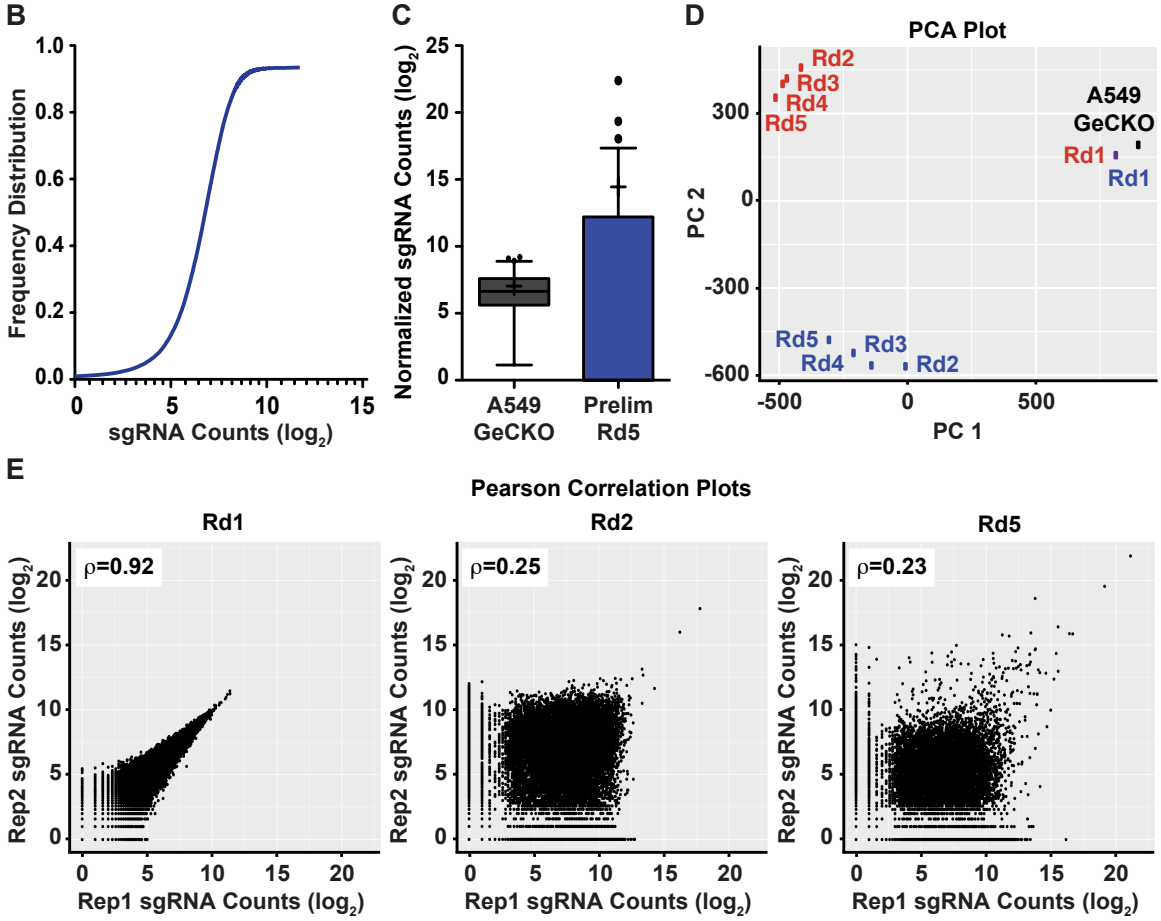


Figure III.2. Analysis of sgRNA Representation in the A549-GeCKO Library and Post H5N1 Selection.

(A) Summary of Illumina reads and sgRNA counts for individual samples. Number of Illumina reads after FastQC analysis and sgRNAs counts (≥10 reads) are shown. (B) Histogram of sgRNA distribution in the A549-GeCKO library. (C) Box plot comparing the sgRNA representation between the A549-GeCKO library and the Preliminary Consecutive Screen (Prelim Rd5). Values are shown in $\log_2$ scale. (D) Principal component analysis of biological replicates at each round (Rd) of the Sequential Screen. A549-GeCKO library is shown in black. Replicate 1 (Rep1) and Replicate 2 (Rep2) are

Fig. III.2, continued. shown in red and blue, respectively. (E) Pearson correlation plots assessing sgRNA representation for biological replicates. A comparison of Rep1 and Rep2 sample sets from Rd1, Rd2 and Rd5 of the Sequential Screen are shown. X and Y axes show sgRNA read counts in the samples (log_2 scale). Pearson correlation coefficients (ρ value) are indicated inside the plots.

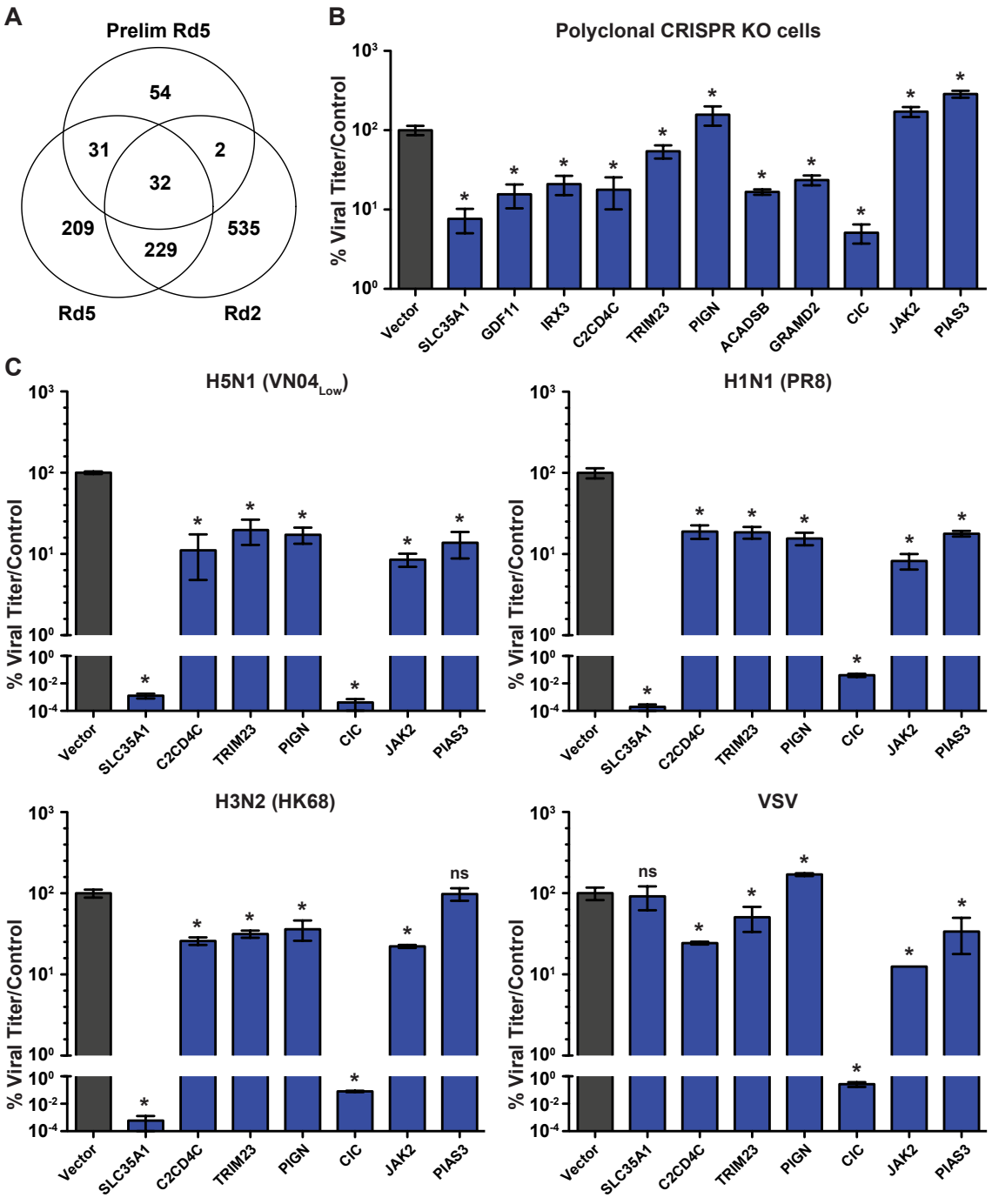


Figure III.3. Validation of Selected Hits with Multiple IAV Strains.
(A) Venn diagram representation of overlapping hits identified in the preliminary consecutive screen (Prelim Rd5) and Rd2 and Rd5 of the sequential screen. See also Table S4 in Han et al., *Cell Reports,* 2018 (Han et al. 2018). (B) Validation of individual hits. Vector control and polyclonal KOs were infected with H5N1 (MOI = 0.001), and viral titers were measured at 48 hpi. (C) Comparison of viral replication. Vector control and clonal KOs were infected with H5N1 (MOI = 0.001), H1N1 (MOI = 0.01), H3N2 (MOI = 0.01), and VSV (MOI = 0.001), and viral titers were measured at 48 hpi. Data are **Fig.**

III.3, continued. represented as a percentage mean titer of triplicate samples relative to vector control cells ± SD. * p-value < 0.05; ns, non-significant. Data are representative of at least three independent experiments. See also Figure III.4.

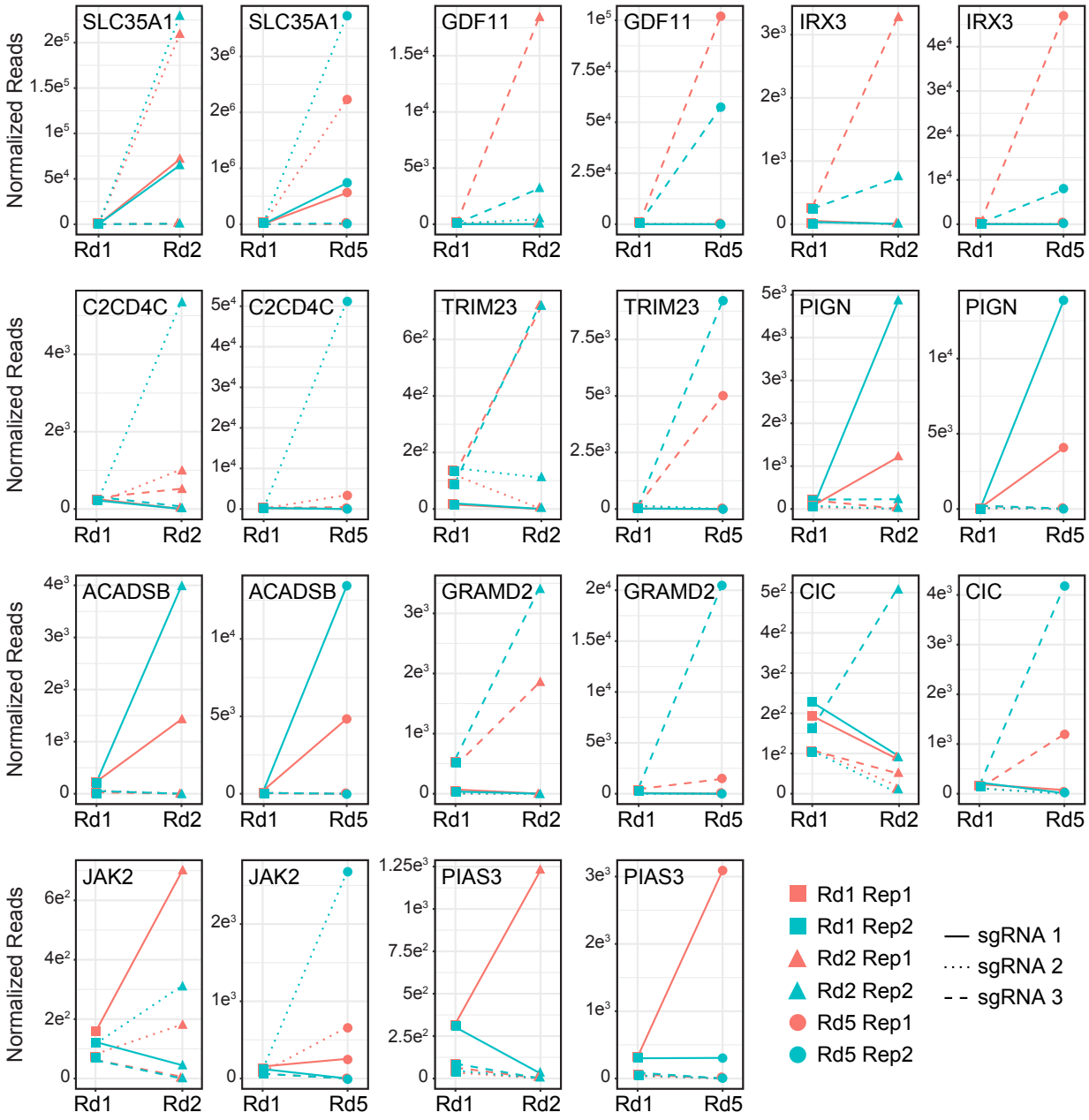


Figure III.4. Depiction of Individual sgRNA Enrichment for Selected Hits. Normalized read counts for individual sgRNAs compared between Rd1 and Rd2 or Rd1 and Rd5 of the Sequential Screen. Rep1 and Rep2 are shown in red and blue, respectively. The three sgRNAs are represented by different dotted lines.

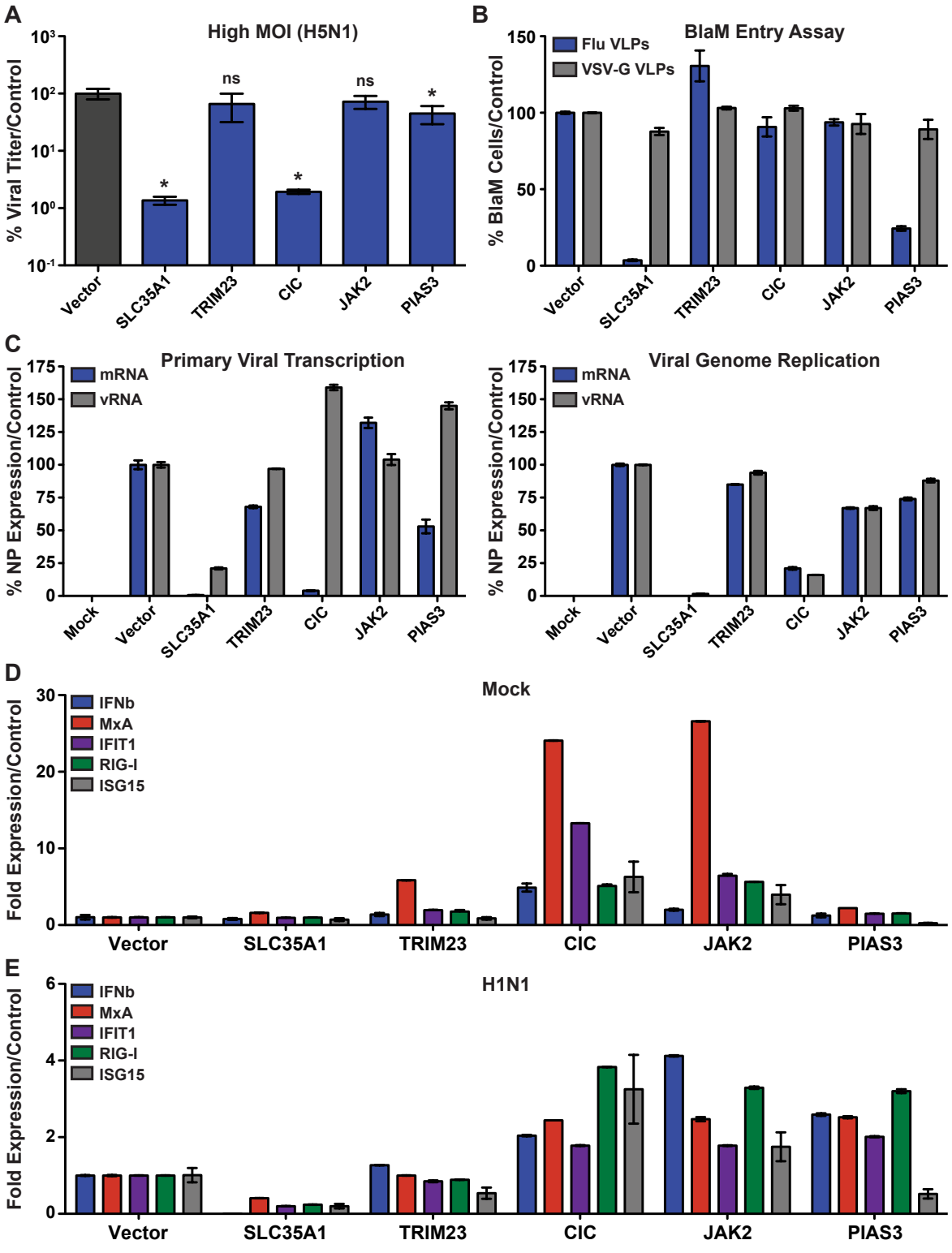


Figure III.5. Identification of Viral Life-Cycle Defects for Selected Hits.
(A) Comparison of viral replication at a high MOI. Vector control and clonal KOs were infected with H5N1 (MOI = 1), and viral titers were measured at 24 hpi. Data are

Fig. III.5, continued. represented as a percentage mean titer of triplicate samples relative to vector control cells ± SD. * p-value < 0.05; ns, non-significant. (B) BlaM VLP entry assay. Vector control and clonal KOs were infected with flu VLPs (HA/NA) or VSV-G VLPs containing a b-lactamase-M1 fusion protein and analyzed by flow cytometry. Values are represented as a percentage of vector control cells ± SD. (C) qRT-PCR analysis of primary viral transcription and viral genome replication. Vector control and clonal KOs were infected with H1N1 (MOI = 3) and NP mRNA, and vRNA levels were analyzed at 3hpi (cycloheximide pretreatment; primary viral transcription) or at 6 hpi (untreated; viral genome replication). Data are represented as a percentage of expression relative to H1N1-infected vector control cells ± SD. (D and E) qRT-PCR analysis of antiviral gene expression in basal (mock) or in H1N1-infected IFNβ conditions. Vector control and clonal KOs were infected with H1N1 (MOI = 5), and mRNA levels for the indicated genes were measured at 16 hpi. Data are represented as the fold expression relative to uninfected (mock) vector control cells ± SD (D) or H1N1-infected vector control cells ± SD (E). Data are representative of at least three independent experiments.

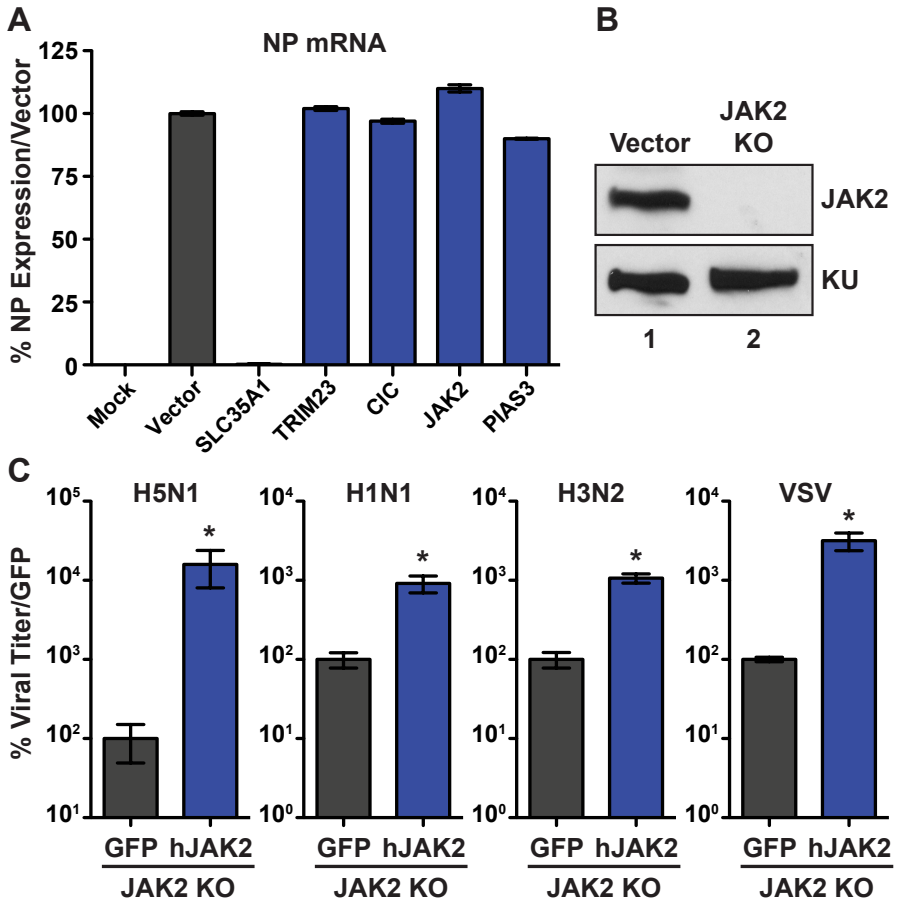


Figure III.6. Complementation of *JAK2* KO cells Increases Viral Replication. (A) NP mRNA levels for antiviral gene expression analysis shown in Figure III.5. Data is represented as percent expression relative to H1N1 infected vector control cells ± SD. (B) Western blot analysis of *JAK2* KO cells. Lysates from vector control or *JAK2* KO cells were subjected to western blot analysis with an anti-JAK2 antibody. Ku levels are shown as loading controls. (C) Expression of *JAK2* cDNA increases viral replication in *JAK2* KO cells. *JAK2* KO cells were complemented with either GFP or hJAK2 expressing vector, infected with H5N1 (MOI=0.001), H1N1 (MOI=0.01), H3N2 (MOI=0.01), and VSV (MOI=0.001), and viral titers were measured at 48hpi. Data are represented as percentage mean titer of triplicate samples relative to GFP expressing *JAK2* KO cells ± SD. * p-value < 0.05. Data are representative of at least three independent experiments.

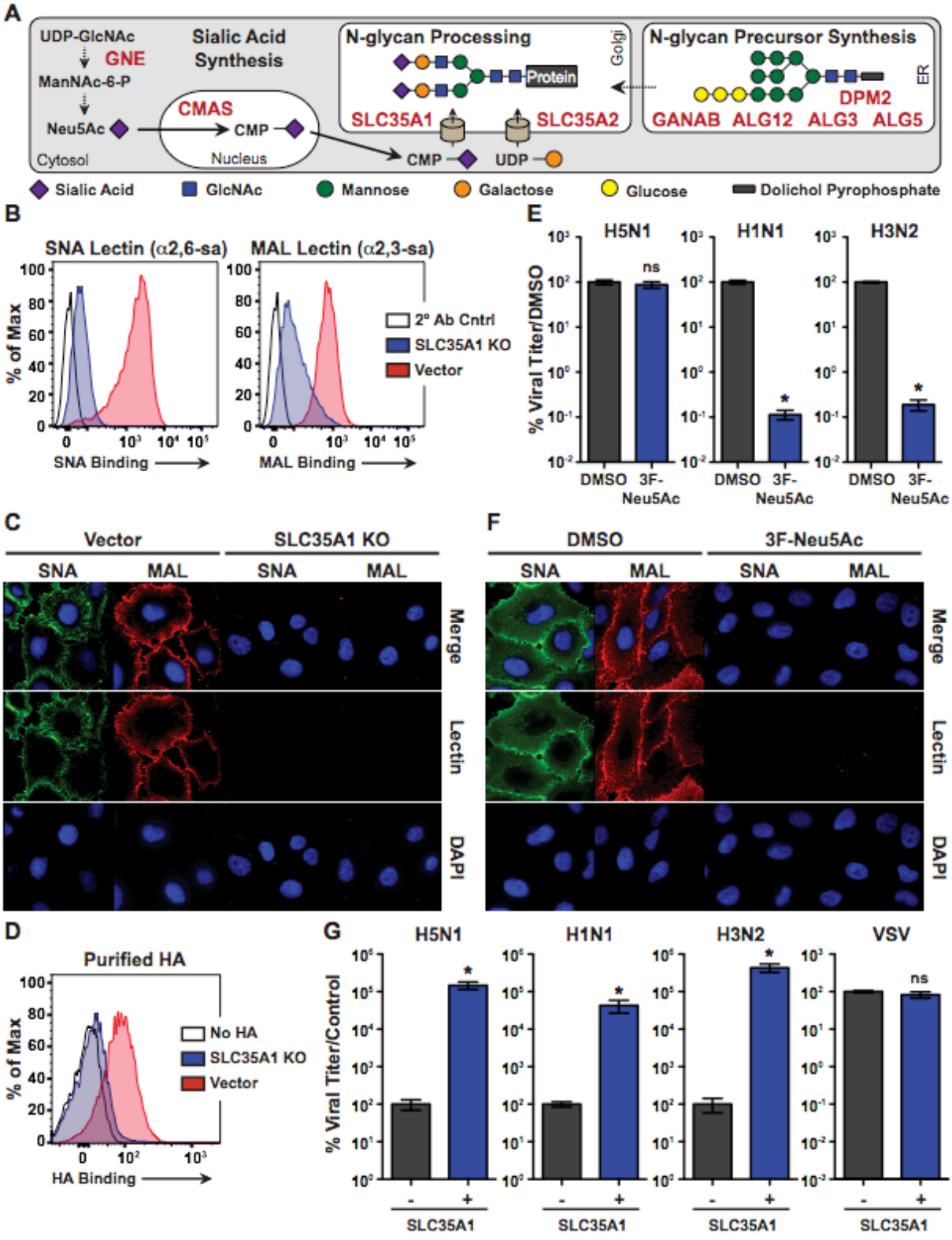


Figure III.7. Sialic Acid Transporter SLC35A1 Is Required for IAV Entry.
Simplified schematic of *de novo* sialic acid biosynthesis and N-glycan processing pathway. Significant genes identified in the GeCKO screen are shown in red.

Fig. III.7, continued. N-acetylglucosamine (GlcNAc), N-acetylmannosamine (ManNAc), and N-acetylneuraminic acid (Neu5Ac), cytidine monophosphate (CMP), and uridine diphosphate (UDP). (B and C) Analysis of sialic acid expression by lectin staining. Vector control and SLC35A1 KOs were treated with lectins that have specificity for 2'-6' (SNA) or 2'-3' (MAL) sialic acids and analyzed by flow cytometry (B) and fluorescent microscopy (C). Histograms depict the intensity of lectin binding relative to cell count. Scale bar, 10 μm. (D) Quantification of HA binding. Vector control and SLC35A1 KOs were incubated with purified HA (H5) and analyzed by flow cytometry. (E) Treatment with sialic acid analog decreases IAV replication. WT A549s were treated with DMSO or 200 μM 3Fax-Peracetyl Neu5Ac (3F-Neu5Ac) for 10 days and infected with the indicated viruses (MOI = 0.1), and viral titers were measured at 18 hpi. (F) Fluorescent microscopy of lectin binding in 3F-Neu5Ac-treated WT A549 cells. SNA and MAL staining was performed as described for (C). Scale bar, 10 μm. (G) Complementation with SLC35A1 cDNA restores IAV replication. SLC35A1 KOs complemented with GFP- or hSLC35A1-expressing vector were infected with H5N1 (MOI = 0.001), H1N1 (MOI = 0.01), H3N2 (MOI = 0.01), and VSV (MOI = 0.001), and viral titers were measured at 48 hpi. Data are represented as mean percentage titer of triplicate samples relative to DMSO-treated WTA549 cells ± SD (E) or GFP-expressing SLC35A1 KOs ±SD (G). * p-value < 0.05; ns, non-significant. Data are representative of at least three independent experiments.

A

Pathway	Gene	Rd2		Rd5	
		p Value	sgRNAs	p Value	sgRNAs
Sialic Acid Biosynthesis	GNE	0.009294	2	0.006349	1
	CMAS	0.003295	2	0.009957	1
N-Glycan Biosynthesis	SLC35A1	2.37E-07	3	2.37E-07	3
	SLC35A2	0.002614	2	0.000267	2
	DPM2	0.001321	3	0.007515	1
	ALG3	0.000866	2	0.00044	2
	ALG5	0.008367	2	0.005932	1
	ALG12	0.045914	1	NS	
	GANAB	NS		0.008286	1
Other Glycan Modifications	A4GALT	0.010851	1	0.005982	1
	B3GAT1	0.031921	1	0.014933	1
	B4GALNT4	NS		0.02268	1
	CHSY1	0.041219	1	0.013057	1
	PIGN	0.001502	1	0.002142	1
	CSGALNACT2	0.00753	2	0.033819	1
	HS3ST6	0.023022	2	0.001233	2

B

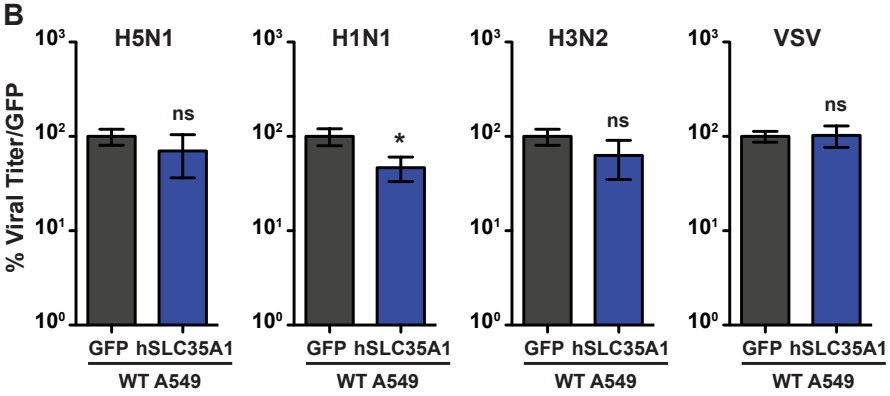


Figure III.8. Enrichment of Host Factors Involved in Sialic Acid Biosynthesis and Related Glycan Modification Pathways. (A) Host factors important for sialic acid biosynthesis and glycan processing identified at Rd2 and Rd5 of the Sequential Screen. Enrichment and number of independent sgRNAs for individual genes are shown. (B) Expression of *SLC35A1* cDNA in WT A549 cells does not alter viral replication. WT A549 cells were transduced with GFP or hSLC35A1 expressing vector, infected with H5N1 (MOI=0.001), H1N1 (MOI=0.01), H3N2 (MOI=0.01), and VSV (MOI=0.001), and viral titers were measured at 48hpi. Data are represented as percentage mean titer of triplicate samples relative to GFP expressing WT A549 cells ± SD. * p-value < 0.05; ns denotes non-significant. Data are representative of at least three independent experiments.

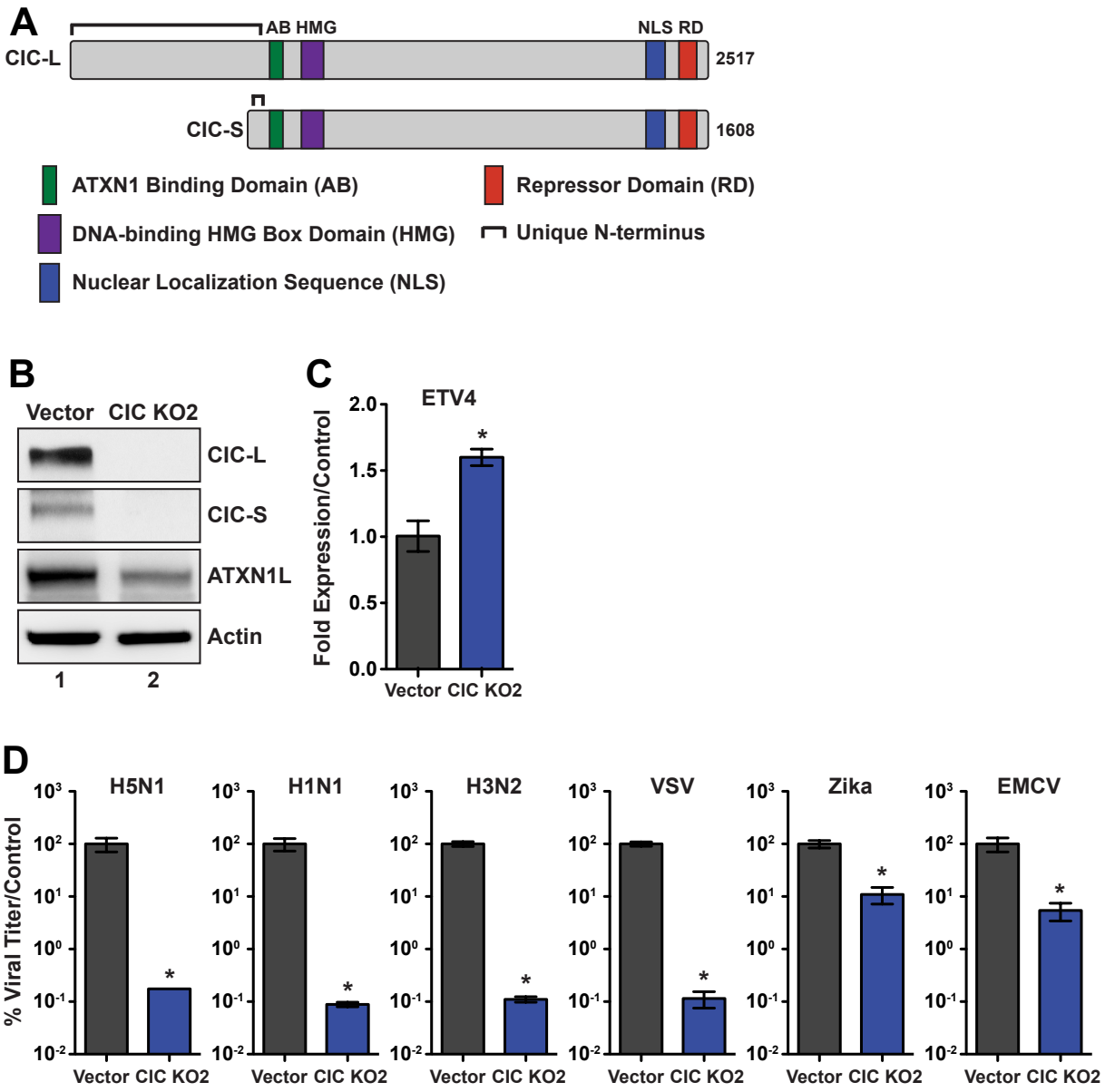


Figure IV.1. Viral Replication is Decreased in CIC KO.
(A) Schematic representation of CIC isoforms. Important functional domains in CIC are indicated. (B) Western blot analysis of *CIC* KO2 cells. Lysates from vector control or *CIC* KO2 cells were subjected to western blot analysis with the indicated antibodies. CIC-Long isoform (CIC-L), CIC-Short isoform (CIC-S) and Ataxin1-Like (ATXN1L) are shown. β-actin levels are shown as loading controls. (C) ETV4 expression is increased in *CIC* KO2 cells. Total RNA was isolated from vector control and *CIC* KO2 cells, and the levels of ETV4 were measured by qRT-PCR. Data is represented as fold expression relative to vector control cells ± SD. * p-value < 0.05. Data are representative of at least three independent experiments. (D) Comparison of viral replication. Vector control or CIC KO2s were infected with H5N1 (MOI = 0.001), H1N1 (MOI = 0.01), H3N2 (MOI = 0.01), VSV (MOI = 0.001), Zika virus (MOI = 0.01), and EMCV (MOI = 0.05) and viral titers were

Fig. IV.1, continued. measured at 48 hpi (EMCV at 24 hpi). Data are represented as a percentage mean titer of triplicate samples relative to vector control cells ± SD.

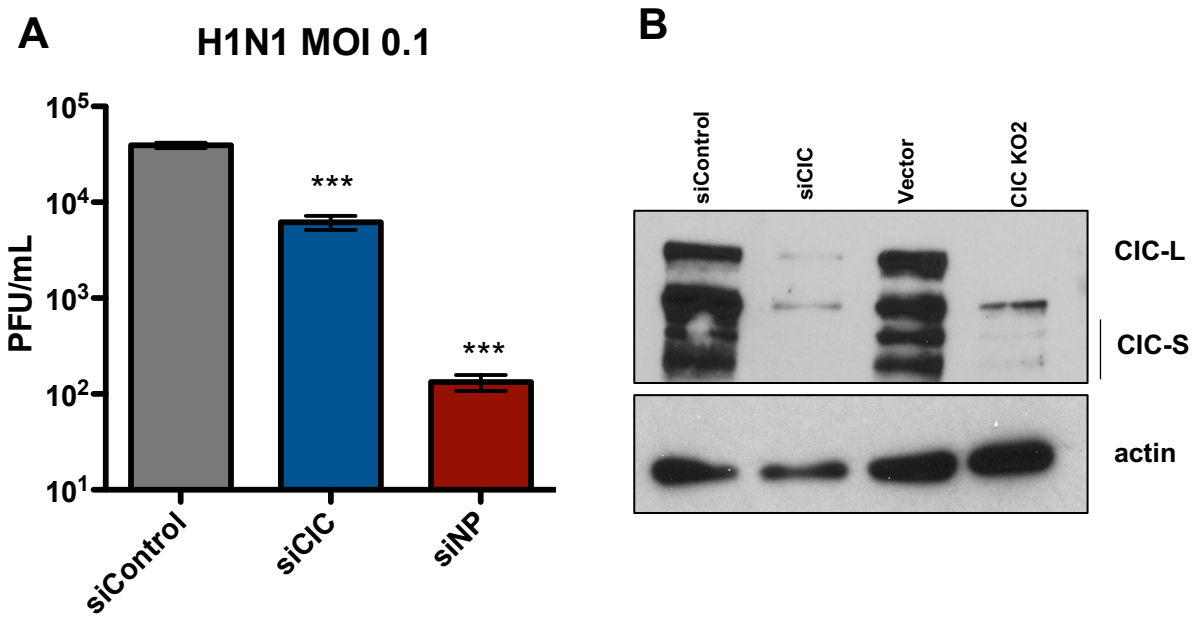


Figure IV.2. Viral Replication is Decreased in CIC Knockdown.
(A) H1N1 replication in WT A549 cells knocked down for CIC or NP mRNA. WT A549s were transfected with siControl, siCIC, or siNP for 24 hours, then infected with H1N1 (MOI = 0.1). Viral titers were measured at 48 hpi. Data are represented as a percentage mean titer of triplicate samples relative to vector control cells ± SD. * p-value < 0.05; ns, non-significant. (B) Western blot analysis of siCIC knockdown in WT A549 cells. Lysates from transfected cells were subjected to western blot analysis with an anti-CIC antibody. Actin levels are shown as loading controls. Data are representative of at least three independent experiments.

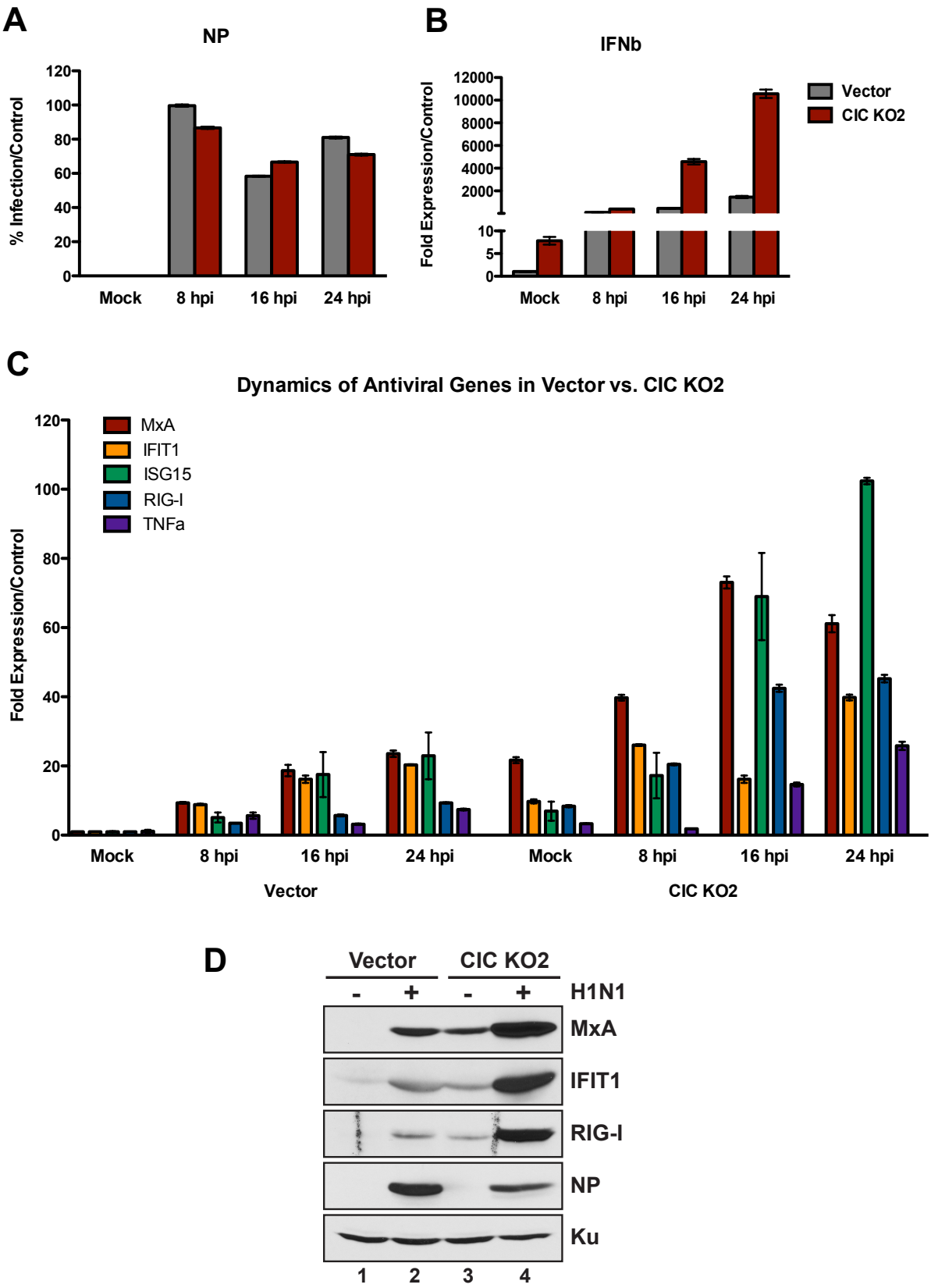


Figure IV.3. CIC Regulates Antiviral Gene Production.

Fig. IV.3, continued. (A-C) qRT-PCR analysis of antiviral gene expression in basal (mock) or in H1N1-infected conditions. Vector control and CIC KO2s were infected with H1N1 (MOI = 5), and mRNA levels for NP (A), IFNβ (B), and antiviral genes (C) were measured from 0-24 hpi. Data are represented as the fold expression relative to uninfected (mock) vector control cells ± SD or H1N1-infected vector control cells ± SD. (D) Western blot analysis of antiviral gene expression in basal (mock) or in H1N1-infected conditions. Vector control and CIC KO2s were infected with H1N1 (MOI = 5), and cell lysates were analyzed at 16 hpi. Ku levels are shown as loading controls. Data are representative of at least three independent experiments.

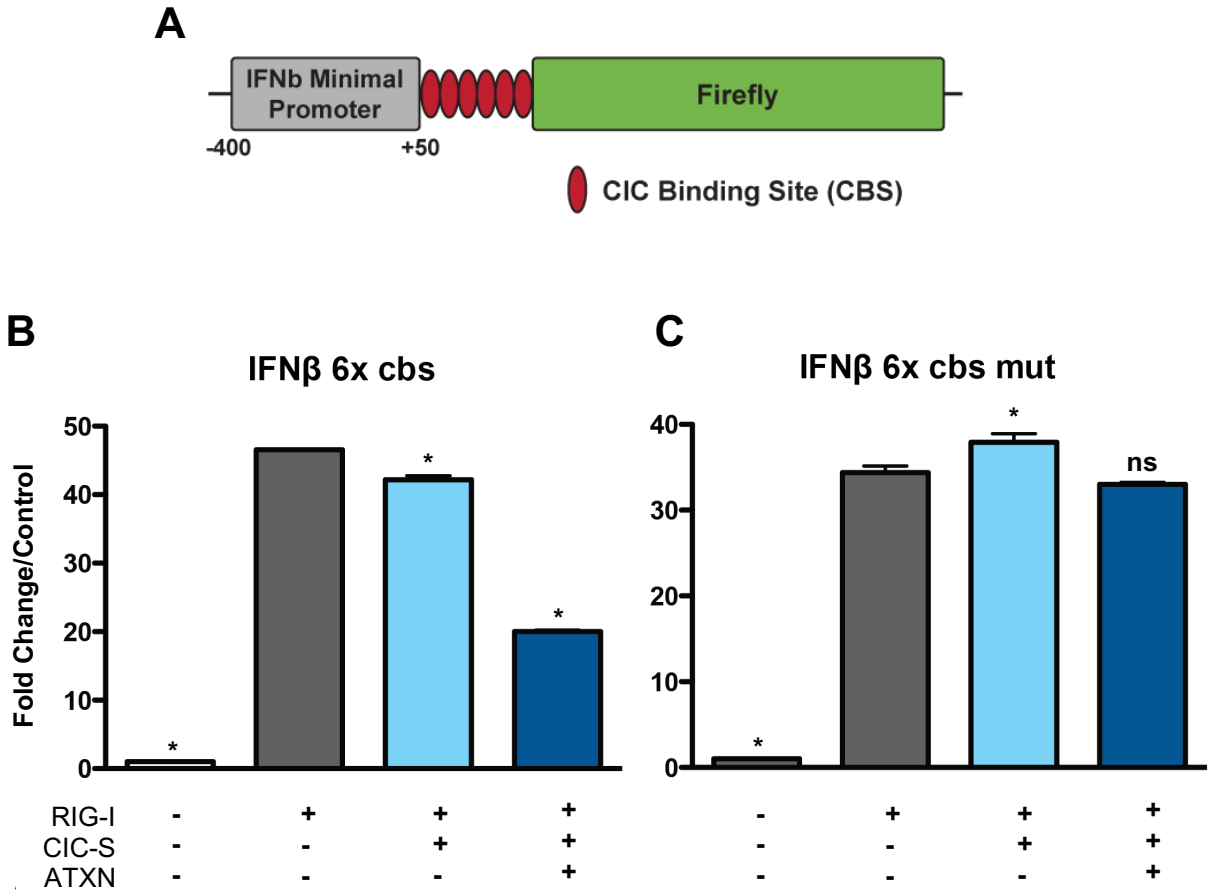


Figure IV.4. CIC Repression of Binding Sites in IFNβ Promoter.
(A) Schematic representation of IFNβ promoter reporter construct with CIC binding sites. CIC binding sites were engineered into the minimal promoter of IFNβ controlling a Firefly luciferase reporter gene. (B) IFNβ 6x cbs and (C) IFNβ 6x cbs mut. reporter activity upon ectopic expression of CIC and ATXN1. Promoter reporter constructs were transfected in the presence or in the absence of RIG-I-2CARD, CIC, and ATXN1, and luciferase activity was measured at 48 hr post-transfection. Data are represented as percent luciferase activity relative to GFP + RIG-I-2CARD-transfected control ± SD. * p-value < 0.05; ns denotes non-significant. Data are representative of at least three independent experiments.

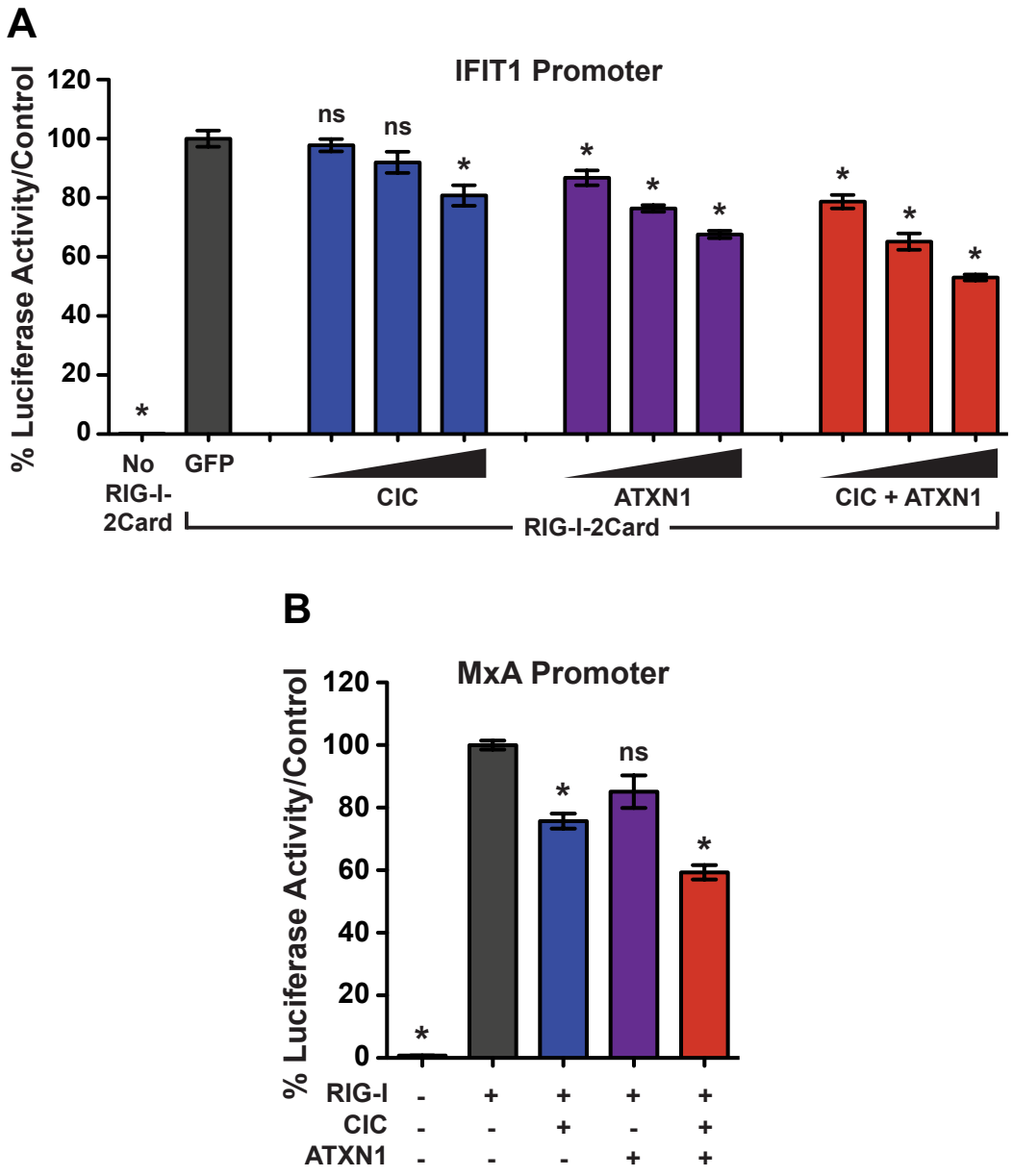


Fig IV.5. CIC Repression of Binding Sites in Endogenous Promoters of ISGs.
(A) IFIT1 and (B) MxA reporter activity upon ectopic expression of CIC and ATXN1. Firefly luciferase reporters under the control of IFIT1 or MxA promoters were transfected in the presence or in the absence of RIG-I-2CARD, CIC, and ATXN1, and luciferase activity was measured at 48 hr post-transfection. Data are represented as percent luciferase activity relative to GFP + RIG-I-2CARD-transfected control ± SD. * p-value < 0.05; ns denotes non-significant. Data are representative of at least three independent experiments.

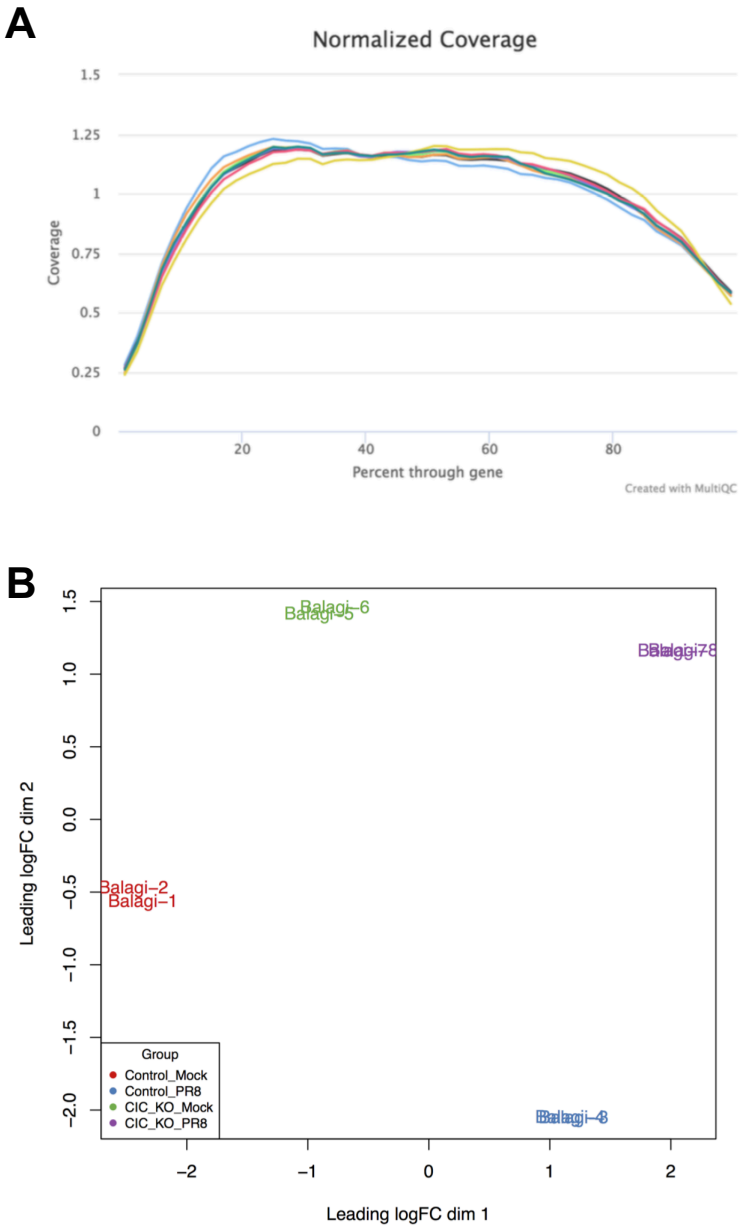


Figure IV.6. Quality Control Checkpoints for RNAseq Analysis of Vector Control and CIC KO2 Cells.

(A) Vector control and CIC KO2s were infected with H1N1 (MOI = 5), total RNA was extracted at 16 hpi, sequencing library was prepared, and samples were sequenced by next generation sequencing. Coverage uniformity was assessed over the gene body for 8 samples in RNAseq analysis. Each transcript was normalized to 100nt, shown from 5' to 3' end. Each curve reflects one sample, and depicts the average read coverage per transcript for all genes in the sample. (B) MDS plot of RNAseq analysis portrays the fold change relationship between replicates and between sample sets.

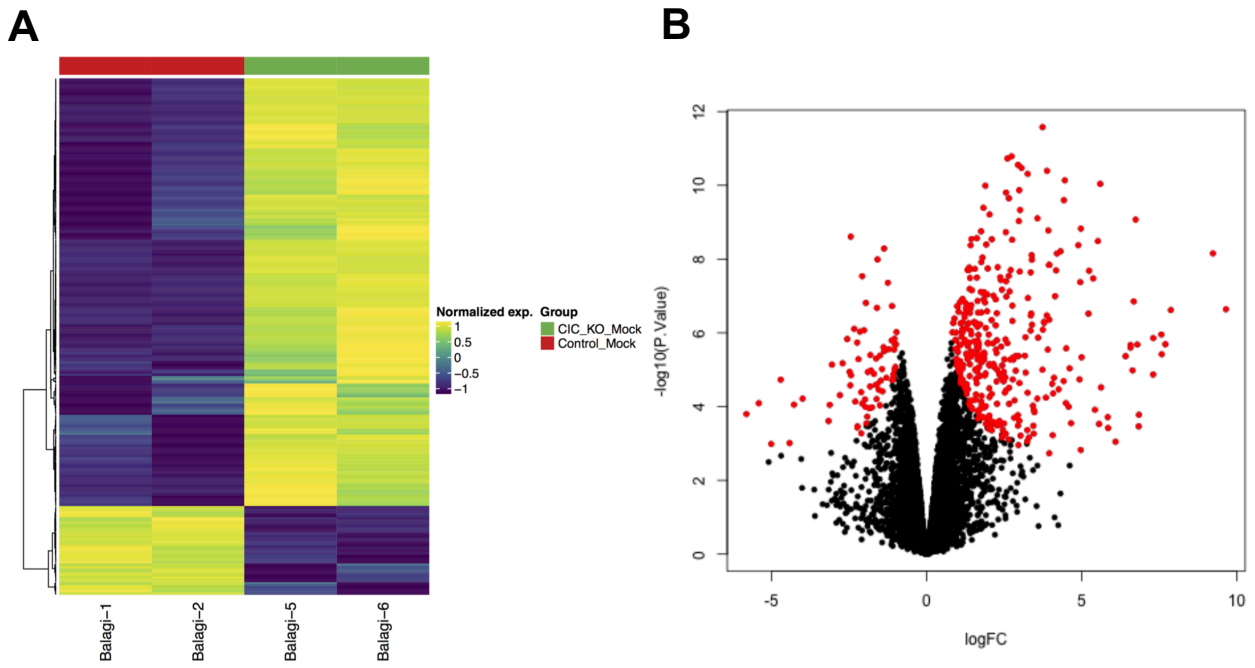


Figure IV.7. Global Change in Gene Expression in CIC KO2 Mock vs. Control Mock.

(A) Heatmap depicting upregulated (yellow) and downregulated (blue) genes in CIC KO2 or Vector control cells under mock conditions by RNAseq analysis. (B) Volcano plot depicting the relationship of fold change (log_2) and statistical strength (log_{10}) of differentially-expressed genes in CIC KO2 vs. Vector control under mock conditions by RNAseq analysis.

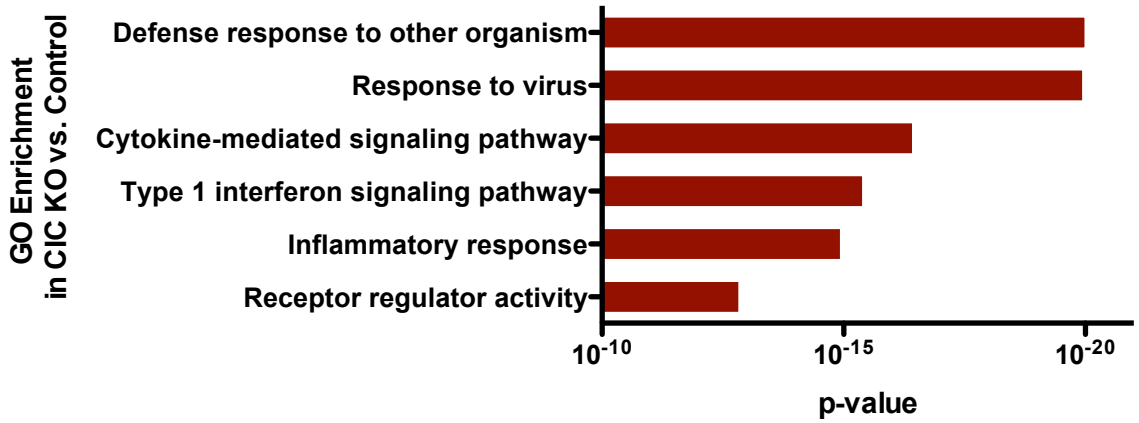


Figure IV.8. Enriched Gene Ontology Categories in CIC KO2 Cells.
Gene ontology pathways enriched in CIC KO2 cells under mock conditions by RNAseq analysis are ranked by statistical strength.

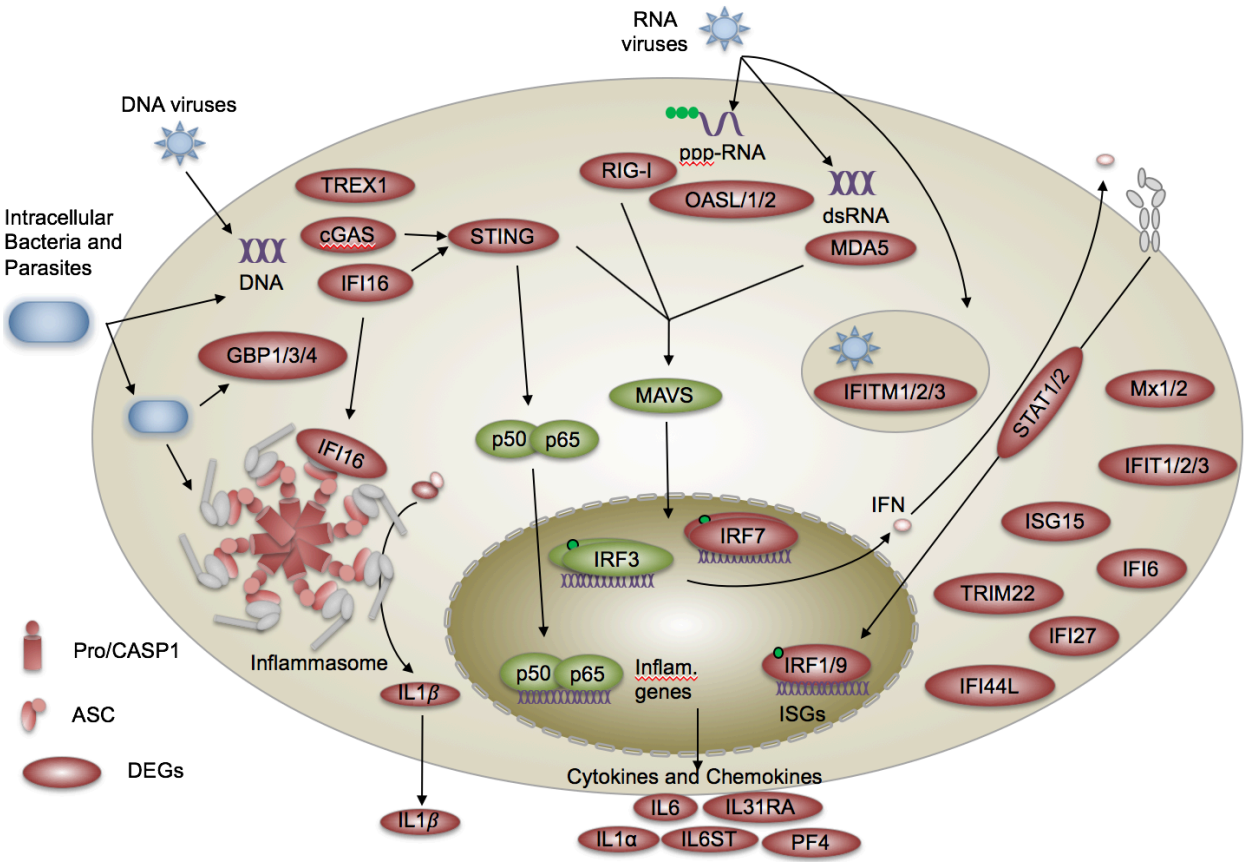


Figure IV.9. CIC KO State: Roadblocks to Multiple Pathogens.
Schematic representation of differentially-expressed genes (DEGs) in CIC KO2 cells under mock conditions determined by RNAseq analysis. We observe upregulation of pathways that sense RNA viruses, DNA viruses, and intracellular parasites and induce type 1 IFN signaling, the inflammasome, and cytokine production.

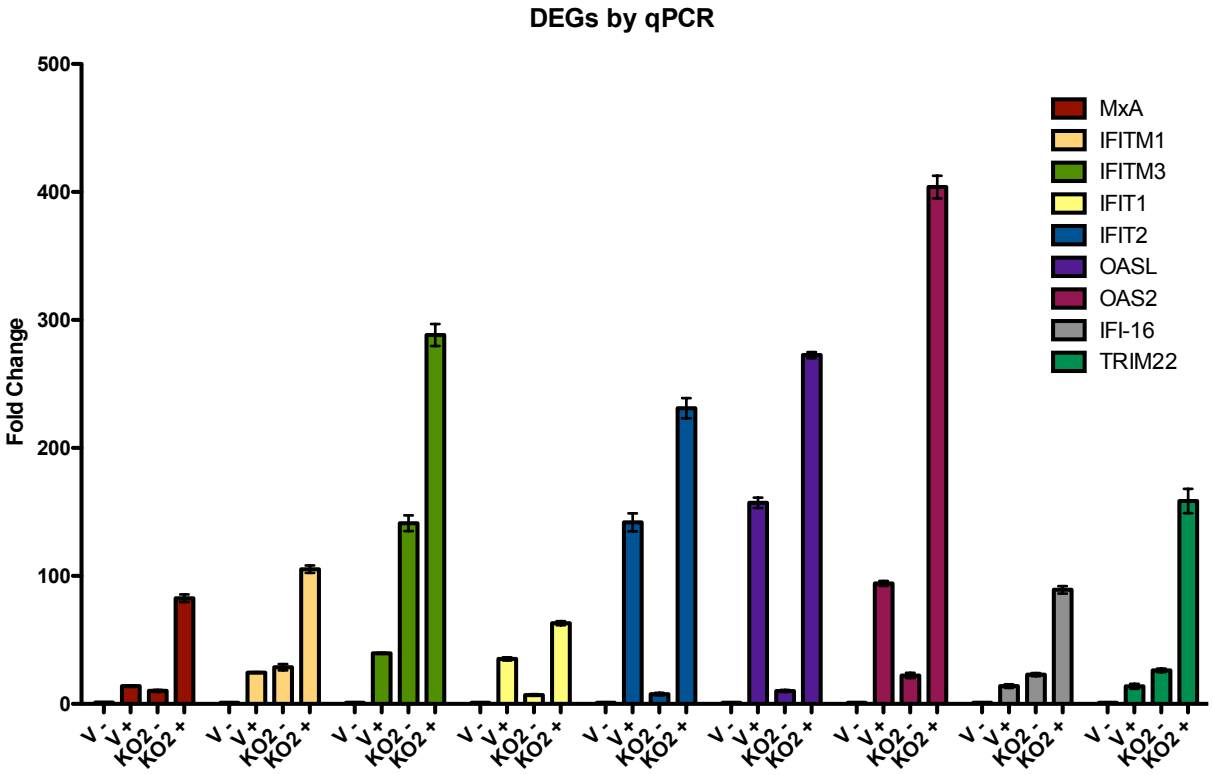


Figure IV.10. qPCR Analysis for Confirming Differentially-Expressed Genes Elicited by RNAseq Analysis.

Quantitative RT-PCR analysis of antiviral gene expression in basal (mock) or in H1N1-infected conditions, using the same total RNA samples submitted for RNAseq analysis. Vector control and CIC KO2s were infected with H1N1 (MOI = 5), and mRNA levels for multiple antiviral genes were measured at 16 hpi. Data are represented as the fold expression relative to uninfected (mock) vector control cells ± SD or H1N1-infected vector control cells ± SD.B. Data are representative of at least three independent experiments.

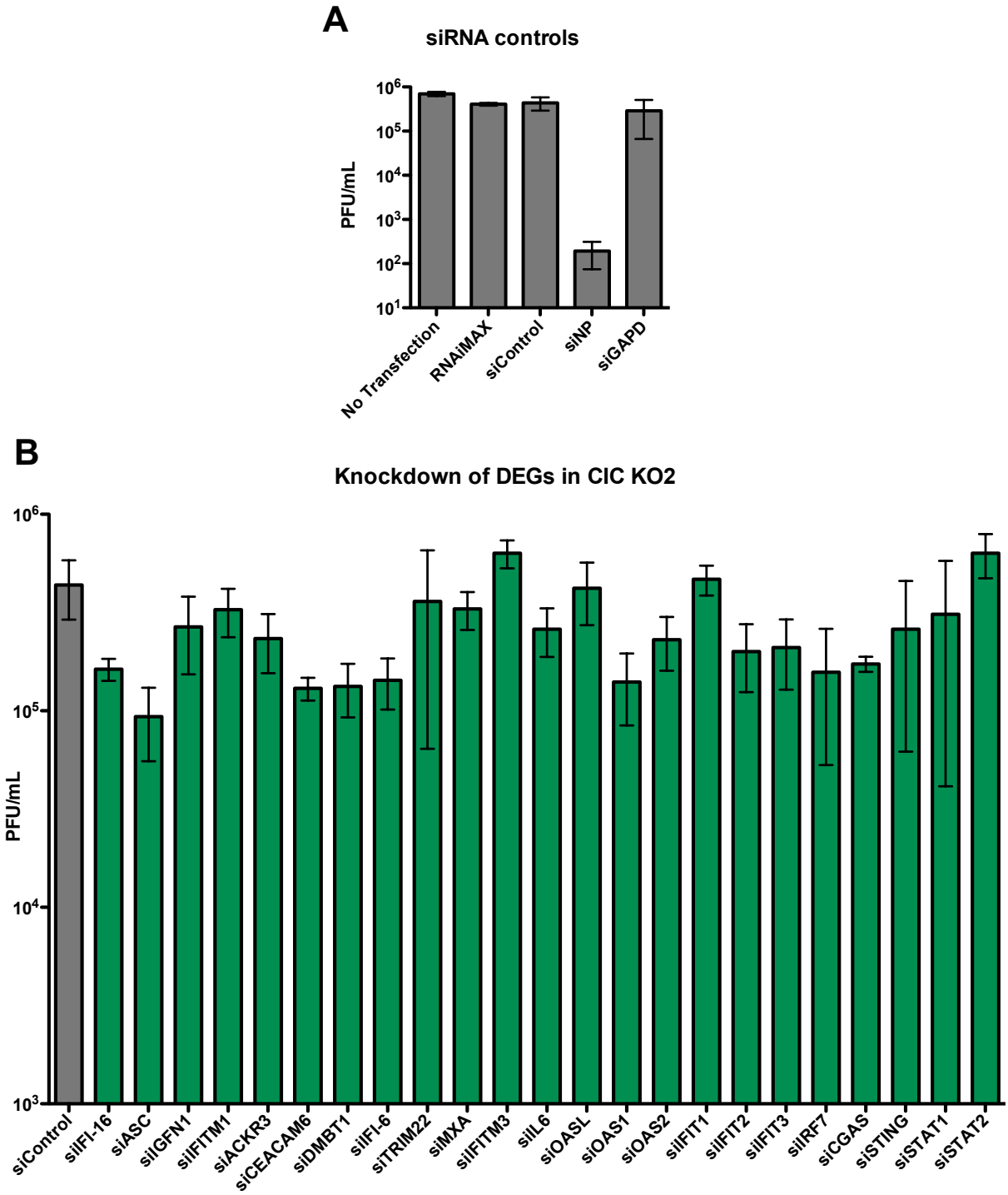


Figure IV.11. Importance of Differentially-Expressed Genes During Viral Infection in CIC KO2s Through siRNA Mini-Screen.

(A and B) H1N1 replication in WT A549 cells knocked down for indicated genes. WT A549s were left untransfected (A), transfected with reagent alone, siControl, siNP, or siGAPD (A), or transfected with siRNA against indicated genes (B) for 24 hours, then infected with H1N1 (MOI = 0.01). Viral titers were measured at 48 hpi. Data are represented as a percentage mean titer of triplicate samples relative to vector control cells

Fig. IV.11, continued. ± SD. * $p < 0.05$; ns, non-significant. Data are representative of at least three independent experiments.

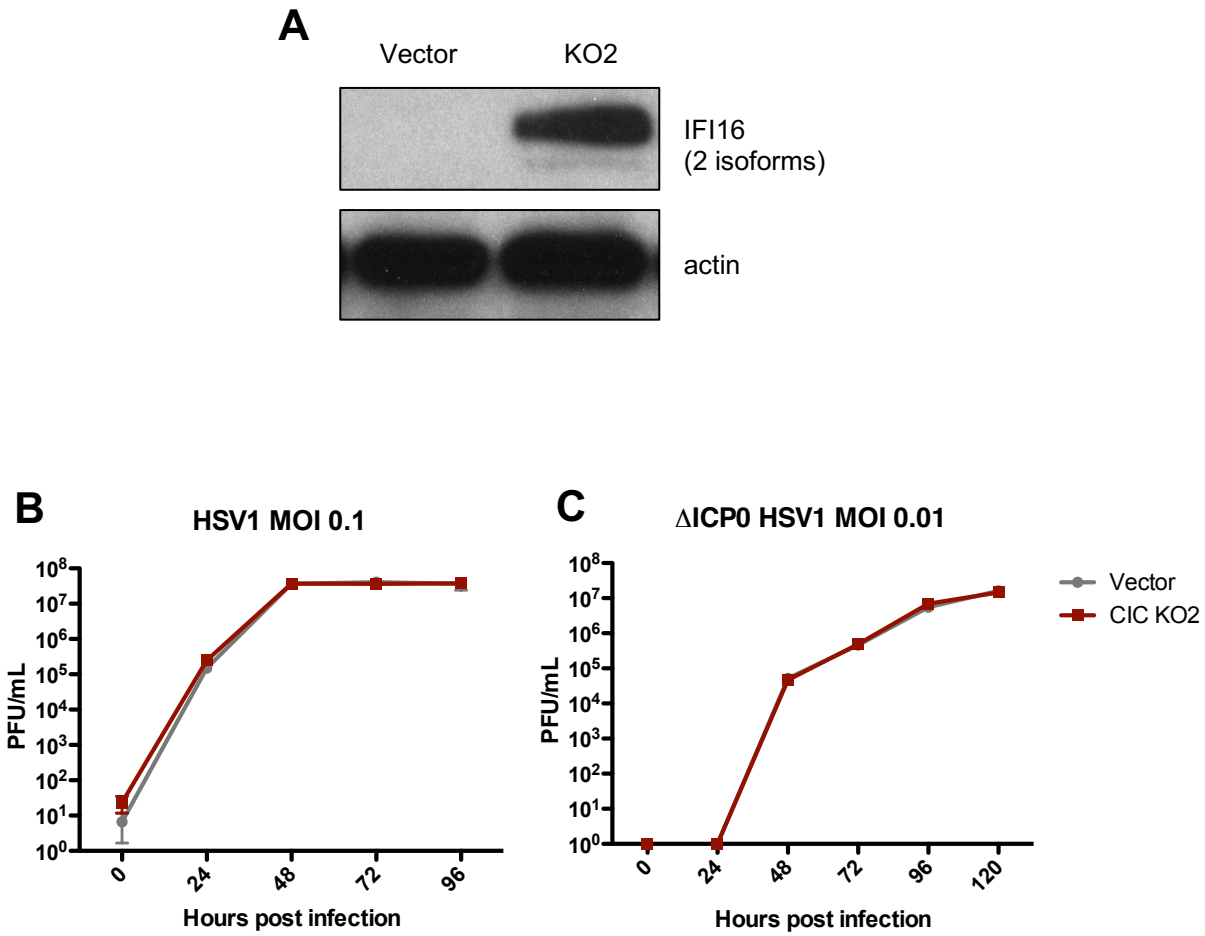


Figure IV.12. HSV1 Replication is Unaffected in CIC KO2 Cells.
(A) Expression of IFI-16, an HSV1 DNA sensor targeted for degradation by ICP0 of HSV1, in Vector control and CIC KO2 cells. Lysates from transfected cells were subjected to western blot analysis with an anti-IFI-16 antibody. Actin levels are shown as loading controls. (B) HSV1 (MOI = 0.1) replication in Vector control or CIC KO2 cells. (C) ΔICP0 HSV1 (MOI = 0.01) replication in Vector control or CIC KO2 cells. Viral titers were measured at indicated time points. Data are represented as a percentage mean titer of triplicate samples relative to vector control cells ± SD. Data are representative of at least three independent experiments.

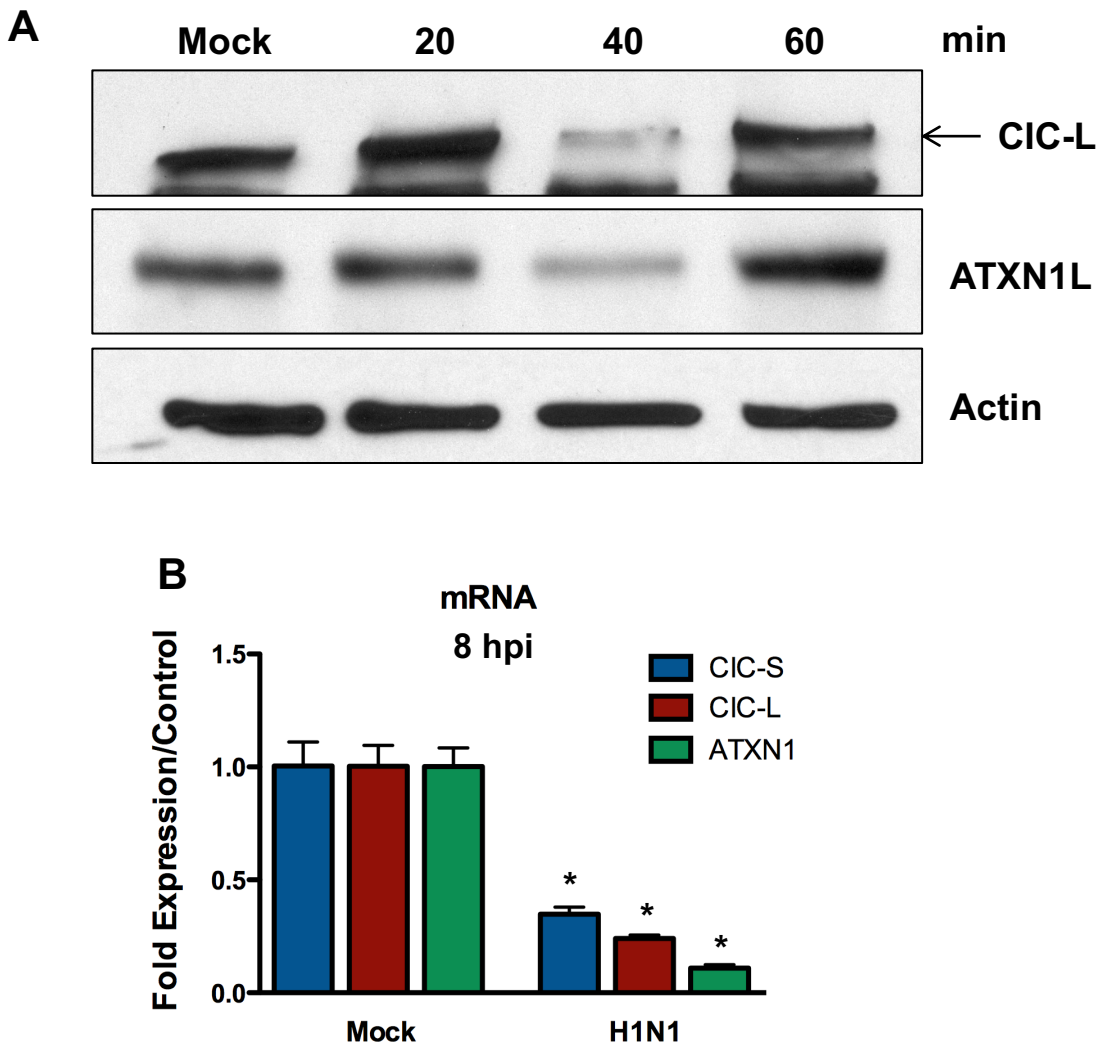


Figure IV.13. CIC is Downregulated in Response to Viral Infection.
(A) Western blot analysis of CIC degradation upon H1N1 infection. WT A549s were infected with H1N1 (MOI = 3), and cell lysates were analyzed at the indicated times. (B) qRT-PCR analysis of CIC downregulation upon H1N1 infection. WT A549s were infected with H1N1 (MOI = 5), and CIC mRNA levels were measured at 8 hpi. Data are represented as the fold expression relative to uninfected (mock) WT A549s ± SD. For (A) actin levels are shown as loading controls. * p-value < 0.05; ns, non-significant. Data are representative of at least three independent experiments.

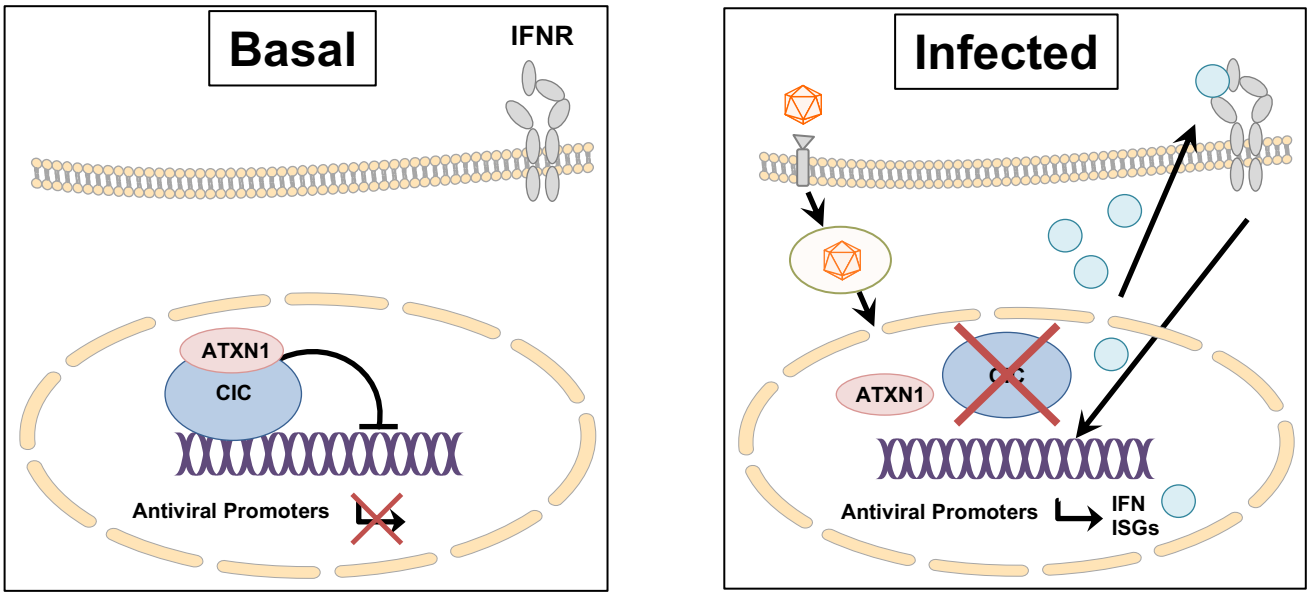


Figure IV.14. Graphical Hypothesis
Under basal conditions, the CIC/ATXN1 complex binds and represses antiviral gene promoters, preventing aberrant induction of the antiviral state. Upon viral infection, the CIC/ATXN1 complex is downregulated and suppression is relieved, enabling expression from antiviral gene promoters and inducing the antiviral state.

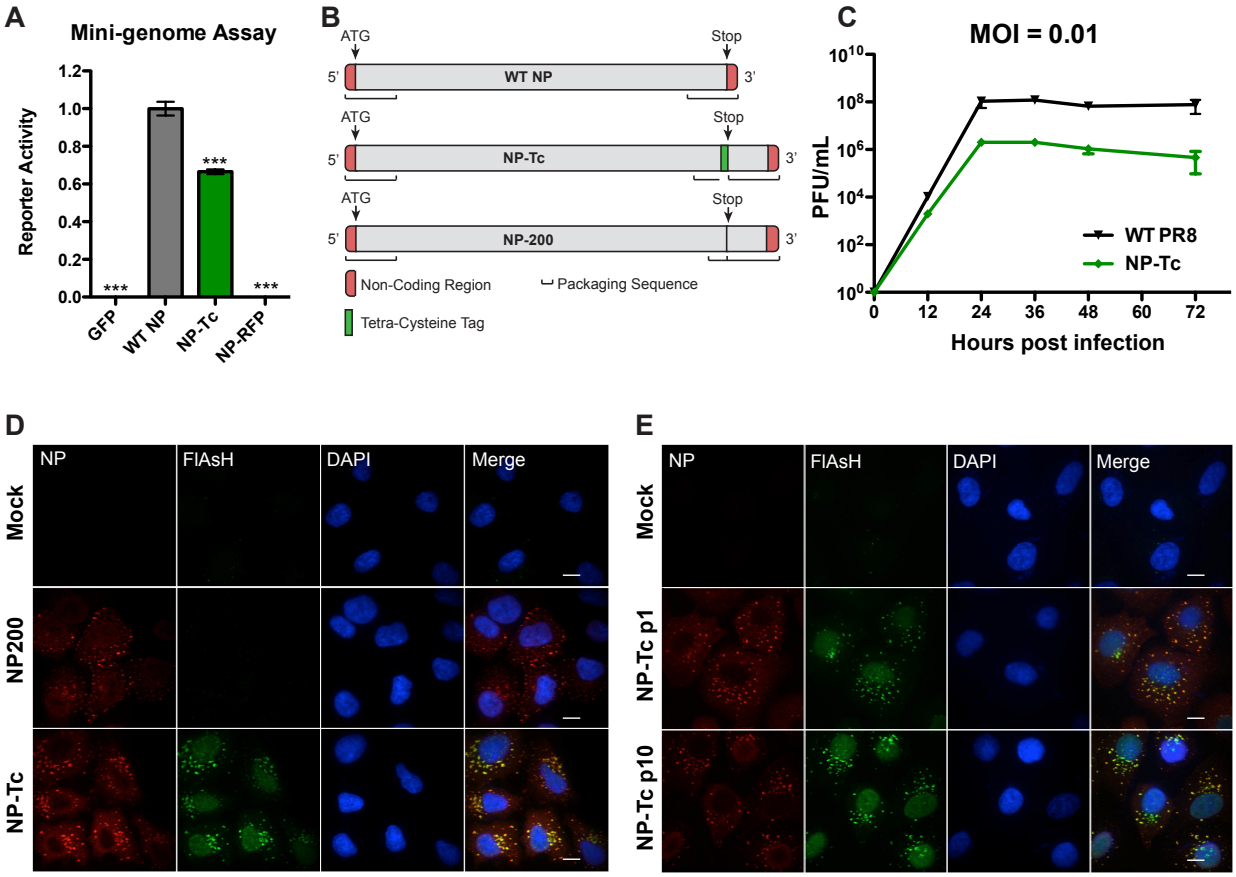


Figure V.1. Design and characterization of first fluorescently-tagged NP virus. (A) Mini-genome activity using tagged versions of NP. PB1, PB2, and PA of H1N1 (A/WSN/1933) were transfected into HEK293T cells along with GFP, WT NP, or tagged NP constructs. Reporter activities of a transfected Firefly luciferase construct controlled by an IAV promoter and Renilla luciferase construct controlled by a cellular promoter were measured. Data are represented as mean reporter activity of 6 samples per condition +/- SD. (B) Schematic of the NP-Tc genomic RNA segment, depicted in the complementary-sense. The WT NP segment contains packaging sequences at both termini. Due to disruption of the 3' packaging sequence by the Tc tag in the NP-Tc segment, the 3' packaging sequence is duplicated after the stop codon. The 3' packaging sequence is duplicated in the NP200 segment as a control. Schematic not to scale. (C) Viral growth kinetics for WT PR8 and NP-Tc viruses. MDCK cells were infected with WT PR8 or NP-Tc virus (MOI = 0.01) and viral titers were measured at indicated time points by plaque assay. Limit of detection = 10 PFU. Data are represented as mean titer of triplicate samples +/- SD. (D) Analysis of FlAsH staining by fluorescence microscopy. A549 cells were infected at MOI = 1 for 9 hours. FlAsH-demarcated puncta co-localized with an NP antibody in NP-Tc infected cells, and NP antibody staining showed a similar cytoplasmic distribution in NP200 infected cells. Scale bar = 10 μm. (E) Tc tag remains stable in virion after passaging. NP-Tc was blindly passaged in A549 cells 10 times. A549 cells were infected with virus from passages 1 and 10 at MOI = 1 for 7 hours. FlAsH-demarcated

Fig. V.1, continued. puncta were present and co-localized with an NP antibody throughout passaging. Scale bar = 10 μm. * p-value < 0.05; ** p-value < 0.01; *** p-value < 0.001; N.S., non-significant. Data are representative of at least three independent experiments.

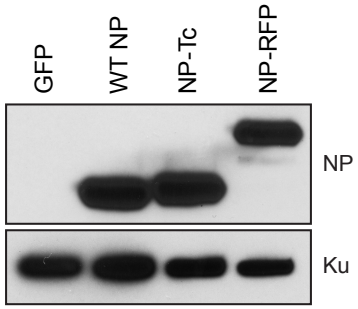


Figure V.2. NP Expression and Dynamics.
(A) Western blot analysis of NP expression. GFP, WT NP, and tagged NP constructs were transfected into HEK293T cells and cell lysates were analyzed at 48 hpt for NP expression. Ku expression is shown as a loading control.

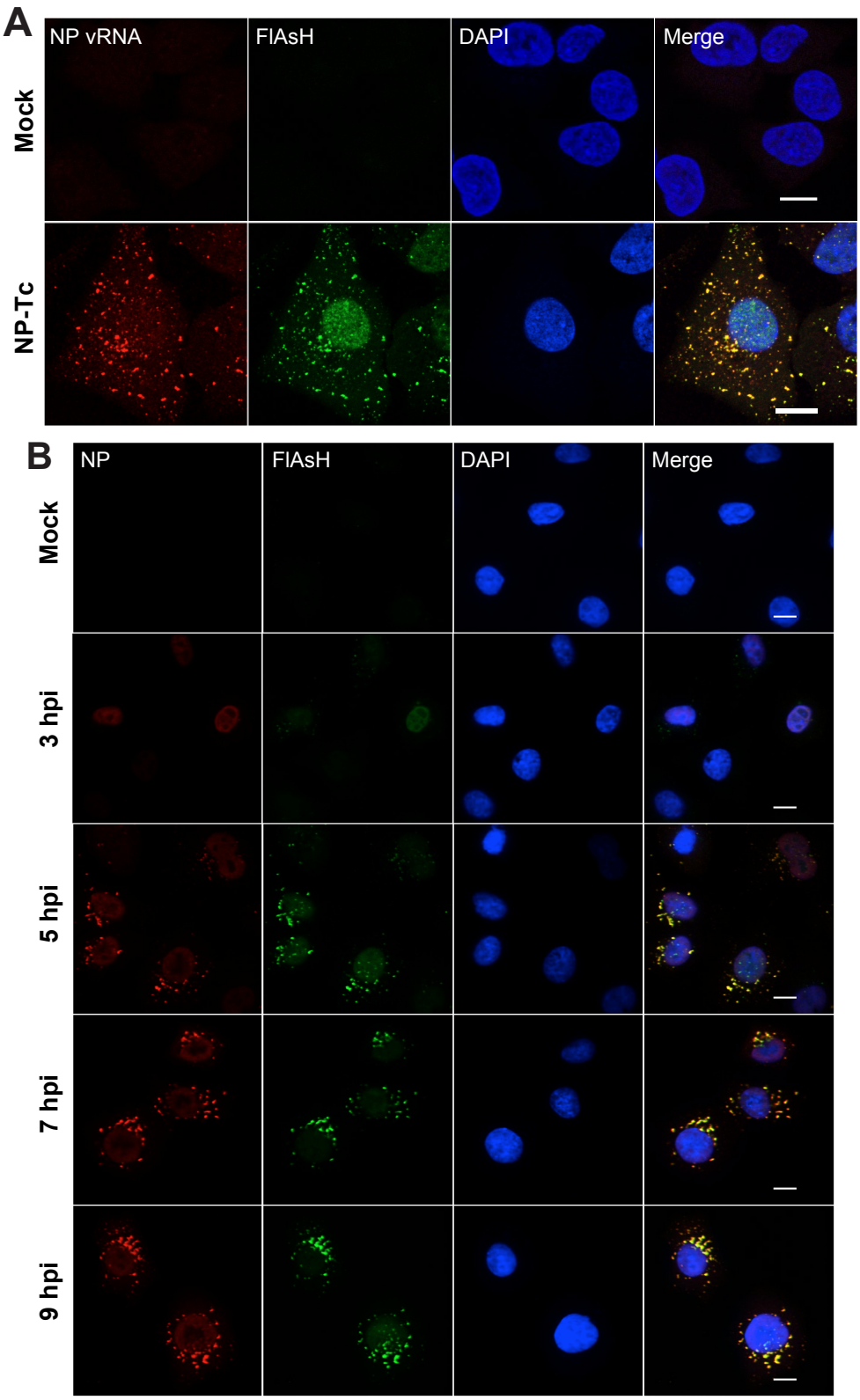


Figure V.3. NP-Tc allows visualization of vRNP dynamics.
(A) NP-Tc marks vRNP complexes. A549 cells were infected with NP-Tc at MOI = 1 for 7 hours. FlAsH puncta co-localized with NP vRNA stained by FISH (Quasar570). Scale bar

Fig. V.1, continued. = 10 μm. (B) Dynamics of vRNP complex export from the nucleus. A549 cells were infected with NP-Tc at MOI = 1 for the indicated time points. FlAsH puncta co-localized with an NP antibody during vRNP egress. Scale bar = 10 μm.

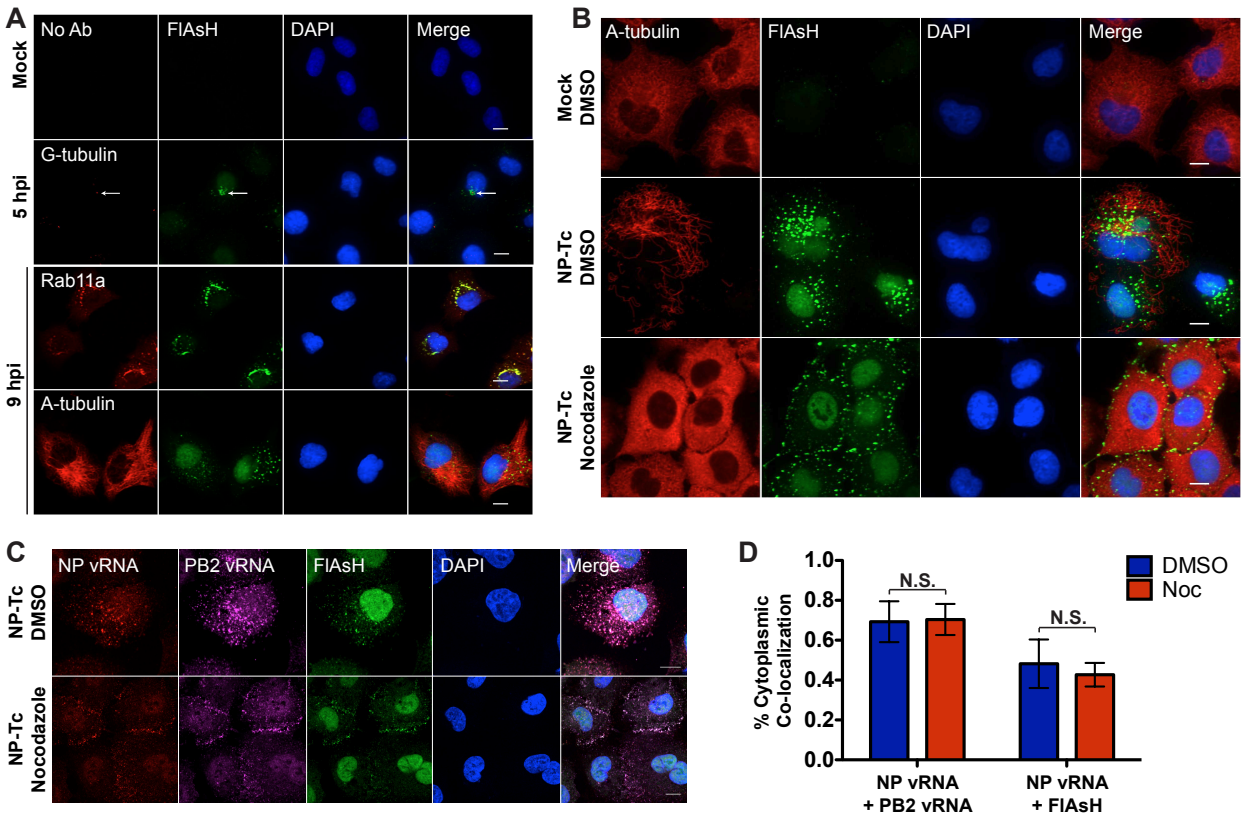


Figure V.4. Cytoskeletal components aide in IAV vRNP export.
(A) Localization of vRNP complexes with cytoskeletal structures and trafficking factors. A549 cells were infected with NP-Tc at MOI = 1 for the indicated time points. FlAsH puncta marked NP, and γ-tubulin, Rab11a, and α-tubulin were marked by antibody staining. Scale bar = 10 μm. (B) Disruption of MT network quickly disperses vRNPs to plasma membrane. A549 cells infected with NP-Tc at MOI = 1 were treated with 30μM nocodazole or DMSO 3 hpi and were stained with FlAsH and α-tubulin 9 hpi. Scale bar = 10 μm. (C and D) Selective packaging of vRNPs may not rely on the microtubule network. A549 cells infected with NP-Tc at MOI = 1 were treated with 30μM nocodazole or DMSO 3 hpi. Five hpi, cells were stained with FlAsH to mark NP as well as FISH Quasar570 and FISH Quasar670 to mark NP vRNA and PB2 vRNA, respectively. Scale bar = 10 μm. Cytoplasmic signals were analyzed for co-localization by fluorescence microscopy (C) and through Manders Coefficient analysis for NP with PB2 vRNA FISH probes and NP vRNA FISH probe with FlAsH (D). At least 9 cells per condition were analyzed (D). * p-value < 0.05; ** p-value < 0.01; *** p-value < 0.001; N.S., non-significant. Data are representative of at least three independent experiments.

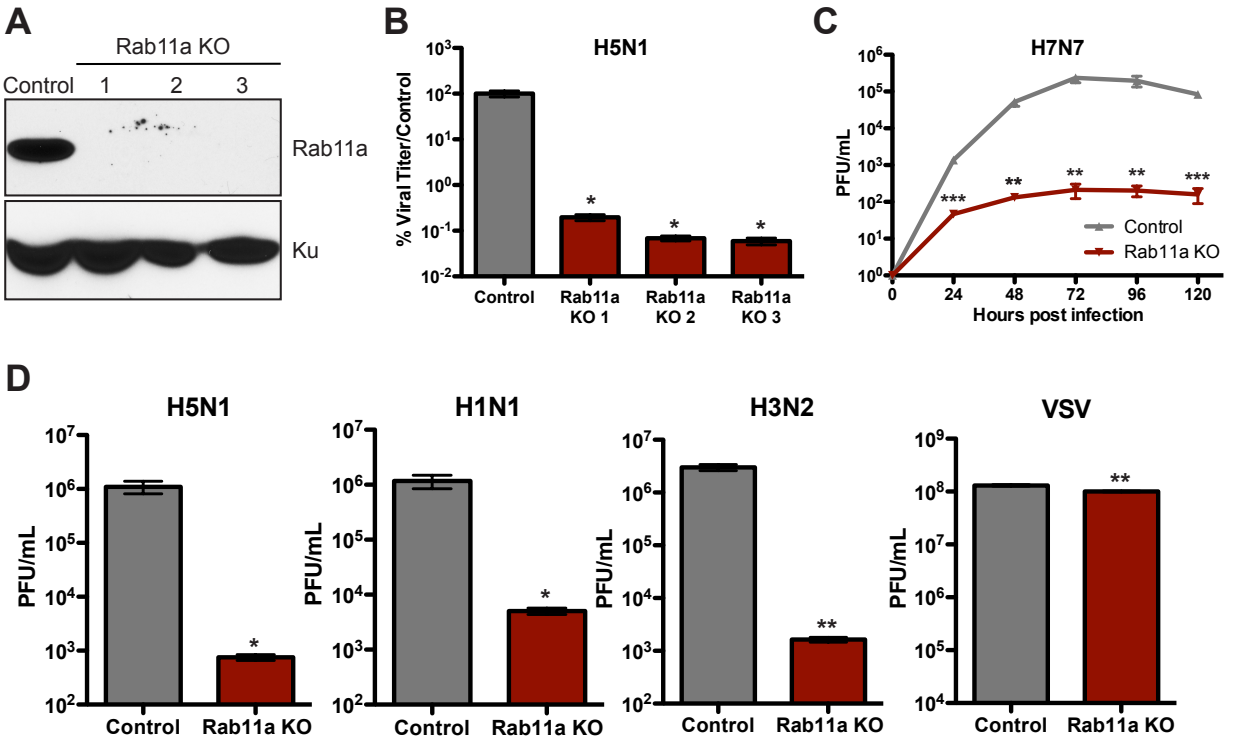


Figure V.5. Rab11a is essential for replication of IAV.
(A) Western blot analysis for Rab11a expression in control and Rab11a KO A549 cells. Cell lysates from control A549 cells and three clonal populations of Rab11a KOs were collected and subjected to western blot analysis for Rab11a expression. Ku expression was used as a loading control. (B) H5N1 relies on Rab11a for replication. Control A549 cells and Rab11a KOs were infected with H5N1 (MOI = 0.001) and viral titers were measured at 48 hpi by plaque assay. Data are represented as mean titer of triplicate samples +/- SD. (C) IAV replication is stunted in Rab11a KOs over a time course of multi-cycle replication. Control A549 cells and Rab11a KOs were infected with H7N7 (MOI = 0.01) and viral titers were measured at indicated time points by plaque assay. Limit of detection = 10 PFU. (D) Multiple strains of IAV, but not VSV, rely on Rab11a for replication. Control A549 cells and Rab11a KOs were infected with H5N1 (MOI = 0.001), H1N1 (MOI = 0.01), H3N2 (MOI = 0.01), and VSV (MOI = 0.001) and viral titers were measured at 48 hpi by plaque assay. Data are represented as mean titer of triplicate samples +/- SD. * p-value < 0.05; ** p-value < 0.01; *** p-value < 0.001; N.S., non-significant. Data are representative of at least three independent experiments.

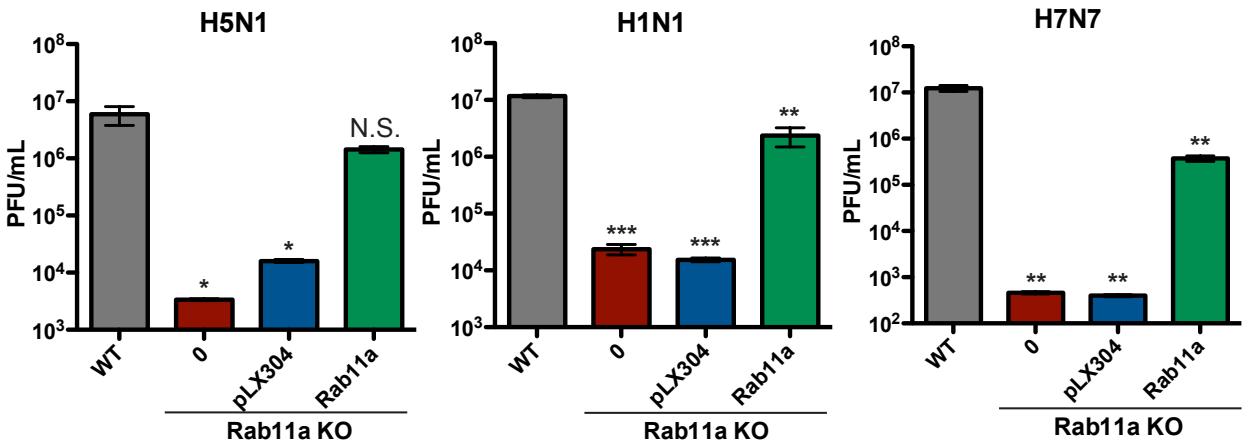


Figure V.6. Complementation of Rab11a Restores IAV Replication in Rab11a KO Cells

Complementation of Rab11a in Rab11a KOs restores IAV replication. Control A549 cells, Rab11a KOs, and Rab11a KOs complemented with transduced empty vector or Rab11a constructs were infected with H5N1 (MOI = 0.001), H1N1 (MOI = 0.01), and H7N7 (MOI = 0.01) and viral titers were measured at 48 hpi by plaque assay. Data are represented as mean titer of triplicate samples +/- SD. * p-value < 0.05; ** p-value < 0.01; *** p-value < 0.001; N.S., non-significant. Data are representative of at least three independent experiments.

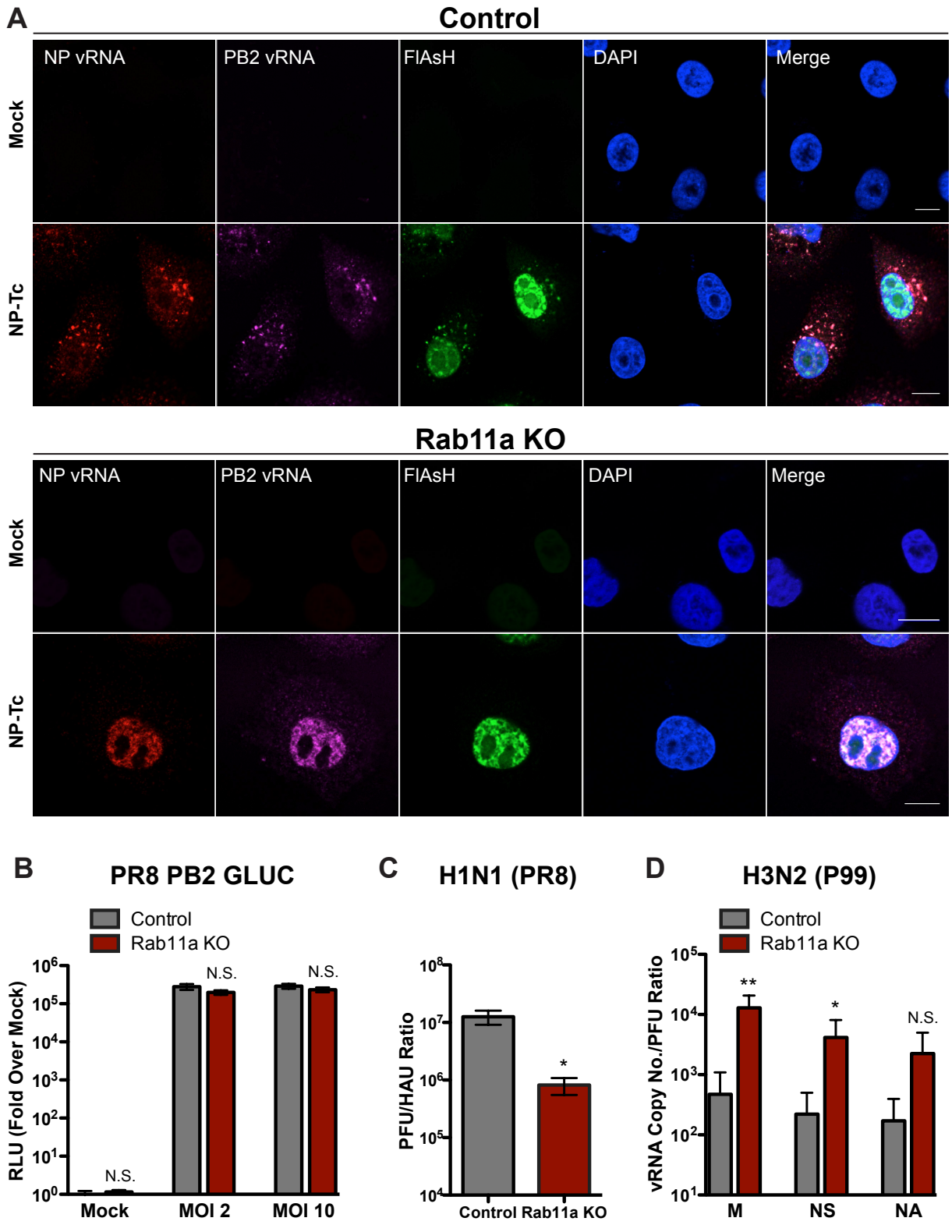


Figure V.7. Loss of Rab11a disrupts trafficking and increases defective particles. (A) vRNP complexes are retained in the nucleus in Rab11a KOs. Control A549 cells and Rab11a KOs were infected with NP-Tc at MOI = 1 for 18 hours. Cells were stained with

Fig. V.7, continued. FlAsH to mark NP as well as FISH Quasar570 and FISH Quasar670 to mark NP vRNA and PB2 vRNA, respectively. Scale bar = 10 μm. (B) Control A549 cells and Rab11a KOs were infected with PR8 PB2-GLUC at MOI 2 and 10. At 16 hpi, cells were lysed and luciferase activity was assessed. (C and D) Rab11a KOs promote production of semi-infectious particles. Control A549 cells and Rab11a KOs were infected with PR8 (C) and P99 (D) at MOI = 0.01 and viral titers were measured at 48hpi by plaque assay. HA assay was performed using 0.5% chicken RBC to determine HA units (HAU) (C). Viral RNA was extracted from the supernatant and digital droplet PCR was performed to determine RNA Copy Number/mL for three segments (M, NS and NA) using sequence specific primers (D). * p-value < 0.05; ** p-value < 0.01; *** p-value < 0.001; N.S., non-significant. Data are representative of at least two independent experiments.

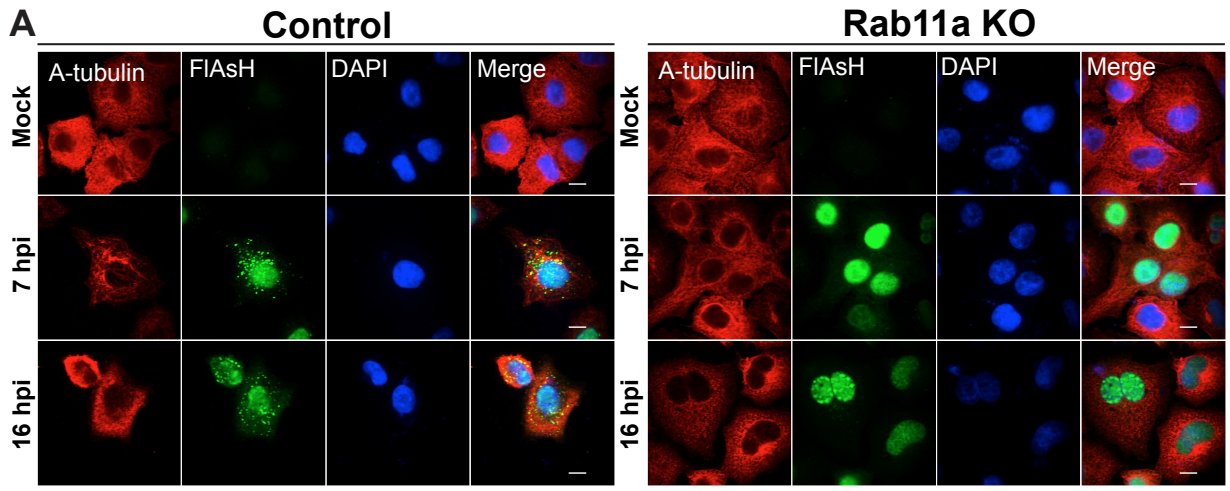


Figure V.8. vRNP trafficking is disrupted in Rab11a KO.
(A) vRNP complexes are retained in the nucleus in Rab11a KOs. Control A549 cells and Rab11a KOs were infected with NP-Tc at MOI = 1 for 7 and 16 hours. Cells were stained with FlAsH and NP Ab to mark NP. Scale bar = 10 μm.

APPENDIX B

Tables

Table II.1. Oligonucleotide Sequences for NP-Tc Virus, Rab11a KO, and Gene Segment Sequencing.

Target	Forward Primer	Reverse Primer
NP-Tc	CTCGTCGACTCAACAACATCCAGGACAACACCCTCCACTCGAGCC	TGAGTCGACGAGGACCGAAATCATAAGGATGATGG
Rab11a promoter gRNA	TAACATCAGCGTAAGTCTCA	TGAGACTTACGCTGATGTTA
Rab11a exon 1 gRNA	CATTTCGAGTAAATCGAGAC	GTCTCGATTTACTCGAAATG
M (sequencing)	GTTGCATGGGCCTCATATAC	ATTGGTTGTTGCCACCATTTG
NS (sequencing)	CCATGTTGGAAAGCAGATTG	GGGCATTAGCATGAACCAGT
NA (sequencing)	ATCAATTTGCCCTTGGACAG	CCCAAATGAAATGGAACACC
NP (amplification)	TGTAAAACGACGGCCAGTAGCAAAAGCAGGGTAGATAATCACTCAC	CAGGAAACAGCTATGACCCAGTATCTGCTTCTCAGTTCAAGG
NP (sequencing)	TGTAAAACGACGGCCAGT	CAGGAAACAGCTATGACC

Table II.2. Oligonucleotide Sequences for Generating and Validating CRISPR KO Cells.

Oligonucleotide Sequences for sgRNAs to Generate CRISPR KO Cells.		
Gene	**Forward Primer**	**Reverse Primer**
SLC35A1	CACCGTGAACAGCATACACTAACGA	AAACTCGTTAGTGTATGCTGTTCAC
GDF11	CACCGTTGCGACTAAAACCCCTAAC	AAACGTTAGGGGTTTTAGTCGCAAC
IRX3	CACCGAACGTGCTCTCGTCCGTGTA	AAACTACACGGACGAGAGCACGTTC
C2CD4C	CACCGGATCCAGATCGAGAGTGCCG	AAACCGGCACTCTCGATCTGGATCC
TRIM23	CACCGGCAGCTCCATACTGACCAAT	AAACATTGGTCAGTATGGAGCTGCC
PIGN	CACCGCGTAAAGTGCATCTGCTCGA	AAACTCGAGCAGATGCACTTTACGC
ACADSB	CACCGATCCACTGTGCTCGTGATAG	AAACCTATCACGAGCACAGTGGATC
GRAMD2	CACCGTCTTCACCCTTCAAGCCTTC	AAACGAAGGCTTGAAGGGTGAAGAC
CIC (sgRNA 1)	CACCGGGGCATACCACCACTCGCCC	AAACGGGCGAGTGGTGGTATGCCCC
CIC (sgRNA 2)	CACCGGTTGCTCATGAACGGCCACC	AAACGGTGGCCGTTCATGAGCAACC
JAK2	CACCGACCTGTGACTCATGAAACAC	AAACGTGTTTCATGAGTCACAGGTC
PIAS3	CACCGTCTTCCGGGGAAAGCGTCGT	AAACACGACGCTTTCCCCGGAAGAC
Primer Sequences for PCR Amplification of sgRNA Target Site		
Gene	**Source**	**Forward Primer**	**Reverse Primer**
SLC35A1	RNA	CTGGTAGTCTGGGTAGATTCAAAGCATC	CAACTGGTAGGTCACCTGGTACACTGCT
C2CD4C	gDNA	GAGACTCCTTGCGCCTCGTG	CAGCAATGTGTTGACGCCCG
TRIM23	gDNA	TCTCTTGGGAATAGTGTTGGCCTTCAGAAC	TTAGACATTAACTACTGAACTATATTAGAAA
PIGN	gDNA	AGTCTTGAGCCAAGTTTGGGAAA	TAGTGCTTATTGTTACCACCACAA
CIC (sgRNA 1)	RNA	ATGAATGCCTTCATGATCTTCAGCAAGC	CCTTGAAGTGGGCCTCCTTCACCTGGAA
CIC (sgRNA 2)	gDNA	GACGCAGCCCCAACAAGGTACTTTATC	CTAACCCCCAGGGGCAGCAGCAGT
JAK2	RNA	ATCTCGAGGTGCTGAAGCTCCTCTTC	TGGATCTTTGCTCGAATACATTTTGGTAAG
PIAS3	gDNA	ATAGAAGGGCAATGGTTTCATGGTGACATC	CTCTGTTTTTCTCCACAGCACATGGTGATG

Table II.3. FISH Probe Sequences for NP vRNA.

Title	Probe Sequences 5'-3'
PR8 NP vRNA _1	GACATGAGGACCGAAATCAT
PR8 NP vRNA _2	GGAATACAGAGGGAAGAACA
PR8 NP vRNA _3	CAACCATTATGGCAGCATTC
PR8 NP vRNA _4	CAGTACAGAGAAATCTCCCT
PR8 NP vRNA _5	GCCAAATCAGCATACAACCT
PR8 NP vRNA _6	AAACACCAATCAACAGAGGG
PR8 NP vRNA _7	TGAACTGAGAAGCAGGTACT
PR8 NP vRNA _8	GAGGAGTTCAAATTGCTTCC
PR8 NP vRNA _9	TTCATCAAAGGGACGAAGGT
PR8 NP vRNA _10	GCCGCATTTGAAGATCTAAG
PR8 NP vRNA _11	AAGAGTCAACTGGTGTGGAT
PR8 NP vRNA _12	ACCAAATGAGAATCCAGCAC
PR8 NP vRNA _13	AGCCAAGTGTACAGCCTAAT
PR8 NP vRNA _14	CCCTTTCAGACTGCTTCAAA
PR8 NP vRNA _15	GGATACTCTCTAGTCGGAAT
PR8 NP vRNA _16	TGGGTACGACTTTGAAAGAG
PR8 NP vRNA _17	TCATATTGAGAGGGTCGGTT
PR8 NP vRNA _18	TCACTTTTCTAGCACGGTCT
PR8 NP vRNA _19	ATGGATCAAGTGAGAGAGAG
PR8 NP vRNA _20	CAAACTGCTGCACAAAAAGC
PR8 NP vRNA _21	GTGCAACATTCTCAAAGGGA
PR8 NP vRNA _22	GGTGAGAATGGACGAAAAAC
PR8 NP vRNA _23	CAATGATCGGAACTTCTGGA
PR8 NP vRNA _24	TGGTCAGGATGATCAAACGT
PR8 NP vRNA _25	GTTGGAACAATGGTGATGGA
PR8 NP vRNA _26	TGATGCAAGGTTCAACTCTC
PR8 NP vRNA _27	AGAGGACAAGAGCTCTTGTT
PR8 NP vRNA _28	CATGATGATCTGGCATTCCA
PR8 NP vRNA _29	ATAATGGTGACGATGCAACG
PR8 NP vRNA _30	AGAAATAAGGCGAATCTGGC
PR8 NP vRNA _31	GGATGAGAGAACTCATCCTT
PR8 NP vRNA _32	GGACCTATATACAGGAGAGT
PR8 NP vRNA _33	CGGGGAAAGATCCTAAGAAA
PR8 NP vRNA _34	ATACCTGGAAGAACATCCCA
PR8 NP vRNA _35	CTGCTTTTGACGAAAGGAGA
PR8 NP vRNA _36	CGGTTGATCCAAAACAGCTT
PR8 NP vRNA _37	CCGAACTCAAACTCAGTGAT

PR8 NP vRNA _38	GTGGAATTGGACGATTCTAC
PR8 NP vRNA _39	GCATCCGTCGGAAAAATGAT
PR8 NP vRNA _40	CCAGAATGCCACTGAAATCA

Table II.3, continued. FISH probe sequences are the same as previously published (Chou et al. 2013).

Table II.4. FISH Probe Sequences for PB2 vRNA.

Title	Probe Sequences 5'-3'
PR8 PB2 vRNA_1	AACTGAGCAACCTTGCGAAA
PR8 PB2 vRNA_2	AAGACAAGAGATATGGGCCA
PR8 PB2 vRNA_3	TTCTGAGGGGATTCCTCATT
PR8 PB2 vRNA_4	AACTGAAGACCCAGATGAAG
PR8 PB2 vRNA_5	TCACAGTTCTCGGAAAGGAT
PR8 PB2 vRNA_6	TATAACAAGGCCACGAAGAG
PR8 PB2 vRNA_7	GGGCAATTCTCCTGTATTCA
PR8 PB2 vRNA_8	GGGATCAGGAATGAGAATAC
PR8 PB2 vRNA_9	GCAGTTCTCCTCATTTACTG
PR8 PB2 vRNA_10	CTCCACCAAAGCAAAGTAGA
PR8 PB2 vRNA_11	AAAACTTCTTCCCTTCGCAG
PR8 PB2 vRNA_12	GACATTTGATACCGCACAGA
PR8 PB2 vRNA_13	CAACAAATGAGGGATGTGCT
PR8 PB2 vRNA_14	GTGGGTTTGTAAGAACTCTG
PR8 PB2 vRNA_15	AAGGCCATTAGAGGCCAATA
PR8 PB2 vRNA_16	CCAGAACCCTACAATGCTAT
PR8 PB2 vRNA_17	CATCAGAAACTGGGAAACTG
PR8 PB2 vRNA_18	CCTGAATCAGTGTTGGTCAA
PR8 PB2 vRNA_19	CGTCAATGATGTGGGAGATT
PR8 PB2 vRNA_20	GGGAACAGAGAAACTGACAA
PR8 PB2 vRNA_21	AATGTACTACTGTCTCCCGA
PR8 PB2 vRNA_22	TTTTGAGAATCCGGGACCAA
PR8 PB2 vRNA_23	TGTAGATGAGTACTCCAGCA
PR8 PB2 vRNA_24	GAGGAGTGAGAATCAGCAAA
PR8 PB2 vRNA_25	CCAAGCATCGAGATGTCAAT
PR8 PB2 vRNA_26	TGGGATATTGCCAGACATGA
PR8 PB2 vRNA_27	TCGACAATGTGATGGGAATG
PR8 PB2 vRNA_28	CAAAATTGGGGAGTTGAACC
PR8 PB2 vRNA_29	GAAGGATGCGAAAGTGCTTT
PR8 PB2 vRNA_30	GCGATTGAATCCTATGCATC
PR8 PB2 vRNA_31	GAATTTCGTCAATAGGGCGA
PR8 PB2 vRNA_32	GATAAAAGCAGTCAGAGGTG
PR8 PB2 vRNA_33	GGCCATGGTATTTTCACAAG
PR8 PB2 vRNA_34	GTCGATTGCCGAAGCAATAA
PR8 PB2 vRNA_35	ATTCAGCTGATAGTGAGTGG
PR8 PB2 vRNA_36	CAGAAAAGCAACCAGGAGAT
PR8 PB2 vRNA_37	AATGGTTGGGAGAAGAGCAA

PR8 PB2 vRNA_38	GCATGAGGGATATGAAGAGT
PR8 PB2 vRNA_39	CGGGCAATCTTCAAACATTG
PR8 PB2 vRNA_40	TCAGTCAAGAGAGAGGAAGA
PR8 PB2 vRNA_41	CCTTCAGTTTTGGTGGATTC
PR8 PB2 vRNA_42	ATGGGACTGAGAATTAGCTC
PR8 PB2 vRNA_43	AAGCCGTGGATATATGCAAG
PR8 PB2 vRNA_44	TTAGGCAGAACCCAACAGAA
PR8 PB2 vRNA_45	GTGGAATTAGGATGGTAGAC
PR8 PB2 vRNA_46	TTATTGGAGATGTGCCACAG
PR8 PB2 vRNA_47	ATCAGCAGATCCACTAGCAT
PR8 PB2 vRNA_48	ACATAGTGAGAAGAGCTGCA

Table II.4, continued. FISH probe sequences are the same as previously published (Chou et al. 2013).

Table III.1. Enrichment of Selected Top Hits for Validation.

Hits	Prelim Rd5	Rd2	Rd5
SLC35A1	1.2072E-05	2.37E-07	2.37E-07
GDF11	0.0045223	0.00038276	0.00032784
IRX3	0.0077903	0.015112	0.00081498
C2CD4C	0.0020496	0.0025642	0.0017149
TRIM23	0.015962	0.025194	0.001811
PIGN	0.0028786	0.0015024	0.0021415
ACADSB	0.011031	0.0023905	0.0021926
GRAMD2	0.021846	0.0059108	0.0028634
CIC	0.0053707	0.31911	0.0053541
JAK2	0.056382	0.16907	0.0063662
PIAS3	0.047231	0.33451	0.0077567

Of the 63 overlapping hits identified in the preliminary consecutive screen (Prelim Rd5) and Rd2 and Rd5 of the sequential screen, 11 genes involved in various biological processes were selected for further validation. p-values for enrichment in the various rounds are shown.

Table III.2. Sequence Analysis of sgRNA Target Sites in Clonal KO Cells.

Clonal KO cells	Type of Mutation (In/Del)
SLC35A1 KO	14nt Del
C2CD4C KO	8nt In
TRIM23 KO	7nt Del, 1nt Del, 3nt In
PIGN KO	1nt In, 61nt Del
CIC KO (sgRNA 1)	4nt Del, 3nt Del, 21nt Del, WT
CIC KO2 (sgRNA 2)	1nt Del, 5nt Del, 6nt Del
JAK2 KO	8nt Del
PIAS3 KO	19nt Del, 39nt Del

Nucleotides = nt; Insertions = In; Deletions = Del

Briefly, a 250bp region flanking the sgRNA target site was amplified by PCR and cloned into the pGEM-T vector for each clonal KO cell line. ~8-12 pGEM-T clones for each KO cell line were analyzed by Sanger sequencing using Lasergene Software (DNASTAR Inc) for disruptions at the sgRNA target site.

Table IV.1. CIC Binding Sites in Antiviral Gene Promoters.

Promoter	Location	Binding Site
IFNβ	-3980	TGAATGGG*
IFNγ	-3209 -327 -2116 -265	TGAATGAA TGAATGAA TGGATGGA* TGAATGGT*
IRF7	-3655 -3400 -1262	TCAATGAG* TCAATGAC* TGAATGGG*
IRF1	-3600	TCAATGAG*
IRF3	-3635 +350	TCAATGAA TGAATGGA
IRF9	-2811 +776	TCAATGAG* TCAATGGC*
MxA	+54	TGAATGGG*
IFIT1	-2874	TGAATGAA
RIG-I	-1853 -1200 -700	TCAATGGA TCAATGGA TGAATGAC*
ISG15	-2129 -1814	TGAATGAA TGAATGGA

*Putative CIC binding sites, differ by 1 nucleotide.

Table IV.2. Top 10 Enriched Gene Ontology Terms Between CIC KO Mock vs. Control Mock.

ID	Description	Gene Ratio	p-value
GO: 0051607	Defense response to virus	36/407	7.98e-20
GO: 0098542	Defense response to other organism	43/407	7.38e-19
GO: 0009615	Response to virus	40/407	3.58e-18
GO: 0019221	Cytokine-mediated signaling pathway	53/407	8.26e-17
GO: 0006954	Inflammatory response	49/407	3.52e-16
GO: 0060337	Type I interferon signaling pathway	21/407	1.28e-15
GO: 0071357	Cellular response to type I interferon	21/407	1.28e-15
GO: 0034340	Response to type I interferon	21/407	6.39e-15
GO: 0030545	Receptor regulator activity	32/407	7.88e-14
GO: 0048018	Receptor ligand activity	30/407	2.65e-13

Gene Ratio = number of DEGs in the GO term out of total DEGs in CIC KO Mock vs. Control Mock conditions present in the GO database.

Table IV.3. Top 10 Enriched Kyoto Encyclopedia of Genes and Genomes Pathways Between CIC KO Mock vs Control Mock.

ID	Description	Gene Ratio	p-value
hsa04610	Complement and coagulation cascades	12/195	2.47e-07
hsa04060	Cytokine-cytokine receptor interaction	19/195	3.19e-07
hsa04621	NOD-like receptor signaling pathway	19/195	4.65e-07
hsa05164	Influenza A	19/195	5.95e-07
hsa04933	AGE-RAGE signaling pathway in diabetic complications	15/195	1.62e-06
hsa04640	Hematopoietic cell lineage	10/195	2.10e-06
hsa05133	Pertussis	12/195	2.12e-06
hsa04064	NF-kappa B signaling pathway	13/195	7.10e-06
hsa05146	Amoebiasis	12/195	7.31e-06
hsa05144	Malaria	7/195	2.53e-05

Gene Ratio = number of DEGs in the KEGG pathway out of total DEGs in CIC KO Mock vs. Control Mock conditions present in the KEGG database.

Table IV.4. Top 10 Enriched Pathways in Ingenuity Pathway Analysis Between CIC KO Mock vs. Control Mock.

Ingenuity Canonical Pathways	p-value
Interferon signaling	2.09e-09
Acute phase response signaling	1.55e-08
GP6 signaling pathway	9.55e-08
Granulocyte adhesion and diapedesis	6.92e-08
Hepatic fibrosis/hepatic stellate cell activation	5.37e-08
Role of pattern recognition receptors in recognition of bacteria and viruses	9.55e-08
Agranulocyte adhesion and diapedesis	8.71e-07
Role of IL-17F in allergic inflammatory airway diseases	2.04e-06
Osteoarthritis pathway	6.76e-06
LXR/RXR activation	8.32e-06

Table IV.5. Top Enriched MSigDB C3 Transcription Factor Target Motifs Between CIC KO Mock vs. Control Mock.

Description	Gene Ratio	p-value
IRF7	18/286	2.24e-05
HNF1	17/286	5.46e-05
ISRE	17/286	6.04e-05
TEF1	22/286	6.65e-05
SRY	16/286	2.88e-04
CRX	16/286	5.20e-04

Gene Ratio = number of DEGs in pathway out of total DEGs in CIC KO Mock vs. Control Mock conditions present in the MSigDB C3 database.

Table IV.6. Top Enriched Genes in CIC KO Mock vs. Control Mock.

Ensembl ID	Entrez	Symbol	Confect*
ENSG00000171345	3880	KRT19	4.59
ENSG00000138650	57575	PCDH10	4.15
ENSG00000170955	112464	CAVIN3	4.07
ENSG00000198848	1066	CES1	3.99
ENSG00000113657	1809	DPYSL3	3.35
ENSG00000153707	5789	PTPRD	3.31
ENSG00000150551	116372	LYPD1	3.28
ENSG00000163565	3428	IFI16	3.25
ENSG00000103490	29108	PYCARD	3.16
ENSG00000197565	1288	COL4A6	3.16

* Confect: CONfident efFECT size; DEG ranking system based on p-value, false discovery rate, and effect size, which is the difference in mean values compared to the standard deviation.

Table IV.7. DEGs in GO Pathway "Defense Response to Other Organism."

Defense Response to Other Organism	Rank	Canonical CBS*	Canonical and Putative CBS*	Gene Function (GeneCards.org)
IFI16	8	10	30	cyto/nuclear DNA sensor
PYCARD (ASC)	9	0	0	mediator in apoptosis and inflammation
IFITM1	12	0	0	inhibitor of viral fusion/release
DMBT1	18	7	21	tumor suppressor, plays role in bacterial defense and viral defense/transmission
TRIM22	23	19	31	ubiquitinates viral proteins
MX1	30	3	9	prevents nuclear import/txn of viral nucleocapsids
IFITM3	31	0	3	prevents viral fusion with cholesterol depleted endosomes
IL6	35	0	18	pro-inflammatory cytokine
OASL	39	0	4	binds dsRNA, but does not activate RNaseL
ISG15	41	2	2	ISGylates viral proteins for degradation and host proteins for activation
IFIT1	43	2	2	binds and sequesters vRNA (5' PPP-RNA)
IFI44L	44	6	19	antiviral activity against hepatitis C
OAS2	48	6	13	binds dsRNA and activates RNaseL
FGB	51	0	0	facilitates antibacterial immune response
IFIT3	52	1	3	adapter that bridges TBK1 to MAVS
IRF7	59	0	25	induces type I IFN expression by binding ISRE
IFIT2	62	2	5	inhibits expression of viral messenger RNAs lacking 2-O-methylation of the 5 cap
GBP3	81	9	30	antiviral activity against influenza virus
RSAD2	97	0	8	inhibits IAV budding, facilitates TLR signaling and T cell activation
PF4	105	0	2	chemokine: chemotactic for neutrophils and monocytes
BST2	119	0	0	tethers budding virions to each other and PM
PARP9	123	7	13	helps induce IFNg responsive genes
IL1B	132	9	15	pro-inflammatory cytokine
SLFN11	136	11	24	inhibits retrovirus protein synthesis
UNC13D	148	5	15	immunological synapse regulation
OAS1	160	4	15	binds dsRNA and activates RNaseL
DDX58 (RIG-I)	163	6	8	major sensor of foreign RNA
MX2	164	10	26	may regulate nucleo-cytoplasmic transport and cell cycle progression
IFITM2	168	0	0	inhibitor of viral fusion/release
MB21D1 (CGAS)	169	4	6	cytosolic DNA sensor
LBP	177	0	1	promotes cytokine release in response to LPS
FGA	189	3	9	facilitates innate immune response
NR1H4	193	9	23	anti-inflammatory protein that prevents bacterial overgrowth
DTX3L	217	0	2	ubiquitin ligase, DNA damage repair
GBP1	225	2	9	antiviral activity against influenza virus

IL31RA	244	3	8	type I IFN cytokine receptor

Table IV.7, continued. DEGs ranked by confect analysis.
*Canonical and putative CBS analysis includes isoforms of each gene.

Appendix C

Soundtrack

An avid lover and amateur performer of music, Albert Einstein once exclaimed, “in scientific thinking are always present elements of poetry. Science and music requires a thought homogeneous.” To enrich your reading experience of this dissertation, I present these pieces, chosen either to match the ethos of the chapter or to reflect my state of mind at each stage of my thesis work.

Chapter I: Introduction

Maurice Ravel: Daphnis et Chloe, Suite No. 2

Recommended recording: London Symphony Orchestra with Arpad Joo, 1995 Arts Music GMBH

Chapter II: Materials and Methods

Sergei Rachmaninoff: Mvt. 1 from Piano Concerto No.2

Recommended recording: Valentina Lisitsa (pianist) with the London Symphony Orchestra and Michael Francis, 2012 Decca Music Group Limited

Chapter III. Genome-wide Crispr/Cas9 Screen Identifies Host Factors Imperative for Influenza Virus Replication

Dmitri Shostakovich: Symphony No. 7 “Leningrad”

Recommended recording: Chicago Symphony Orchestra with Leonard Bernstein, 1989 Deutsche Grammophon GMBH

Chapter IV. Regulation of Cell Intrinsic Immunity by the Transcriptional Repressor CIC

Gustav Mahler: Mvt. 1 from Symphony No. 2 "Resurrection"

Recommended recording: Vienna Philharmonic with Gilbert Kaplan, 2003 The Kaplan Foundation

Chapter V: Tetracysteine Tagged NP Reveals the Role of Rab11a in Production of Infectious Influenza Virus Particles

Richard Strauss: Till Eulenspiegel lustige Streiche (Till Eulenspiegel's Merry Pranks)

Recommended recording: Chicago Symphony Orchestra with Sir George Solti, 1976, 2017 Decca Music Group Limited

Chapter VI: Discussion

Richard Strauss: Don Juan

Recommended recording: Berlin Philharmonic with Riccardo Muti, 2015 Decca Music Group Limited